Coventry University

DOCTOR OF PHILOSOPHY

Nonlinear instabilities and transition to turbulence in magnetohydrodynamic channel flow

Hagan, Jonathan Paul

Award date:
2013

Awarding institution:
Coventry University

Link to publication

General rights
Copyright and moral rights for the publications made accessible in the public portal are retained by the authors and/or other copyright owners and it is a condition of accessing publications that users recognise and abide by the legal requirements associated with these rights.

- Users may download and print one copy of this thesis for personal non-commercial research or study
- This thesis cannot be reproduced or quoted extensively from without first obtaining permission from the copyright holder(s)
- You may not further distribute the material or use it for any profit-making activity or commercial gain
- You may freely distribute the URL identifying the publication in the public portal

Take down policy
If you believe that this document breaches copyright please contact us providing details, and we will remove access to the work immediately and investigate your claim.

Download date: 04. May. 2023

Nonlinear instabilities and transition to turbulence in magnetohydrodynamic channel flow

Jonathan Hagan
1667024
Coventry University

"A thesis submitted in partial fulfilment of the University's requirements for the Degree of Doctor of Philosophy."

September, 2013

Abstract

The present study is concerned with the stability of a flow of viscous conducting liquid driven by a pressure gradient between two parallel walls in the presence of a transverse magnetic field, which is investigated using a Chebyshev collocation method. This magnetohydrodynamic counterpart of the classic plane Poiseuille flow is generally known as Hartmann flow. Although the magnetic field has a strong stabilizing effect, the turbulence is known to set in this flow similarly to its hydrodynamic counterpart well below the threshold predicted by the linear stability theory. Such a nonlinear transition to turbulence is thought to be mediated by unstable equilibrium flow states which may exist in addition to the base flow. Firstly, the weakly nonlinear stability analysis carried out in this study shows that Hartmann flow is subcritically unstable to small finite-amplitude disturbances regardless of the magnetic field strength. Secondly, two-dimensional nonlinear travelling wave states are found to exist in Hartmann flow at substantially subcritical Reynolds numbers starting from $Re_n = 2939$ without the magnetic field and from $Re_n \sim 6.50 \times 10^3 Ha$ in a sufficiently strong magnetic field defined by the Hartmann number Ha. Although the latter value is by a factor of seven lower than the linear stability threshold $Re_l \sim 4.83 \times 10^4 Ha$ and by almost a factor of two lower than the value predicted by the mean-field (monoharmonic) approximation, it is still more than an order of magnitude higher than the experimentally observed value for the onset of turbulence in this flow. Three-dimensional disturbances are expected to bifurcate from these two-dimensional travelling waves or infinity and to extend to significantly lower Reynolds numbers.

The by-product of this study are two developments of numerical techniques for linear and weakly nonlinear stability analysis. Firstly, a simple technique for avoiding spurious eigenvalues is developed for the solution of the Orr-Sommerfeld equation. Secondly, an efficient numerical method for evaluating Landau coefficients which describe small amplitude states in the vicinity of the linear stability threshold is introduced. The method differs from the standard approach by applying the solvability condition to the discretised rather than the continuous problem.

Acknowledgements

First, I would like to thank my supervisor Dr. Janis Priede for the support, guidance and encouragement that he has offered during my studies.

A special thanks to my friends, Chris, Paul, Dr. David, Ryan and Rich, for ensuring that I have found time to enjoy myself in between studying.

Finally, I would like to thank my Mum and Dad, Lisa, Amy and James, the rest of my family, and especially Sarah for their constant love and support that have allowed me to complete this thesis.

Thank you all.

Contents

List of Figures

List of Tables

Nomenclature

t	Time
V	Volume
ρ	Density
m	Mass
p	Pressure
h	Length scale
ν	Kinematic viscosity
Re	Reynolds number
Ha	Hartmann number
Rm	Magnetic Reynolds number
Pm	Prandtl number
Re_l	Critical Reynolds number
R_l	Critical Reynolds number based on Hartmann layer thickness
R_n	Critical Reynolder number for nonlinear modes
R_t	Reynolds number for transition to turbulence
c	Wave speed
ω	Frequency
α	Wavenumber in x-direction
β	Wavenumber in z-direction
α_l	Critical wavenumber in x-direction
$T_n(x)$	Chebyshev polynomials of the first kind
$\boldsymbol{e}_x$	Unit vector in x-direction
$\boldsymbol{e}_y$	Unit vector in y-direction
$\boldsymbol{e}_z$	Unit vector in z-direction
λ	Complex temporal growth rate
$\boldsymbol{k}$	Wave vector
$\boldsymbol{B}$	Magnetic field

$\boldsymbol{j}$	Electric current
σ	Electrical conductivity
τ_m	Magnetic diffusion time
μ_0	Permeability of a vacuum
ϕ	Electrostatic potential
$\boldsymbol{k}$	Wave vector

Chapter 1

Introduction

The main topic of this thesis is the stability of incompressible plane Poiseuille flow and Hartmann flow. Plane Poiseuille flow is the flow of a liquid between two infinite parallel plates, driven by a constant pressure gradient. This is one of the simplest and most widely studied models of hydrodynamic instabilities and transition to turbulence in shear flows. Hartmann flow has a similar set-up, but the liquid is an electrically conducting fluid and a magnetic field is applied transverse to the flow. The mathematical model describing these flows is the Navier-Stokes equations. By first considering the hydrodynamic stability problem of plane Poiseuille flow, methods can be developed which will be extended to investigate the stability characteristics of Hartmann flow. The mathematical model of the fluid will assume conservation of mass, that the fluid is incompressible and Newtonian, and the continuum hypothesis is applicable [1]. Figure 1.1 is a sketch of the set-up and velocity profiles for plane Poiseuille flow and Hartmann flow.

Of particular interest in both cases is the point at which laminar flow breaks down and becomes turbulent. Osbourne Reynolds [2] showed that the laminar flow of pipe Poiseuille flow broke down when the ratio of the velocity of the fluid times the radius of the pipe to the kinematic viscosity of the fluid exceeded a certain value. The dimensionless value representing this ratio is known as the Reynolds number, and specifies any class of dynamically similar flows for a given geometry [3]. The transition

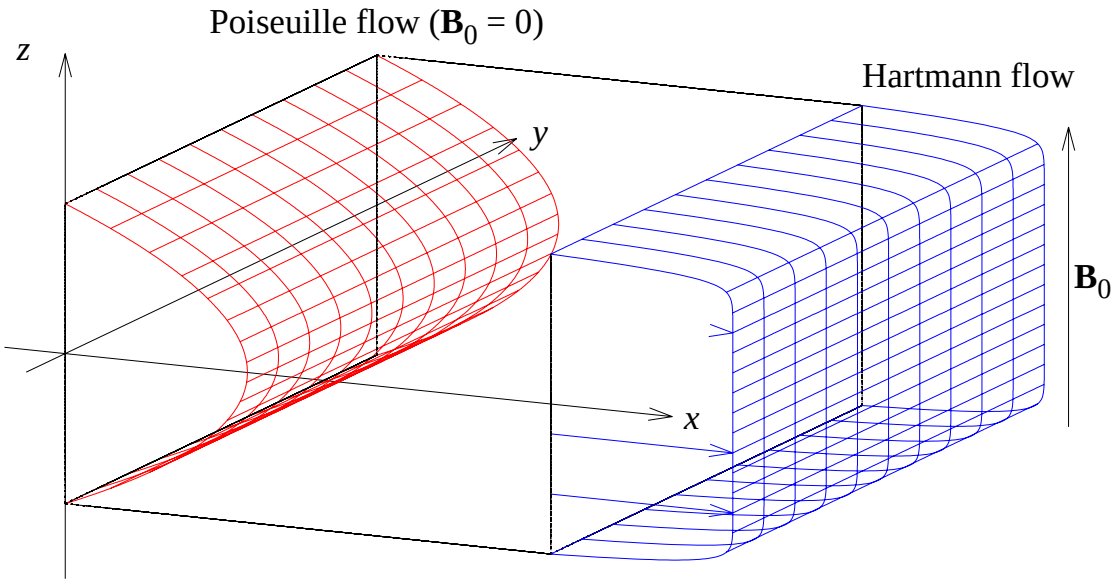

Figure 1.1: Sketch of the set-up and velocity profiles of plane Poiseuille flow and Hartmann flows.

from laminar flow to turbulent flow is characterised by the *critical* Reynolds number, and calculating this value for Hartmann flow will be the primary task.

Consider a laminar flow that is subject to a small amplitude disturbance. If the flow returns to its original state, then the flow can be described as stable. If the disturbance grows and the laminar flow is changed into another state, then it can be described as unstable. This state can either be a turbulent flow or a more complicated laminar flow. Of interest is the mathematical analysis of the evolution of the disturbances superposed on a laminar base flow [4]. When discussing the stability of a flow, then it is the stability of this basic flow that is being referred to. Physically, it is of interest if the basic flow can be observed. The transition point occurs when there is a bifurcation, when the flow becomes unstable to a certain disturbance.

Hartmann flow has a similar set-up to plane Poiseuille flow, except the flow is an electrically conducting liquid and there is a transverse magnetic field applied. As well as a Reynolds number, similar Hartmann flows have a Hartmann number, which is a dimensionless parameter that is a square root of the ratio of the electromagnetic body (Lorentz) force to the viscous force.

Practically, interactions between conducting shear layers and magnetic fields have applications in industry that include nuclear fusion reactors and in pumping, stirring and levitating liquid metals. Other examples include the Earth's magnetic field, which is maintained by the motion of fluid in the Earth's core, and solar magnetic fields which generate solar sunspots [5, 6]. The study of these flows is known as magnetohydrodynamics.

The thesis is ordered as follows. In the first section, the background of the topics covered is discussed. In Sec. 2 the Chebyshev collocation method is introduced, in particular the Chebyshev-Gauss-Lobatto points. In Sec. 3 a simple numerical technique for avoiding spurious eigenvalues is presented, demonstrated using linear stability analysis of plane Poiseuille flow. In Sec. 4 a numerical method for calculating Landau coefficients in weakly nonlinear analysis is shown. Left eigenvectors are used to apply the solvability condition directly to the discretised problem as opposed to the continuous problem. In Sec. 5 the stability of Hartmann flow is investigated. Results are presented for linear stability analysis and weakly nonlinear analysis. Then two dimensional travelling waves are traced into the subcritical regime. Sec. 6 contains a summary and conclusions.

1.1 Hydrodynamic stability

1.1.1 Linear Stability analysis

For over a century the study of hydrodynamic stability has been one of the cornerstones of fluid mechanics. The field of hydrodynamic stability concerns the stability of various flows when subjected to disturbances. This is important because a stationary unstable flow cannot exist in reality. The main interest is to find out when, why and how the flow transitions; be it from a laminar flow to a turbulent flow, from a laminar flow to a different laminar flow or whether there is no transition and the flow is stable to some infinitesimally small perturbation. Mathematically, the hydrodynamic stability

problem can be considered as follows: Suppose there is a time-independent solution

$$u_i(x_j), p(x_j), \tau(x_j) \tag{1.1}$$

for the components of velocity, pressure and temperature. This solution is analysed for a class of perturbations, and if the solution approaches a steady-state solution (1.1) as time $t \to \infty$, the flow is classed as asymptotically stable. If the solution jumps to another state and remains there, this is a metastable solution. Linearised stability analysis gives an upper bound for the critical parameter (Reynolds number, wavenumber), a necessary condition for instability. For a more accurate solution, it is necessary to conduct a non-linear analysis. Early work on the hydrodynamic stability of a pressure driven flow of a Newtonian fluid between parallel plates was carried out most notably by Helmholtz [7], Kelvin [8] and Rayleigh [9]. This work consisted mainly of analytical studies of purely inertial stability of parallel shear flows of inviscid fluids. The experimental work by Reynolds [2] first demonstrated the instabilities of parallel shear flows . It was Orr [10] and Sommerfeld [11] who derived the governing equation for the flow of a viscous fluid, the Orr-Sommerfeld equation, at the beginning of the 20^{th} century. It is a homogeneous, eigenvalue equation that describes the linear, two-dimensional modes of a disturbed viscous parallel flow. The Orr-Sommerfeld equation was derived by considering the linearised version of the Navier-Stokes equation for a perturbed velocity field. For viscous parallel flows, such as for plane Poiseuille flow which will be considered here, the eigenvalue spectrum is discrete and infinite [105]. For unbounded flows, for example the Blasius boundary layer flow, there is a finite number of discrete eigenvalues, which increases with the Reynolds number, but there is also a continuous spectrum of eigenvalues [12, 3]. For a given Reynolds number and wavenumber, that are real and fixed, the eigenvalue relation defines a discrete set of eigenvalues. If these are ordered from largest to smallest, then it is the leading eigenvalue, or the first few eigenvalues that will be of most interest. The sign of the real part of this eigenvalue will be of particular importance, showing whether the solution is stable or unstable. The Orr-Sommerfeld equation is difficult to solve directly,

so asymptotic methods or numerical methods are required in order to find solutions. Asymptotic solutions of the Orr-Sommerfeld equation were developed by Heisenberg [13], Tollmien [14] and Lin [15, 16]. Numerical methods were later developed to locate the critical Reynolds number [17]. In 1953, Thomas [18] published the first numerical solution of the Orr-Sommerfeld equation. He hoped to resolve the controversies surrounding asymptotic methods of approximation. Using a finite difference method, he validated the conclusions of Heisenberg [13] and Lin [15], that plane Poiseuille flow is unstable.

Davey and Drazin [19] showed that unbounded Poiseuille flow (pipe Poiseuille flow) is stable. They used two different methods, integration of the stability equation with a 'shooting' method and an expansion of the eigenfunction as a series of orthogonal functions, with the numerical results of both methods agreeing, joining up with known asymptotic results, and showing conclusively that all axisymmetric disturbances are stable at all Reynolds numbers. Davey [20] applied an initial 'shooting' value method to solve the Orr-Sommerfeld equation. This works by considering the Orr-Sommerfeld equation as a system of first order differential equations, normalising and then solving the resulting eigenvalue relation for fixed Reynolds number and wavenumber iteratively. There are many difficulties that arise in this method, some of which have been overcome, but it is generally more efficient than using a finite difference method. For a detailed discussion see Lee and Reynolds [21] or Davey [20].

Orszag [17] found an accurate solution of the Orr-Sommerfeld equation, using expansions in Chebyshev polynomials and the QR matrix eigenvalue algorithm. When this method was applied to the stability of plane Poiseuille flow the critical Reynolds number was found to be $Re_l = 5772.22$, with corresponding wavenumber $\alpha_l = 1.02055$. Orszag showed that the use of spectral methods (in this case Lanczos' Chebyshev Tau method [22]) was superior to either finite difference methods [18] or initial value (shooting) methods [19], as spectral methods obtained results with a higher degree of accuracy, and required less computation. This value of the Reynolds number, whilst considered accurate, is vastly different from those results obtained experimentally.

Whilst the results obtained by Orszag were at the time the most accurate, the method resulted in spurious unstable modes with large growth rates [23]. For more information on spurious modes and a more detailed discussion of spectral methods, see 1.4.

A number of fluid flows that are theoretically linearly stable can become turbulent, for example, plane Couette flow and circular pipe (Hagen-Poiseuille) flows. These flows are linearly stable to all infinitesimal disturbances, but can become unstable to small, finite disturbances. This suggests that linear stability theory may not give the whole picture of what is happening, and nonlinear effects may need to be accounted for.

1.1.2 Experimental Background

Historically, it has been difficult for experimentalists to observe periodic disturbances predicted theoretically in plane Poiseuille flow. This is because it is required to produce a laminar flow that is close to the critical Reynolds number. Physically, it is necessary to have a large width to height aspect ratio, as well as a channel that is long enough for the fully developed laminar flow to develop. It is necessary to avoid contamination from the side walls; this can cause problems as a small channel height results in a higher probability that the walls cause imperfections. The earliest experimental work on studying the transition to turbulence appears to have been carried out by Davis and White [24], and along with Patel and Head [25], they were able to obtain a critical Reynolds number of $Re \approx 1000$, though these experiments were rather crude. Both demonstrated that plane Poiseuille flow is unstable to finite amplitude disturbances.

Nishioka et al. [26] were able to experimentally obtain laminar flow up to $Re \approx 8000$, seemingly obtaining a critical Reynolds number higher than that predicted by linear stability theory. This proved to be false; their experiment was flawed as the channel length used was too short to allow the disturbances to sufficiently grow and cause transition. The aspect ratio used was 27.4 with background turbulence below 0.05%. When the disturbance levels were increased, instabilities were demonstrated at lower Reynolds numbers.

Kozlov and Ramazanov [27] were able to achieve a turbulence level of 0.1% and

claimed to have achieved laminar flow up to $Re = 7000$, but whilst using a longer channel than Nishioka *et al.* It is likely that the flow was not fully developed once they achieved $Re > 4000$.

Whilst Carlson *et al.* [28] did not record the value of their background turbulence, it can be assumed that it was of lower intensity than Davies & White and Patel & Head. Turbulent spots initiated a transition at $Re = 1000$. Using three different disturbances, each introduced to a fully developed flow, Nishioka and Asai [29] showed that the transition occurs at $Re \approx 1000$. Further, the threshold amplitude was the same as the amplitude of the disturbances in fully turbulent flow. Alavyoon et al. [30] found that laminar flow was always maintained for $Re < 1100$. Turbulent spots were observed to form and evolve in the region $1100 < Re < 2200$.

These last three experiments seem to confirm the crude predictions of Davies & White and Patel & Head. It is expected that $Re \approx 1000$ is required for transition in plane Poiseuille flow. Linear stability theory predicts transition to occur at $Re_l = 5772.22$ [17]. In order to resolve this discrepancy it is necessary to consider the nonlinear terms that were neglected for linear stability theory, and also to consider an amplitude that is small, but no longer infinitesimal.

1.2 Weakly nonlinear analysis

Theoretically, plane Poiseuille flow is known to be linearly stable up to the critical Reynolds number $Re_l = 5722.22$ [17]. Experimentally it has been observed that plane Poiseuille flow becomes turbulent at Reynolds numbers as low as $Re \approx 1000$ [30, 28, 29]. Furthermore, turbulence is observed to develop in the flow on the time scales which are several orders of magnitude shorter than those predicted by the linear stability analysis [31]. Such a subcritical transition to turbulence can be accounted for by a positive feedback of perturbation on its growth rate, which is a non-linear effect beyond the scope of linear stability theory. So, perturbations of sufficiently large amplitude can acquire large, positive growth rates at a subcritical Reynolds number, where all

small-amplitude perturbations are linearly stable. For small-amplitude perturbations in the vicinity of the linear stability threshold, this type of phenomenon is described generally by the so-called Landau (Stuart-Landau) equation [32, 33]. Whether the instability is sub- or super-critical is determined by the coefficients of this equation, referred to as Landau coefficients. It is necessary to calculate these for each individual case.

Nonlinear disturbances in flows were considered historically by several authors, including Reynolds in 1883 [2] and theoretically by Bohr in 1909, Noether in 1921 and Heisenberg in 1924 for a variety of problems. It was the work by Landau in 1944 [32] that provided the basis for nonlinear hydrodynamic stability, with the derivation of the so-called Landau equation. Around the same time, Hopf [34] considered similar ideas of how turbulence may develop with an increasing Reynolds number by repeatedly bifurcating the solution representing the flow. Work was carried out by Stuart [35], Gor'kov [36] and Malkus and Veronis [37] who all carried out similar work for various problems. Palm [38] in 1960 was the first to show how the Landau equations can be derived from a system of partial differential equations that govern a flow. Stuart [39] and Watson [40] were the first to derive the Landau equation for plane parallel flows. They provided the basic formalism for the work in this area. A more recent account is given by Schmid and Henningson [4], Huerre and Rossi [41] and Yaglom [42].

The method of Stuart and Watson was later extended and modified by Reynolds and Potter [43], who used it to show that plane Poiseuille flow with a fixed flow rate is indeed sub-critically unstable. Both of these methods were compared by Sen and Venkateswarlu, [44] who applied them to calculate higher-order Landau coefficients for plane Poiseuille flow driven by a fixed pressure gradient. Not much difference was detected in the supercritical range of instability, however the Watson method was found difficult to apply in the subcritical region, which represents the main area of interest for this type of flow. These types of asymptotic expansion methods have been reconsidered and surveyed by Herbert [45], and substantially extended by Stewartson and Stuart [46] who included a slow spatial variation so deriving the complex Ginzburg-

Landau equation [47]. The method of multiple scales was shown to be the equivalent of amplitude expansion by Fujimura [48], as well as to that of centre manifold reduction, another technique that can be used to derive the Landau equation [49].

Weakly non-linear stability analysis requiring the evaluation of the Landau coefficients is technically rather complicated. This may explain why most hydrodynamic stability problems are restricted to the linear analysis, which is of limited practical significance when the instability happens to be subcritical. A significant technical hindrance to the implementation of the conventional weakly non-linear stability analysis is the adjoint eigenfunction which needs to be found by solving the adjoint problem. Then several inner product integrals containing the adjoint eigenfunction need to be numerically evaluated in order to obtain Landau coefficients.

A simpler but numerically more accurate method to evaluate Landau coefficients was developed as part of this study. The method is based on the application of the solvability condition to the discretised rather than the original continuous equations. This allows us to evaluate Landau coefficients without using the adjoint eigenfunction which in this approach is replaced by the left eigenvector. Such a possibility seems to have been mentioned by Crouch and Herbert [50], and a similar approach employing Gaussian elimination was noted by Sen and Venkateswarlu [44]. The approach differs from that of Jeffrey and Kawahara [51], who just consider a straightforward extension of the standard solvability condition from a single partial differential equation to a system of such equations using the left eigenvector of continuous adjoint functions.

1.3 Hartmann Flow

Magnetohydrodynamics is an area of continuum mechanics, in which moving, electrically conducting fluids interact with magnetic fields. The movement of an electrically conducting fluid through a magnetic field generates an electromotive force that can induce an electric current, which in turn produces its own magnetic field [52].

The magnetic Reynolds number, the ratio of the advection of the magnetic field to

the diffusion of the magnetic field, is found to be negligible at laboratory scales [52], where the fluid flow has little effect on the magnetic field. When a medium is highly conducting, then the magnetic Reynolds number is large, $Rm \gg 1$, and the fluid flow induces a magnetic field which strongly affects the imposed magnetic field. When the medium is a poor conductor, the magnetic Reynolds number is small, $Rm \ll 1$, which is typical for Hartmann flow. In this situation, the magnetic field induced by the fluid flow is negligible relative to the imposed magnetic field. This leads to simplifications in the Lorentz force and Ohm's law (see 5.1).

The earliest theoretical work on the flow of an electrically conducting liquid between two infinite plates with a transverse magnetic field was carried out by Hartmann [53], and then the first experimental work by Hartmann and Lazarus [54]. The first work investigating the linear stability of Hartmann flow was by Lock [55]. By considering that the magnetic Prandtl number, Pm, is very small for this setup, Lock simplified the governing equations and applied the method of asymptotic solutions. The magnetic Prandtl number is the ratio of the magnetic Reynolds number to the Reynolds number, *i. e.*, the ratio of the magnetic diffusivity to the viscosity. He demonstrated that the magnetic field had a strong stabilising effect on the flow, with the critical Reynolds number increasing as $Re_l = R_l Ha$. In particular, when the Hartmann number, $Ha > 20$, the critical Reynolds number based on the Hartmann layer thickness, R_l, is $R_l \approx 5 \times 10^4$. Lock comments on the discrepancy between this result and the experiments. These show that the critical Reynolds number at which the transition from turbulent to laminar flow is two orders of magnitude lower, $R_t \approx 225$, which was observed experimentally by Murgatroyd [56]. Lock hypothesised that this difference may be resolved by considering instability to finite amplitude disturbances. The transition may be caused by unstable equilibrium states which exist in addition to the base flow.

Stuart [57] conducted a similar study for a parallel magnetic field, using similar simplifications, and showed that the magnetic field again had a stabilising effect on the flow. Hunt [58] presented a theoretical analysis on a parallel flow with an applied parallel magnetic field. He shows that when a uniform magnetic field is oriented

parallel to the flow, and is sufficiently strong, the wave vector of the most unstable disturbance is not parallel to the flow. This invalidates the conclusions of Stuart [57], who said the most unstable wave vector was parallel to the flow, and so only considered a two dimensional disturbance. Hunt goes on to prove that a parallel magnetic field, however strong, can never completely stabilise a flow.

Potter and Kutchey [59] repeated the study by Lock of a transverse magnetic field, but without making the same simplifications. They demonstrated that the stability of the flow increased with Pm. However, Takashima [60] suggested that the boundary conditions on the magnetic field perturbations seem to be incorrect, and argued that the magnetic field can have a destabilising effect, and as Pm increases the fluid flow becomes more unstable. This effect was more prominent the larger the Hartmann number (stronger the magnetic field).

The extremely high critical Reynolds number found by Lock [55], which is typical for exponential velocity profiles [61, 19] has been confirmed by more recent studies. Likhachev [62] found $R_l \approx 48310$. Lifshits and Shtern [63] obtained hydrodynamic plane Poiseuille flow results of similar accuracy to those calculated by Orszag [17]. They also calculated the linear stability result for Hartmann flow to be $R_l \approx 48300$, with corresponding wave number $\alpha_l = 0.16 \times Ha$ and wave speed $c = 0.154$. Using a monoharmonic (mean-field) approximation, they found $R_n \approx 12300$. The authors state that this is 'the simplest model, the first step towards realisation of an escalating process'. Both of the linear stability results calculated by Likhachev and Lifshits & Shtern are very close to the highly accurate result obtained later by Takashima. Takashima [60] found, for sufficiently large Hartmann number, $Re_l = 48311.016 \times Ha$. with corresponding wave number $\alpha_l = 0.161531 \times Ha$ and wave speed $c = 0.155029 \times Ha$.

More recently, rather than considering the full Hartmann flow, work has been carried out on the Hartmann layer. A Hartmann layer develops at any boundary in an electrically conducting fluid where the magnetic field is not tangential to the boundary [64]. Lingwood and Alboussière [64], working on a single Hartmann layer, with a transverse magnetic field, found the critical Reynolds number to be $Re = 48\,250 \times Ha$.

The result is within 1.5% of Takahshima's [60], and the authors explain the discrepancy as 'probably due to differences in calculation method used'.

Experimentally, the earliest work was carried out by Hartmann and Lazarus [54], who introduced the concept of a Hartmann layer. The experimental work carried out was on pressure driven duct flow. They discovered that an applied transverse magnetic field caused the velocity profile of the flow to change; it flattened in the middle and two boundary layers developed at the walls. These boundary layers are now known as Hartmann layers.

Murgatroyd [56], Lykoudis [65] and Branover [66], all performed experiments to determine if a duct flow is laminar or turbulent in the presence of a transverse magnetic field. All are in agreement that the laminarisation occurs at $150 < Re/Ha < 250$ for sufficiently high Hartmann number. This result holds for both circular pipes and rectangular cross sections. More recently, Moresco and Alboussière [67] were able to obtain a result of $Re/Ha \approx 380$ for the Hartmann layer. This discrepancy in value, it being much higher than that achieved previously, may be due to the higher value of the Hartmann number that was used in the experiments. This value was supported by a numerical study by Krasnov *et al.* [68], who proposed that the value for Re_t is in the range between 350 and 400.

As conjectured by Lock [55], the discrepancy between the experimental and theoretical values could be due to finite amplitude disturbances not being accounted for by linear stability analysis. The weakly nonlinear analysis of a physically similar problem, that of an asymptotic suction boundary layer found by Hocking [69] and Likhachev [62], was found to be subcritically unstable to small but finite amplitude disturbances. Moresco and Alboussière [70] studied the weakly nonlinear stability of Hartmann boundary layers and showed that working from the critical linear stability results, there is a subcritical instability, confirming that the same is true for Hartmann flow.

The first quantitative results for finite amplitude subcritical travelling waves were reported by Lifshits and Shtern [63]. By assuming the perturbation took the form

of one harmonic, they used the mean-field approximation. They showed that two-dimensional travelling waves existed down to $R_n \approx 12300$. For the non-magnetic case, *i.e.* plane Poiseuille flow, this approximation yields surprisingly good results, namely $Re_n \approx 2825$ [71]. This is only 4% away from the accurate result $Re_n \approx 2939$ [72]. This approximation is only qualitatively correct even in the weakly nonlinear limit, where it overestimates the Landau coefficient, which is used to determine the evolution of small finite amplitude disturbances, by about 30% [43].

Other approaches to explaining the transition to turbulence in Hartmann flow have been attempted by considering the energetic stability and the transient growth theories. Although, formally, energy stability applies to arbitrary disturbance amplitudes, it is essentially a linear and amplitude-independent approach. This is because the nonlinear term neither produces nor dissipates the energy, and so drops out of the disturbance energy balance. Lingwood & Alboussière [64] used this approach and found that the Hartmann layer is energetically stable, i.e. all disturbances decay at any time, provided that the Reynolds number is below $R \approx 26$, which is an order of magnitude lower than that observed experimentally. As shown by the numerical study by Krasnov *et al.* [68], likewise linear is also the optimal transient growth mechanism. This has been studied for the Hartmann boundary layer by Gerard-Varet [73] and the whole Hartmann flow by Airiau & Castets [74]. The transition to turbulence is essentially a nonlinear process that is mediated by a strongly nonlinear but necessarily stable equilibrium states that have little to do with the nonnormality of the linear problem that underlies the transient growth [75]. At sufficiently high Reynolds numbers, the basins of attraction of such intermediate nonlinear equilibrium states can approach very close to the laminar base flow where they are reachable by small, finite amplitude disturbances [76].

In this project, of interest is finding these two-dimensional travelling wave states in Hartmann flow. Beginning with plane Poiseuille flow, subcritical equilibrium states can be traced as the strength of the magnetic field is increased using an accurate numerical method, that is based on the Chebyshev collocation approximation and a

sufficiently large number of harmonics, it is expected that these states will extend to subcritical Reynolds numbers.

1.4 Spectral methods

Spectral methods became increasingly popular in the second half of the 20^{th} century, with the developments in the fast transform methods. They are known to achieve exponential convergence [77]. Spectral methods have applications in weather prediction and turbulent flows, especially where high accuracy is required for complicated solutions [23]. The rapid rate of convergence makes them ideal for solving eigenvalue problems found in hydrodynamic stability analysis, such as the Orr-Sommerfeld equation [17], that are numerically demanding [78]. Previously used methods, such as finite difference methods [18]and initial 'shooting' methods [19], are inferior to spectral methods for solving these types of problems because although all the methods have a similar rate of convergence, spectral methods require less computational power. For simple problems this is not important, but for more complex, numerically demanding problems this is desirable as computations can be solved quicker and more efficiently.

There are 3 main types of spectral methods; the Tau method, the Galerkin method and the collocation method.

The monograph by Gottlieb and Orszag [23], first published in 1977, was the first comprehensive work on the theory of spectral methods. Spectral methods first developed in the early 20^{th} century, but their use was not widespread until advances were made in computational power. The earliest work carried out on spectral methods, in the guise of the method of weighted residuals, is thought to have been in the 1930's. Canuto *et al.* [77] makes reference to the work by Slater [79] and Kantorovic [80], both in 1934, who applied the collocation method to some basic, but specific, problems. This work was taken further by Frazer, Jones and Skan [81], who then used the collocation method to solve some ordinary differential equations for the first time. However, it was Cornelius Lanczos, in 1938, after previously working on purely mathematical physics

papers, who published his first work on numerical analysis. This paper contained both the first τ-method, as well as the pseudospectral method (though it was not termed this until 1972 by Steven A. Orszag) [22]. Further work on matrices over the next few years lead to what was later realised to be the Fast Fourier Transform, which although not dealt with in this project, is very important for spectral methods.

Whilst spectral methods can accurately and efficiently calculate a number of leading eigenvalues for an eigenvalue problem, they can also produce physically spurious unstable modes. Increasing the resolution will still result in these modes appearing [23]. These spurious modes are not unique to spectral methods; they also appear when solving the Orr-Sommerfeld equation using a finite difference method [23]. There are two kinds of spurious eigenvalues. Physically spurious eigenvalues are numerically computed eigenvalues that are incorrect because of an incorrect boundary condition or other incorrect physics. Numerically spurious eigenvalues are poorly approximated exact eigenvalues; by sufficiently increasing the numerical resolution, these can be accurately calculated [82]. Both of these kinds of spurious eigenvalues will occur in the solutions, but it is the physically spurious which are the most concerning. They appear in all spectral methods; Galerkin [83], Tau [84] and collocation approximations [77], unless a modification is made to the method to avoid them. It is desirable to avoid them, as when searching for unstable modes, physically spurious modes of positive large real part could be confused with genuine instabilities.

For the Galerkin method, spurious eigenvalues can be removed by using the basis functions also as the test functions instead of separate Chebyshev polynomials [83]. Gardner *et al.* [85] developed a modified Chebyshev tau method, which eliminated these spurious eigenvalues found in [17]. It was also shown that the modified Chebyshev Tau method had solutions that converged at least as quickly as the original method. Zebib [86] calculated the eigenvalues for plane Poiseuille flow, using the Orr-Sommerfeld equation obtained via linear stability analysis, and compared the results to Orszag's [17]. It was claimed that his were more accurate, whilst using the same number of expansion coefficients. It should be noted that Zebib did not use the

Galerkin or Tau methods, but instead used an expansion procedure using the Chebyshev polynomials as base functions. Zebib also encountered spurious eigenvalues, but proposed no method to eliminate these [86]. As previously stated, Gardner et al. [85] proposed a way to eliminate these spurious values, whilst maintaining a similar rate of convergence to the actual solution, by modification of a tau spectral method. Weideman and Reddy [89] used the same method as proposed by Huang and Sloan [88] when solving the Orr-Sommerfeld equation, with the method employing different boundary conditions which lead to the elimination of the spurious eigenvalues. The result is of the same order of accuracy as previous results, as well as having a similar rate of convergence. Following the approach of McFadden *et al.* [78] for the tau method, Huang and Sloan [88] use a Lagrange interpolating polynomial for second-order terms which is by two orders lower than the Hermite interpolant used for other terms. The choice of the latter polynomial depends on the particular combination of the boundary conditions for the problem to be solved [89].

This work will follow the method of Hagan and Priede [90]. This outlines a simple method for avoiding spurious eigenmodes in the Chebyshev collocation method which uses only the Lagrange interpolating polynomial applicable to general boundary conditions. The approach is based on the capacitance matrix technique which is used to eliminate fictitious boundary conditions for a vorticity-type auxiliary variable. The elimination can be performed in one of two basically different ways which respectively produce a pair of infinite and zero spurious eigenvalues. In the latter case, the eigenvalues can be shifted to any prescribed value by a simple modification of the second approach. The main advantage of this method is not only its simplicity but also applicability to more general problems with complicated boundary conditions. This means that it can be incorporated in all of the work that will be covered.

Chapter 2

Chebyshev Collocation Method

The problems in this project will be solved using a Chebyshev collocation method. For the purposes here, the Chebyshev polynomials will be the choice of orthogonal trial function, and the Chebyshev Gauss Lobatto points will be chosen as the points at which the solution will be approximated.

2.1 Chebyshev Polynomials

Chebyshev polynomials of the first kind, $T_n(x)$, are polynomials in x of degree n that are defined by the relation:

$$T_n(\cos\theta) = \cos n\theta, \tag{2.1}$$

where $x = \cos\theta$ [91, 92]. The range of x is obviously $[-1, 1]$. The boundary values are $T_n(1) = T_n(\cos 0) = \cos(n0) = 1$ and $T_n(-1) = T_n(\cos n\pi) = \cos(n\pi) = (-1)^n$.

There is a recurrence relation defined by

$$T_{n+1} = 2xT_n - T_{n-1}.$$

along with the initial conditions $T_0(x) = 1$ and $T_1(x) = x$. As shown in Fig (2.1), $T_n(x)$ can be an even or odd function.

When n is even, all the powers of x in the polynomial are even, and when n is odd, all the powers of x are odd. This implies that the function is even and odd as n is

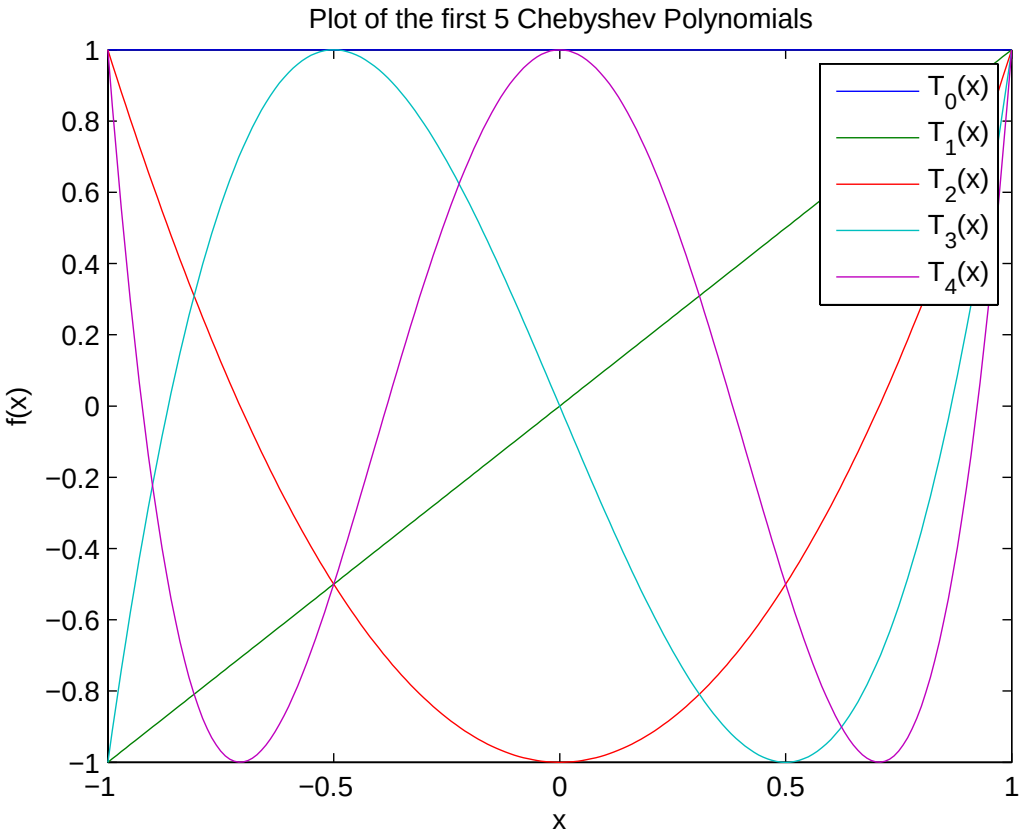

Figure 2.1: The first five Chebyshev polynomials, $T_n(x)$ over the range $-1 \leq x \leq 1$.

even and odd [92]:

$$T_n(-x) = \begin{cases} T_n(x), & n \text{ is even} \\ -T_n(x), & n \text{ is odd.} \end{cases} \tag{2.2}$$

$T_n(x)$ is a solution of the differential equation

$$\left(\sqrt{1-x^2}T_n'(x)\right)' + \frac{n^2}{\sqrt{1-x^2}}T_n(x) = 0,$$

which has been expressed in Sturm-Liouville form, with $p(x) = \sqrt{(1-x^2)}$, $q(x) = 0$ and the weight function, $w(x) = (1-x^2)^{-\frac{1}{2}}$ [77].

Consider two Chebyshev polynomials, $T_n(x)$ and $T_m(x)$, defined as in Eq. (2.1), and take the integral of their product:

$$\int_0^\pi T_n(\cos\theta)T_m(\cos\theta)d\theta = \int_0^\pi \cos(n\theta)\cos(m\theta)d\theta. \tag{2.3}$$

Substituting $\cos n\theta \cos m\theta = \frac{1}{2}\left[\cos((n+m)\theta + \cos((n-m)\theta)\right]$ into Eq. (2.3)

$$\begin{aligned} \frac{1}{2}\int_0^\pi \left(\cos(n+m)\theta + \cos(n-m)\theta\right)d\theta &= \frac{1}{2}\left[\frac{sin(n+m)\theta}{n+m} + \frac{\sin(n-m)\theta}{n-m}\right]_0^\pi \\ &= \begin{cases} 0 & m \neq n \\ \pi & m = n = 0 \\ \frac{\pi}{2} & m = n \neq 0 \end{cases} \end{aligned} \tag{2.4}$$

By differentiating $x = \cos\theta$ with respect to θ, giving $\frac{dx}{d\theta} = -\sqrt{1-x^2}$, a change of variable from θ to x can be performed on the left hand side of Eq. (2.3). Note that the limits change from π and 0 to -1 and 1 respectively. Combining this with Eq. (2.3) and Eq. (2.4) gives the orthogonality relation for the Chebyshvev polynomials:

$$\int_{-1}^1 \frac{T_n(x)T_m(x)}{\sqrt{1-x^2}}dx = \begin{cases} 0 & m \neq n \\ \pi & m = n = 0 \\ \frac{\pi}{2} & m = n \neq 0. \end{cases} \tag{2.5}$$

2.2 Lagrange Polynomials

Consider a function, $f(x)$, expressed in terms of the Lagrange polynomials:

$$f(x) = \sum_{i=0}^{N} f_i \psi_i(x), \tag{2.6}$$

where $f_i = f(x_i)$ and $\psi_i(x_j) = \delta_{ij}$. The Lagrange interpolant is then constructed as follows. Consider now the following polynomial:

$$\varphi_i^N(x) = \frac{\Pi_{j=0}^N (x - x_j)}{x - x_i} = \frac{P_N(x)}{x - x_i}, \tag{2.7}$$

which will be 0 for each of the collocation points except $x = x_i$. This means that it is zero everywhere, except for when $i = j$. When $i = j$, this gives $x = x_i$, and when this happens, Eq. (2.7) results in division by zero. This means that l'Hôpital's rule must be used to evaluate the expression. This results in the following:

$$\varphi_i^N(x_j) = \begin{cases} 0, & i \neq j \\ P_N'(x_i), & i = j. \end{cases} \tag{2.8}$$

Combining Eqs. (2.7) and (2.8) the following function can be defined:

$$\psi_i(x) = \frac{\varphi_N}{\varphi_N(x_i)} = \frac{P_N(x)}{(x - x_i)P_N'(x_i)}. \tag{2.9}$$

Equation (2.9) yields 1 at the point x_i and 0 at all other collocation points. This is a form of the expression for the Lagrange interpolant polynomial ([93, p. 49][77, p. 69]). Hereafter, Eq. (2.9) it will be referred to as the Lagrange polynomial. In this form it is expressed in terms of a polynomial $P_N(x)$, which has its roots at the collocation points. The Lagrange polynomial and its derivatives are not yet expressed in terms of Chebyshev polynomials; that will come in the next section. First, the first and second derivatives of the Lagrange polynomial must be found.

By differentiating Eq. (2.9) with respect to x and using the product rule, the

following equation is obtained:

$$\psi_i^{'}(x) = \frac{P_N^{'}(x)}{(x-x_i)P_N^{'}(x_i)} - \frac{P_N(x)}{(x-x_i)^2 P_N^{'}(x_i)}. \tag{2.10}$$

Equation (2.10) is now evaluated at the $n+1$ collocation points x_j, and with some simplification the following is derived:

$$\psi_i^{'}(x_j) = \begin{cases} \frac{P_N^{'}(x_j)}{(x_j-x_i)P_N^{'}(x_i)} & i \neq j \\ \frac{1}{2}\frac{P_N^{''}(x_j)}{P_N^{'}(x_i)} & i = j \end{cases} \tag{2.11}$$

In the next section, the polynomials $P_N(x)$ will be found in terms of Chebyshev polynomials, and evaluated, to give the equations for the differentiation matrices that will be used to write the MATLAB code.

By differentiating Eq. (2.11), using the product rule, and by some simplification the following relationship is found:

$$\psi_i^{''}(x) = -\frac{2P_N^{'}(x)}{(x-x_i)^2 P_N^{'}(x_i)} + \frac{P_N^{''}(x)}{(x-x_i)P_N^{'}(x_i)} + \frac{2P_N(x)}{(x-x_i)^3 P_N^{'}(x_i)} \tag{2.12}$$

Again, this Eq. (2.12) can be evaluated at x_j, and by using the relationships shown above, and further simplification:

$$\psi_i^{''}(x) = \begin{cases} \frac{1}{(x_j-x_i)P_N^i(x_i)}\left[P_N^{''}(x_j) - \frac{2P_N^{'}(x_j)}{x_j-x_i}\right] & ; i \neq j \\ \frac{1}{3}\frac{P_N^{'''}(x_j)}{P_N^{'}(x_i)} & ; i = j \end{cases} \tag{2.13}$$

In the next section, these Lagrange polynomials, and derivatives thereof, will be revisited once relationships between $P_N(x)$ and $T_N(x)$, the Chebyshev polynomials, have been established.

2.3 Chebyshev Gauss Lobatto collocation points

Suppose that the $n+1$ collocation points that were discussed in the previous subsection are the points $x_k = \cos\theta_k = \cos\left(\frac{\pi k}{N}\right)$, $k = 0, 1, \ldots, N$, which minimise and maximise $T_N(x)$, including the boundary points $x = \pm 1$. Consequently, these points are roots of $(1-x^2)T_N'(x)$, which can thus be chosen as $P_N(x)$.

Before continuing, it is worth mentioning that there are many different types of collocation points. These include Chebyshev-Gauss and Chebyshev-Gauss-Radau collocation points, but here only the Chebyshev-Gauss-Lobatto collocation points will be considered. This is standard practice, and Canuto et al. [77] only mentioned the other collocation points in passing, before using the Chebyshev Gauss Lobatto points for the main part, their points being defined as:

$$x_k^N = \cos\theta_k^N = \cos\left(\frac{k\pi}{N}\right); \qquad k = 0, \ldots, N. \tag{2.14}$$

If these points are then substituted into the original expression for the Chebyshev polynomials:

$$T_n(\cos\theta) = \cos n\theta, \tag{2.15}$$

then the result is the following expression:

$$T_N(\cos\theta_k^N) = \cos(k\pi) = (-1)^k. \tag{2.16}$$

It is necessary to show the equations for the first and second derivatives of Eq. (2.15):

$$T_N'(\cos\theta) = N\frac{\sin(N\theta)}{\sin\theta} \tag{2.17}$$

$$T_N''(\cos\theta) = -\frac{N}{\sin\theta}\left(\frac{N\cos(N\theta)}{\sin\theta} - \frac{\cos\theta\sin(N\theta)}{\sin^2\theta}\right) \tag{2.18}$$

Taking Eq. (2.17), the first derivative, and multiplying both sides by $\sin^2\theta$ gives:

$$\sin^2\theta T_N'\cos\theta = (1-x^2)T_N'(x) = N\sin\theta\sin(N\theta). \tag{2.19}$$

By then applying the same basic trigonometric formulae that have been used previously, the Eq. (2.19) can be rewritten as:

$$\begin{aligned} N\sin\theta\sin(N\theta) &= \frac{N}{2}\left[\cos((N-1)\theta) - \cos((N+1)\theta)\right] \\ &= \frac{N}{2}\left[T_{N-1}(x) - T_{N+1}(x)\right]. \end{aligned} \tag{2.20}$$

This allows the polynomial $P_N(x)$ to be expressed in terms of Chebyshev polynomials as:

$$P_N(x) = T_{N-1}(x) - T_{N+1}(x) = \frac{2}{N}(1-x^2)T_N^{'}(x). \tag{2.21}$$

Equation (2.21) is $P_N(x)$, and it is necessary to note that it is slightly different to how it was described in the first paragraph of this section, as it now has a factor of $2/N$.

The derivative of $P_N(x)$ is also required, so by differentiating Eq. (2.21) and then substituting using Eq. (2.17), yields:

$$\begin{aligned} P_N^{'}(x) &= T_{N-1}^{'}(x) - T_{N+1}^{'}(x) \\ &= (N-1)\frac{\sin((N-1)\theta)}{\sin\theta} - (N+1)\frac{\sin((N+1)\theta)}{\sin\theta}. \end{aligned} \tag{2.22}$$

Equation (2.22) can then be expanded by using the basic trigonometric rules once again, resulting in:

$$\begin{aligned} P_N^{'}(x) = (N-1)&\frac{\sin(N\theta)\cos\theta - \cos(N\theta)\sin\theta}{\sin\theta} \\ -(N+1)&\frac{\sin(N\theta)\cos\theta + \cos(N\theta)\sin\theta}{\sin\theta}. \end{aligned} \tag{2.23}$$

Having derived an expression for the derivative of the polynomial, $P_N^{'}(x)$, it is necessary to evaluate Eq. (2.23), at both the boundary points, $x = \pm 1$, and the internal collocation points, x_j. First consider the derivative of the polynomial at the boundary:

$$P_N^{'}(\pm 1) = (\pm 1)^N\left((N-1)^2 - (N+1)^2\right) = -(\pm 1)^N 4N. \tag{2.24}$$

Evaluating Eq. (2.23) at x_j yields:

$$P_N^{'}(x_j) = -(N-1)(-1)^j - (N+1)(-1)^j = (-1)^{j+1}2N. \tag{2.25}$$

The final expression for the derivative of the polynomial evaluated at x_j is:

$$P_N^{'}(x_j) = \bar{c_j}(-1)^{j+1}2N, \tag{2.26}$$

where $\bar{c}_j = 1$ for $j = 1 \ldots n-1$ and $\bar{c}_j = 2$ for $j = 0$ or N.

This means that the Lagrange polynomial, Eq. (2.9) from earlier, can now be re-written as:

$$\psi_i^N(x) = \frac{T_{N-1}(x) - T_{N+1}(x)}{(x - x_i)\bar{c}_i(-1)^{i+1}2N}. \tag{2.27}$$

However, because the Lagrange polynomial has already been differentiated, it is not necessary to differentiate Eq. (2.27) directly, but simply to derive equations that can be substituted into Eq. (2.10), which is the first derivative of the Lagrange polynomial.

We differentiate Eq. (2.22) this to get the second derivative of the polynomial, $P_N(x)$:

$$P_N^{''}(x) = T_{N-1}^{''}(x) - T_{N+1}^{''}(x). \tag{2.28}$$

In order to evaluate Eq. (2.28), it is necessary to return to Eq. (2.18), and multiply both sides by $\sin^2\theta$:

$$\sin^2\theta T_N^{''}(\cos\theta) = -N\sin\theta\left(\frac{N\cos(N\theta)}{\sin\theta} - \frac{\cos\theta\sin(N\theta)}{\sin^2\theta}\right). \tag{2.29}$$

Now, by simple algebraic manipulation, and substituting in Eqs. (2.15) and (2.17) it follows directly that from Eq. (2.29):

$$\begin{aligned} T_N^{''}(x) &= \frac{1}{1-x^2}\left[N^2 T_N(x) - xT_N^{'}(x)\right] \\ &= \frac{1}{1-\cos^2\theta}\left[N^2\cos(N\theta) - N\cos\theta\frac{\sin N\theta}{\sin\theta}\right]. \end{aligned} \tag{2.30}$$

Returning to the second derivative of the polynomial, Eq. (2.28), the result from Eq.

(2.30) can be substituted in to give:

$$\begin{aligned} P_N''(x) &= T_{N-1}''(x) - T_{N+1}''(x) \\ &= -\frac{1}{1-x^2}\left[(N-1)^2 T_{N-1}(x) - (N+1)^2 T_{N+1}(x)\right] \\ &\quad + \frac{1}{1-x^2}\left[x\left(T_{N-1}'(x) - T_{N+1}'(x)\right)\right] \\ &= -\frac{1}{1-x^2}\left[(N^2+1)P_N(x) - 2N(T_{N-1}(x) + T_{N+1}(x)) - xP_N'(x)\right] \\ &= -\frac{1}{1-x^2}\left[(N^2+1)^2 P_N(x) - 4NxT_N(x) - xP_N'(x)\right]. \end{aligned} \tag{2.31}$$

After the substitution has been made, Eq. (2.31) has been simplified and rearranged to give a more manageable form.

The second derivative of the polynomial, Eq. (2.31) is now evaluated at $x = \pm 1$ and x_j, as before for the first derivative. First, for x_j:

$$\begin{aligned} P_N''(x_j) &= +\frac{1}{1-x_j^2}\left[4Nx_j(-1)^j + x_j(-1)^j 2N\right] \\ &= \frac{2Nx_j}{1-x_j^2}(-1)^j. \end{aligned} \tag{2.32}$$

Now the second derivative needs to be evaluated at $x = \pm 1$, but first:

$$P_N''(x) = \left[(N^2+1)P_N'(x) - 4N(T_N(x) + xT_N'(x)) - P_N'(x) - xP_N''(x)\right] \tag{2.33}$$

So by using simple algebraic manipulation the final expression for $P_N''(\pm 1)$ can be derived as follows:

$$\begin{aligned} P_N''(\pm 1) &= \frac{\pm 1}{3}\left[N^2(-(\pm 1)^N 4N) - 4N\left((\pm 1)^N \pm (\pm 1)^{N+1}N^2\right)\right] \\ &= \pm\frac{1}{3}(\pm 1)^N\left[-4N^3 - 4N(1+N^2)\right] \\ &= -(\pm 1)^{N+1}\frac{4}{3}N(2N^2+1). \end{aligned} \tag{2.34}$$

This gives everything required to substitute into the first derivative of the Lagrange polynomial. When this is done, the following expression for the first derivative of the

Lagrange interpolant polynomial is found:

$$\psi_i^{'}(x_j) = \begin{cases} \frac{2N^2+1}{6} & ; j = 0 \\ \frac{c_j}{c_i}\frac{(-1)^{i+j}}{(x_j - x_i)} & ; i \neq j \\ -\frac{x_j}{2(1-x_j^2)} & ; 0 < i = j < N \\ -\frac{2N^2+1}{6} & ; j = N. \end{cases} \tag{2.35}$$

This is also the expression for the first differentiation matrix that is discussed in more depth in the next section. It will be used to write the MATLAB code that will enable the differential equations to be solved using the collocation method.

For now, it remains to derive the final equations for the second derivative of the Lagrange polynomial. This requires $P_N^{'''}(x)$ to be calculated. This is done by differentiating Eq. (2.31):

$$\begin{aligned} P_N^{'''}(x) &= \frac{2x}{1-x^2}P_N^{''}(x) \\ &\quad - \frac{1}{1-x^2}\left[(N^2+1)P_N^{'}(x) - 4N(T_N(x) + xT_N^{'}(x)) - P_N^{'}(x) - xP_N^{''}(x)\right] \\ &= \frac{3x}{1-x^2}P_N^{''}(x) - \frac{1}{1-x^2}\left[N^2P_N^{'}(x) - 4N\left(T_N(x) + xT_N^{'}(x)\right)\right]. \end{aligned} \tag{2.36}$$

Again, it is required that Eq. (2.36) is evaluated at x_j:

$$\begin{aligned} P_N^{'''}(x_j) &= \frac{3x_j}{1-x_j^2}\cdot\frac{2Nx_j}{1-x_j^2}(-1)^j - \frac{1}{1-x_j^2}\left[N^2(-1)^{j+1}2N - 4N(-1)^j\right] \\ &= \frac{x_j^2 6N}{(1-x_j^2)^2}(-1)^j + \frac{2N^3+4N}{1-x_j^2}(-1)^j \\ &= 2N(-1)^j\left[\frac{3x_j^2}{(1-x_j^2)^2} + \frac{N^2+2}{1-x_j^2}\right]. \end{aligned} \tag{2.37}$$

Before proceeding with $P_N^{'''}(x)$, it is necessary to evaluate $T_n^{''}(\pm 1)$:

$$T_N^{''}(\pm 1) = \pm\frac{1}{2}\left[-T_N^{'}(\pm 1) \mp T_N^{''}(\pm 1) + N^2T_N^{'}(\pm 1)\right]. \tag{2.38}$$

Substituting in Eqs. (2.17) and (2.30) allows $T_N''(\pm 1)$ to be evaluated:

$$\begin{aligned} T_N''(\pm 1) &= \pm\frac{1}{3}(N^2-1)N^2(\pm 1)^{N+1} \\ &= \frac{1}{3}(\pm 1)^N N^2(N^2-1). \end{aligned} \tag{2.39}$$

Finally, it is left to evaluate $P_N'''(\pm 1)$. First, it is required to simplify the Eq. (2.37) to give:

$$P_N'''(\pm 1) = \pm\frac{1}{2}\left[3P_N''(\pm 1) \pm 3P_N'''(\pm 1) - N^2 P_N''(\pm 1) + 4N\left(2T_N'(\pm 1) \pm T_N''(\pm 1)\right)\right] \tag{2.40}$$

Then it is left to perform the final algebraic manipulations:

$$\begin{aligned} P_N'''(\pm 1) &= \pm\frac{1}{2}\left[3P_N''(\pm 1) \pm 3P_N'''(\pm 1) - N^2 P_N''(\pm 1) + 4N\left(2T_N'(\pm 1) \pm T_N''(\pm 1)\right)\right] \\ &= \pm\frac{1}{2}\left[(N^3-3)P_N''(\pm 1) - 4N\left(2T_N'(\pm 1) \pm T_N''(\pm 1)\right)\right] \\ &= -\frac{(\pm 1)^N}{2} N\left[\frac{4}{3}(N^3-3)(2N^2+1) + 8N^2 + \frac{4}{3}N^2(N^2-1)\right] \\ &= -(\pm 1)^N 2N(N^4-1) \end{aligned} \tag{2.41}$$

Now, by substituting all of the derived equations into the formula for the second derivative of the Lagrange polynomial, Eq. (2.13) gives:

$$\psi_i''(x_j) = \begin{cases} \frac{(-1)^{i+j}}{\bar{c}_j}\frac{x_i^2+x_i x_j-2}{(1-x_j^2)(x_i-x_j)^2} & ;1 \le i \le N-1, 0 \le j \le N, i \ne j \\ -\frac{(N^2-1)(1-x_i^2)+3}{3(1-x_i^2)^2} & ;1 \le i = j \le N-1 \\ \frac{2}{3}\frac{(-1)^j}{\bar{c}_j}\frac{(2N^2+1)(1-x_j)-6}{(1-x_j)^2} & ;i = 0, 1 \le j \le N \\ \frac{2}{3}\frac{(-1)^{j+N}}{\bar{c}_j}\frac{(2N^2+1)(1+x_j)-6}{(1+x_j)^2} & ;i = N, 0 \le j \le N-1 \\ \frac{N^4-1}{15} & ;i = j = 0 \text{ and } i = j = N. \end{cases} \tag{2.42}$$

This is also the equation for the second differentiation matrix, and is used as the basis for writing the MATLAB code that is used in the Collocation method to solve differential equations.

Chapter 3

Avoiding spurious eigenmodes

In this chapter, a simple technique for avoiding physically spurious eigenmodes is introduced for the Chebyshev collocation method. This method is demonstrated on the solution of the Orr Sommerfeld equation for plane Poiseuille flow. The results obtained are used to confirm the accuracy of the method by comparing them to those of Orszag [17], who carried out a linear stability analysis of plane Poiseuille flow using a Chebyshev Tau numerical method.

3.1 Hydrodynamic stability problem

Consider a flow of an incompressible liquid with density ρ and kinematic viscosity ν. The flow is driven by a constant pressure gradient $\boldsymbol{\nabla} p_0 = -\boldsymbol{e}_x P_0$ in the gap between two parallel walls located at $z = \pm h$ in the Cartesian system of coordinates with the x and z axes directed streamwise and transverse to the walls, respectively (see Fig. 1.1).

The velocity distribution of $\boldsymbol{v}(\boldsymbol{r}, t)$ is governed by the Navier-Stokes equation

$$\partial_t \boldsymbol{v} + (\boldsymbol{v} \cdot \boldsymbol{\nabla})\boldsymbol{v} = -\rho^{-1}\boldsymbol{\nabla} p + \nu \boldsymbol{\nabla}^2 \boldsymbol{v} \tag{3.1}$$

and subject to the incompressibility constraint $\boldsymbol{\nabla} \cdot \boldsymbol{v} = 0$. Subsequently, all variables are non-dimensionalised by using h and h^2/ν as the length and time scales, respectively. Instead of the commonly used maximum flow velocity, the viscous diffusion speed ν/h

is employed as the characteristic velocity. This non-standard choice allows testing of the numerical method against the analytical eigenvalue solution for a quiescent liquid. Note that this scaling means the Reynolds number appears as a factor at the convective term as opposed to a reciprocal at the viscous term. The problem admits a rectilinear base flow

$$\boldsymbol{v}_0(z) = Re\bar{u}(z)\boldsymbol{e}_x \tag{3.2}$$

where $\bar{u}(z) = 1 - z^2$ is the parabolic velocity profile and $Re = U_0 h/\nu$ is the Reynolds number defined in terms of the maximum flow velocity $U_0 = 2P_0h^2/\rho\nu$. In dimensionless form, the Navier-Stokes equation (3.1) becomes

$$\partial_t \boldsymbol{v} + (\boldsymbol{v} \cdot \boldsymbol{\nabla})\, \boldsymbol{v} = -2Re\boldsymbol{\nabla}p + \boldsymbol{\nabla}^2\boldsymbol{v}. \tag{3.3}$$

In linear analysis, the effect of an infinitesimal perturbation on the base flow is considered. Non-linear terms are all neglected. Of particular interest is when a linear infinitesimal perturbation is introduced to the system, will it decay, persist with similar magnitude or grow. If it decays, the system is said to be stable, if the magnitude remains constant then the system is neutrally stable and if the perturbation grows enough so that the basic flow is changed to another laminar sate or a turbulent flow then the system is unstable. Note that for the disturbance to be considered linear, it must be sufficiently small that all nonlinear terms can be neglected. From Squire's theorem [104], it is known that parallel shear flows first become unstable to two-dimensional perturbations at a value of the Reynolds number that is smaller than any value for which unstable three-dimensional perturbations exist. At sufficiently high Re number, the base flow can become unstable with respect to infinitesimal perturbations $\boldsymbol{v}_1(\boldsymbol{r}, t)$, and as the base flow is invariant with respect to t and $\boldsymbol{x} = (x, y)$, the perturbation can be sought as

$$\boldsymbol{v}_1(\boldsymbol{r}, t) = \hat{\boldsymbol{v}}(z)\mathrm{e}^{\lambda t + \mathrm{i}\boldsymbol{k}\cdot\boldsymbol{x}} + \text{c.c.}, \tag{3.4}$$

where $\hat{\boldsymbol{v}}(z)$ is the complex amplitude distribution and λ is the complex temporal growth rate with the wave vector $\boldsymbol{k} = (\alpha, \beta)$.

The incompressibility constraint, which takes the form $\boldsymbol{D} \cdot \hat{\boldsymbol{v}} = 0$, where $\boldsymbol{D} \equiv \boldsymbol{e}_z \frac{d}{dz} + \mathrm{i}\boldsymbol{k}$ is a spectral counterpart of the nabla operator, is satisfied by expressing the component of the velocity perturbation in the direction of the wave vector as $\hat{u}_{\shortparallel} = \boldsymbol{e}_{\shortparallel} \cdot \hat{\boldsymbol{v}} = \mathrm{i}k^{-1}\hat{w}'$, where $\boldsymbol{e}_{\shortparallel} = \boldsymbol{k}/k$ and $k = |\boldsymbol{k}|$. Taking the *curl* of the linearised counterpart of Eq. (3.3) to eliminate the pressure gradient and then projecting it onto $\boldsymbol{e}_z \times \boldsymbol{e}_{\shortparallel}$, after some transformations we obtain the Orr-Sommerfeld equation

$$\lambda \boldsymbol{D}^2 \hat{w} = \boldsymbol{D}^4 \hat{w} + \mathrm{i}\alpha Re(\bar{u}'' - \bar{u}\boldsymbol{D}^2)\hat{w}, \tag{3.5}$$

which is written in a non-standard form corresponding to our choice of the characteristic velocity. Note that the growth rate λ differs by a factor Re from its standard definition. The same difference, in principle, applies also to the velocity perturbation amplitude which, however, is not important as long as only the linear stability is concerned. In this form, Eq. (3.5) admits a regular analytical solution at $Re = 0$, which is used as a benchmark for the numerical solution below.

The no-slip and impermeability boundary conditions require

$$\hat{w} = \hat{w}' = 0 \quad \text{at} \quad z = \pm 1. \tag{3.6}$$

Because three control parameters Re and (α, β) appear in Eq. (3.5) as only two combinations αRe and $\alpha^2 + \beta^2$, solutions for oblique modes with $\beta \neq 0$ are equivalent to the transverse ones with $\beta = 0$ and a larger α and, thus, a smaller Re which keeps both parameter combinations constant [3]. Therefore, it is sufficient to consider only the transverse perturbations ($k = \alpha$).

To avoid spurious eigenvalues in the discretised version of Eq. (3.5), it is necessary

to represent Eq. (3.5) as a system of two second order differential equations [23]

$$\lambda\hat{\zeta} = \boldsymbol{D}^2\hat{\zeta} + \mathrm{i}\alpha Re(\bar{u}''\hat{w} - \bar{u}\hat{\zeta}), \tag{3.7}$$

$$\hat{\zeta} = \boldsymbol{D}^2\hat{w}, \tag{3.8}$$

where $\hat{\zeta}$ is a vorticity-type auxiliary variable with no explicit boundary conditions. This system is solved using a Chebyshev collocation method.

3.2 Numerical Method

The problems will be solved numerically using a collocation method with $N+1$ Chebyshev-Gauss-Lobatto nodes

$$z_i = \cos\left(i\pi/N\right), \quad i = 0, \cdots, N. \tag{3.9}$$

at which the discretised solution $(\hat{w}, \hat{\zeta})(z_i) = (w_i, \zeta_i) = (\mathbf{w}, \boldsymbol{\zeta})$ and its derivatives are sought. The latter are expressed in terms of the former by using the so-called differentiation matrices, which for the first and second derivatives are denoted by $D^{(1)}_{i,j}$ and $D^{(2)}_{i,j}$ with explicit expressions given in Sec. (2.3). Requiring Eqs. (3.7,3.8) to be satisfied at the internal collocation points $0 < i < N$ and the boundary conditions (3.6) at the boundary points $i = 0, N$, the following system of $2N$ algebraic equations is obtained for the same number of unknowns

$$\lambda\boldsymbol{\zeta}_0 = \mathbf{A}\boldsymbol{\zeta}_0 + \mathbf{B}\boldsymbol{\zeta}_1 + \mathbf{g}_0, \tag{3.10}$$

$$\boldsymbol{\zeta}_0 = \mathbf{A}\mathbf{w}_0, \tag{3.11}$$

$$\tilde{0}_1 = \mathbf{C}\mathbf{w}_0, \tag{3.12}$$

where $\tilde{0}$ is the zero matrix and the subscripts 0 and 1 denote the parts of the solution at the inner and boundary collocation points, respectively; $\tilde{w}_1 = \tilde{0}_1$ due to the first

boundary condition (3.6) and

$$g_i = \mathrm{i}\alpha Re(\bar{u}_i'' w_i - \bar{u}_i \zeta_i). \tag{3.13}$$

The matrices

$$A_{i,j} = (\boldsymbol{D}^2)_{i,j}, \quad 0 < (i,j) < N, \tag{3.14}$$

$$B_{i,j} = (\boldsymbol{D}^2)_{i,j}, \quad 0 < i < N, j = 0, N, \tag{3.15}$$

represent the parts of the collocation approximation of the operator

$$(\boldsymbol{D}^2)_{i,j} = D^{(2)}_{i,j} - \alpha^2 I_{i,j} \tag{3.16}$$

using the inner and boundary points, respectively; $I_{i,j}$ is the unity matrix. Equation (3.12) is a discretised version of the second boundary condition (3.6) imposed on $\hat{w}'$ which is defined by the matrix

$$C_{ij} = D^{(1)}_{i,j}, \quad i = 0, N; 0 < j < N. \tag{3.17}$$

Our goal is to reduce Eqs. (3.10-3.12) to the standard matrix eigenvalue problem for $\hat{w}_0$. First, $\tilde{\zeta}_0$ is eliminated from Eq. (3.10) by using Eq. (3.11), which results in

$$\lambda \mathbf{A}\mathbf{w}_0 = \mathbf{A}^2\mathbf{w}_0 + \mathbf{B}\boldsymbol{\zeta}_1 + \mathbf{g}_0. \tag{3.18}$$

Next, we can use Eq. (3.12) to eliminate $\boldsymbol{\zeta}_1$ from the equation above. This, as shown in the next section, can be done in two basically different ways.

3.2.1 Elimination of the vorticity boundary values

Eliminating $\boldsymbol{\zeta}_1$ from Eq. (3.18) using Eq. (3.12) is achieved by employing a modified capacitance (or influence) matrix method. For the basics of this method, see [93, p. 178] and references therein. Modifications to the method are due to the structure of

the matrix eigenvalue problem which must be conserved in the elimination process. The general capacitance matrix approach suggests to express $\mathbf{w}_0$ from Eq. (3.18) and then to substitute it into Eq. (3.12), which then would result in a system of linear equations for $\boldsymbol{\zeta}_1$. However, as noted above, the elimination procedure must be linear in λ for the eigenvalue problem structure to be conserved. It means that $\mathbf{w}_0$ can be expressed either from the right or left hand side of Eq. (3.18) but not from the combination of both sides as in the standard capacitance matrix approach for the time stepping schemes.

The first approach is to express $\mathbf{w}_0$ from the r.h.s. of Eq. (3.18) by inverting $\mathbf{A}^2$ and then substituting it into the boundary condition (3.12), which results in

$$\mathbf{C}\mathbf{w}_0 = \mathbf{C}\mathbf{A}^{-2}(\lambda\mathbf{A}\mathbf{w}_0 - \mathbf{B}\boldsymbol{\zeta}_1 - \mathbf{g}_0) = \mathbf{0}_1. \tag{3.19}$$

Next, solving the equation above for

$$\boldsymbol{\zeta}_1 = (\mathbf{C}\mathbf{A}^{-2}\mathbf{B})^{-1}\mathbf{C}\mathbf{A}^{-2}(\lambda\mathbf{A}\mathbf{w}_0 - \mathbf{g}_0) \tag{3.20}$$

and substituting it into Eq. (3.18), obtaining

$$\lambda\mathbf{E}\mathbf{A}\mathbf{w}_0 = (\mathbf{A}^2 + \mathbf{E}\mathbf{G})\mathbf{w}_0, \tag{3.21}$$

where $\mathbf{G}\mathbf{w}_0 = \mathbf{g}_0$ and

$$\mathbf{E} = \mathbf{I} - \mathbf{B}(\mathbf{C}\mathbf{A}^{-2}\mathbf{B})^{-1}\mathbf{C}\mathbf{A}^{-2}. \tag{3.22}$$

It is important to notice that $\mathbf{E}\mathbf{B} = 0\mathbf{B}$, which means that $\mathbf{E}$ is singular. That is, it has a zero eigenvalue of multiplicity two corresponding to two eigenvectors represented by the columns of $\mathbf{B}$. By representing Eq. (3.21) as

$$(\mathbf{A}^2 + \mathbf{E}\mathbf{G})^{-1}\mathbf{E}\mathbf{A}\mathbf{w}_0 = \lambda^{-1}\mathbf{w}_0, \tag{3.23}$$

which is a standard eigenvalue problem for λ^{-1}, it is obvious that zero eigenvalues of

$\mathbf{E}$ result in two zero eigenvalues λ^{-1}, which in turn correspond to infinite eigenvalues λ of the original Eq. (3.21). A way to avoid these spurious eigenvalues is described below.

An alternative approach to eliminating $\boldsymbol{\zeta}_1$ is to express $\lambda\mathbf{w}_0$ from the l.h.s. of Eq. (3.18) by inverting $\mathbf{A}$ and then substituting it into the boundary condition (3.12), which results in

$$\lambda\mathbf{C}\mathbf{w}_0 = \mathbf{C}\mathbf{A}^{-1}(\mathbf{A}^2\mathbf{w}_0 + \mathbf{B}\boldsymbol{\zeta}_1 + \mathbf{g}_0) = \mathbf{0}_1. \tag{3.24}$$

This equation can be solved for $\tilde{\zeta}_1$ similarly to Eq. (3.19) as

$$\boldsymbol{\zeta}_1 = -(\mathbf{C}\mathbf{A}^{-1}\mathbf{B})^{-1}\mathbf{C}\mathbf{A}^{-1}(\mathbf{A}^2 + \mathbf{G})\mathbf{w}_0, \tag{3.25}$$

which substituted in Eq. (3.18) leads to

$$\lambda\mathbf{A}\mathbf{w}_0 = \mathbf{F}(\mathbf{A}^2 + \mathbf{G})\mathbf{w}_0, \tag{3.26}$$

where the transformation matrix

$$\mathbf{F} = \mathbf{I} - \mathbf{B}(\mathbf{C}\mathbf{A}^{-1}\mathbf{B})^{-1}\mathbf{C}\mathbf{A}^{-1} \tag{3.27}$$

is singular with two zero eigenvalues because it satisfies $\mathbf{F}\mathbf{B} = 0\mathbf{B}$ similarly to the $\mathbf{E}$ considered above. In contrast to the previous eigenvalue problem defined by Eq. (3.21), now the singular transformation matrix appears on the r.h.s. of Eq. (3.26) and thus it produces two zero rather than infinite eigenvalues λ.

It is important to notice that zero eigenvalues represent an alternative solution to Eq. (3.24), which can be satisfied not only by the boundary condition (3.12) but also by $\lambda = 0$. Consequently, these spurious eigenvalues can be shifted from zero to any value λ_0 by subtracting $\lambda_0\mathbf{C}\mathbf{w}_0$ from both sides of Eq. (3.24), which obviously does not affect the true eigenmodes satisfying Eq. (3.12). As a result, the equation for $\boldsymbol{\zeta}_1$ is obtained

$$\boldsymbol{\zeta}_1 = -(\mathbf{C}\mathbf{A}^{-1}\mathbf{B})^{-1}\mathbf{C}\mathbf{A}^{-1}(\mathbf{A}(\mathbf{A} - \lambda_0\mathbf{I}) + \mathbf{G})\mathbf{w}_0, \tag{3.28}$$

which when substituted in Eq. (3.18) leads to the following standard eigenvalue problem

$$\lambda \mathbf{w}_0 = (\mathbf{A}^{-1}\mathbf{F}(\mathbf{A}(\mathbf{A} - \lambda_0 \mathbf{I}) + \mathbf{G}) + \lambda_0 \mathbf{I})\mathbf{w}_0. \tag{3.29}$$

The complex matrix eigenvalue problems outlined above are solved using the LAPACK's ZGEEV routine [94].

3.3 Results

$N = 8$	$N = 16$	$N = 32$	Exact
5.4285×10^{16}	1.2597×10^{17}	3.5670×10^{16}	–
3.1699×10^{16}	-1.1600×10^{17}	-6.0842×10^{18}	–
-9.3120595	-9.3137399	-9.3137399	-9.3137399
-20.709030	-20.570571	-20.570571	-20.570571
-39.297828	-38.947806	-38.947789	-38.947789
-66.057825	-60.054233	-60.055435	-60.055435
-73.670710	-88.285123	-88.299997	-88.299997
	-119.43366	-119.27480	-119.27480
	-157.89593	-157.38866	-157.38866
	-199.64318	-198.23234	-198.23234
	-226.99053	-246.21576	-246.21576
	-384.38914	-296.92876	-296.92874
	-409.06660	-354.78191	-354.78176
	-961.90740	-415.36266	-415.36420
	-961.99676	-483.07721	-483.08684
		-553.58796	-553.53879
		-711.16464	-711.45255
		$\vdots$	$\vdots$

Table 3.1: The eigenvalues found numerically by solving Eq. (3.23) (method I) with various number of collocation points N for $\alpha = 1$ and $Re = 0$. The exact eigenvalues values are the roots of the characteristic equation resulting from analytical solution of Eq. (3.5) for $Re = 0$.

To validate the method developed, start by setting $Re = 0$ for which Eq. (3.5) can easily be solved analytically leading to the characteristic equation

$$\frac{\tanh(k)}{\tan(\sqrt{k^2 - \lambda})} = \pm \left(\frac{k}{\sqrt{k^2 - \lambda}} \right)^{\pm 1}, \tag{3.30}$$

which defines two branches of eigenvalues λ for the even and odd modes corresponding

to the plus and minus signs in the above expression. The eigenvalues resulting from Eq. (3.23), which represents the first approach, are shown in Table 3.1 for various numbers of collocation points along with the exact solution defined by Eq. (3.30). As can be seen, this approach produces a couple of very large physically spurious eigenvalues, which are due to the singularity of the transformation matrix $\mathbf{E}$ (3.22) pointed out above. At the same time, the numerical solution accurately reproduces the leading eigenvalues of the exact solution. The accuracy, however, decreases down the spectrum so that only a half of the exact eigenvalues are reproduced by the numerical solution. The other half are numerically spurious eigenvalues which are due to the discretization of the problem [82]. Increasing the number of collocation points will yield a larger number of accurate eigenvalues, but half will still be numerically spurious.

The second approach, defined by Eq. (3.26), produces exactly the same eigenvalues as the first one for the given N except for the two spurious eigenvalues which are now machine-size zeroes rather than infinities. Using the modification of the second approach defined by Eq. (3.29), these zero eigenvalues can be shifted to any prescribed value λ_0 without affecting other eigenvalues. Further, by using $\lambda_0 = 4(N/4)^4$ the two physically spurious eigenvalues are shifted to the region of numerically spurious eigenvalues located in the lower part of spectrum. The variation of the five leading eigenvalues with the number of collocation points N plotted in Fig. 3.1 shows an exponential convergence rate characteristic for the spectral numerical methods [77].

Next, the solution of Eq. (3.29) is considered for $Re = 10^4$ and $\alpha = 1$, which is a standard test case for the linear stability analysis of plane Poiseuille flow. The leading eigenvalue for this case is shown in table 3.2 in terms of the commonly used phase velocity $c = -\mathrm{i}\lambda/Rek$. For $N \gtrsim 60$ the solution is seen to converge to the reference value obtained in [17] using a tau method with $M \gtrsim 30$ even Chebyshev polynomials. As seen in Fig. 3.1, however the convergence rate for $Re = 10^4$ is somewhat slower than for $Re = 0$, it is still exponential with the final accuracy comparable to the previous case.

The number of collocation points can be reduced by a half by considering even and

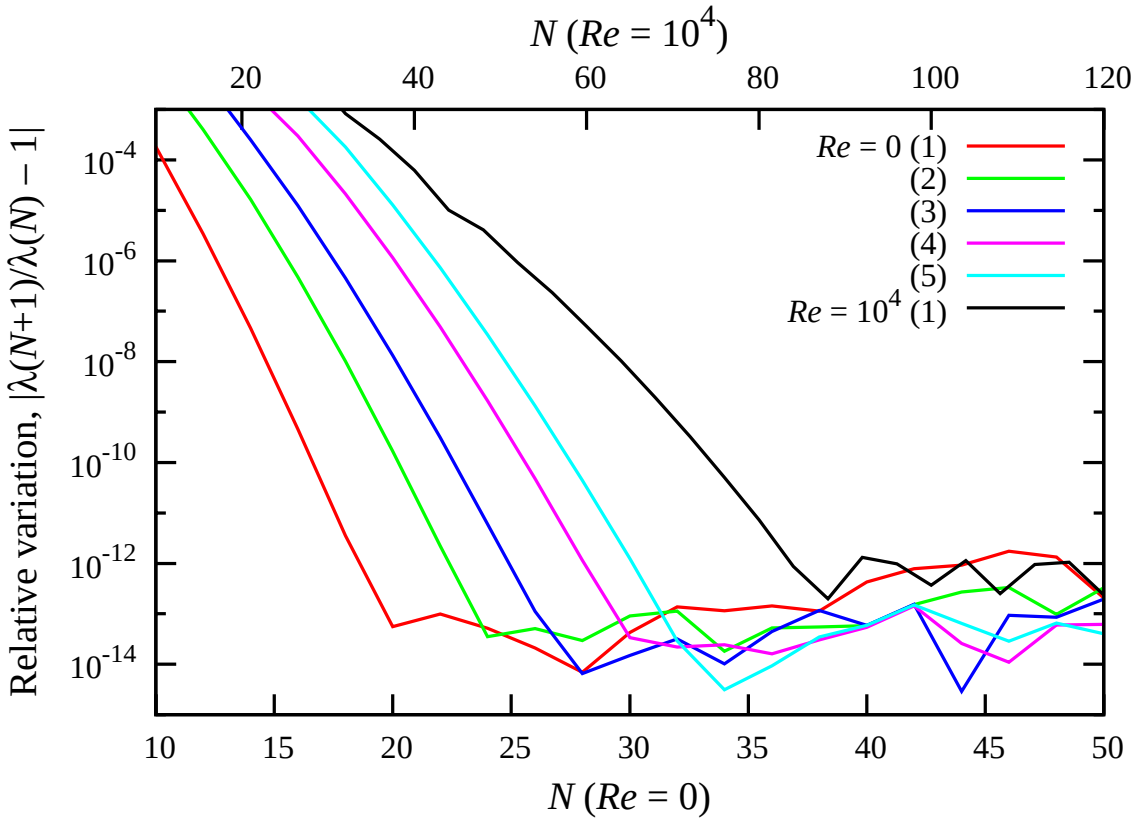

Figure 3.1: Relative variation of leading eigenvalues with the number of collocation points N for $\alpha = 1$, $Re = 0$ and $Re = 10^4$.

odd modes separately as done in [17]. Here, this would require substitution of differentiation matrices (2.41,2.42) for general functions with their half-size counterparts for even and odd functions.

N	c
16	(0.23272286, 0.00922887)
20	(0.23814366, 0.00566303)
24	(0.23842504, 0.00282919)
28	(0.23735182, 0.00357013)
32	(0.23747200, 0.00372519)
36	(0.23752527, 0.00375400)
40	(0.23752494, 0.00373917)
44	(0.23752716, 0.00374012)
48	(0.23752633, 0.00373961)
52	(0.23752653, 0.00373969)
56	(0.23752648, 0.00373967)
60	(0.23752649, 0.00373967)
64	(0.23752649, 0.00373967)

Table 3.2: Phase velocity $c = -\mathrm{i}\lambda/(Rek)$ of the most unstable mode depending on the number of collocation points N for $\alpha = 1$ and $Re = 10^4$.

Chapter 4

Weakly nonlinear analysis

In linear stability analysis the eigenvalues are independent of the amplitude of the disturbance, which is predicted to decay or grow exponentially. The linear stability analysis finds the marginal values of Reynolds number depending on the wave number α for which neutrally stable perturbations defined by zero growth are possible. The lowest value, the so-called critical Reynolds number, Re_l, and the corresponding critical wavenumber α_l give the starting point for weakly non-linear stability analysis. For $Re > Re_l$, linear stability theory predicts exponentially growing perturbations. Evolution of these unstable perturbations depends on the nonlinear effects. Depending on whether these inhibit or enhance the growth rate, then there will be either a super- or subcritical instability respectively.

4.1 Formulation of problem

Consider a flow of incompressible liquid with density ρ and kinematic viscosity ν driven by a constant pressure gradient $\boldsymbol{\nabla} p_0 = -\boldsymbol{e}_x P_0$ in the gap between two parallel walls located $z = \pm h$ in Cartesian system of coordinates with the x and z axes directed streamwise and transverse to the walls, respectively. The velocity distribution $\boldsymbol{v}(\boldsymbol{r}, t)$ is governed by the Navier-Stokes equation

$$\partial_t \boldsymbol{v} + (\boldsymbol{v} \cdot \boldsymbol{\nabla})\boldsymbol{v} = -\rho^{-1}\boldsymbol{\nabla} p + \nu \boldsymbol{\nabla}^2 \boldsymbol{v} \tag{4.1}$$

and is subject to the incompressibility constraint $\boldsymbol{\nabla} \cdot \boldsymbol{v} = 0$. Subsequently, all variables are non-dimensionalised by using h and h^2/ν as the length and time scales, respectively. In order to simplify the expressions of Landau coefficients obtained in the following, the viscous diffusion speed ν/h is employed as the characteristic velocity instead of the commonly used maximum flow velocity. Due to this non-standard scaling Reynolds number appears as a factor at the convective term rather reciprocal at the viscous term. The problem admits a rectilinear base flow

$$\boldsymbol{v}_0(z) = Re\bar{u}(z)\boldsymbol{e}_x, \tag{4.2}$$

where $\bar{u}(z) = 1 - z^2$ is the parabolic velocity profile and $Re = U_0 h/\nu$ is Reynolds number defined in terms of the center-line velocity $U_0 = 2P_0h^2/\rho\nu$. At sufficiently high Re, this base flow can become unstable with respect to infinitesimal perturbations $\boldsymbol{v}_1(\boldsymbol{r}, t)$, which due to the invariance of the base flow in both t and $\boldsymbol{x} = (x, y)$ can be sought as

$$\boldsymbol{v}_1(\boldsymbol{r}, t) = \hat{\boldsymbol{v}}_1(z)\mathrm{e}^{\lambda t + \mathrm{i}\boldsymbol{k}\cdot\boldsymbol{x}} + \text{c.c.}, \tag{4.3}$$

where λ is complex temporal growth rate for the Fourier mode defined by the wave vector $\boldsymbol{k} = (\alpha, \beta)$ and complex amplitude distribution $\hat{\boldsymbol{v}}_1(z)$. The linear stability analysis finds marginal values of Re depending on $\boldsymbol{k}$ for which neutrally stable perturbations defined by $\Re[\lambda] = 0$ are possible. The lowest marginal value of Re, referred to as the critical Reynolds number, for this flow is known to be $Re_l = 5772.22$ and it is attained at the critical wave vector $\boldsymbol{k}_l = (1.02055, 0)$, [17] which corresponds to purely transversal perturbations defined by $\beta = 0$. For $Re > Re_l$ the linear stability theory predicts exponentially growing perturbations. Evolution of these unstable perturbations depends on the non-linear effects which may either inhibit or enhance the growth rate leading to what is known as super- and sub-critical instabilities, respectively. In the first case, instability is expected to saturate at $Re > Re_l$, while in the second case instability can be triggered by sufficiently large finite amplitude perturbations at sub-critical Reynolds numbers. In the latter case, unstable equilibrium states are possible

at $Re < Re_l$.

4.2 Two-dimensional equilibrium states

In order to identify the type of instability, the approach of Reynolds and Potter,[43] is followed, which is known as the method of "false problems" [95, 45]. One searches for equilibrium solutions in the vicinity of the linear stability threshold Re_l using the following considerations. The neutrally stable mode (4.3) with purely real frequency $\omega = -\mathrm{i}\lambda$ interacts with itself through the quadratically nonlinear term in Eq. (4.1) to produce a streamwise-invariant and steady perturbation of the mean flow, and a second harmonic $\sim \mathrm{e}^{2\mathrm{i}(\omega t+\alpha x)}$, which varies as with double frequency of the fundamental mode. Further nonlinear interactions produce higher harmonics, which similarly to the fundamental and second harmonic travel synchronously with the same phase velocity $c = -\omega/\alpha$. Thus, the equilibrium solution represents a travelling wave of the form

$$\boldsymbol{v}(\boldsymbol{r},t) = \sum_{n=-\infty}^{\infty} E^n \hat{\boldsymbol{v}}_n(z), \tag{4.4}$$

where $E = \mathrm{e}^{\mathrm{i}(\omega t+\alpha x)}$ contains ω which, in general, needs to determined together with $\hat{\boldsymbol{v}}_n$ by solving a non-linear eigenvalue problem. The reality of solution requires $\hat{\boldsymbol{v}}_{-n} = \hat{\boldsymbol{v}}_n^*$, where the asterisk stands for the complex conjugate. The incompressibility constraint for the nth velocity harmonic can be written concisely as $\boldsymbol{D}_n \cdot \hat{\boldsymbol{v}}_n = 0$ by using the operator $\boldsymbol{D}_n \equiv \boldsymbol{e}_z \frac{d}{dz} + \mathrm{i}\boldsymbol{e}_x \alpha_n$ with $\alpha_n = \alpha n$, which is a spectral counterpart of the nabla operator for the respective harmonic. This constraint is satisfied by expressing the streamwise component of the velocity perturbation as

$$\hat{u}_n = \boldsymbol{e}_x \cdot \hat{\boldsymbol{v}}_n = \mathrm{i}\alpha_n^{-1}\hat{w}_n' \tag{4.5}$$

in terms of the transverse velocity component $\hat{w}_n = \boldsymbol{e}_z \cdot \hat{\boldsymbol{v}}_n$, which is employed instead of the commonly used stream function. Note that this equation is not applicable to the zeroth harmonic $n = 0$, which thus needs to be considered separately. Taking the

curl of Eq. (4.1) to eliminate the pressure gradient and then projecting it onto $\boldsymbol{e}_y$, then after some transformations the following equation is obtained

$$[\boldsymbol{D}_n^2 - \mathrm{i}\omega n]\hat{\zeta}_n = \hat{h}_n, \tag{4.6}$$

where

$$\hat{\zeta}_n = \boldsymbol{e}_y \cdot \boldsymbol{D}_n \times \hat{\boldsymbol{v}}_n = \begin{cases} \mathrm{i}\alpha_n^{-1}\boldsymbol{D}_n^2\hat{w}_n, & n \neq 0; \\ \hat{u}_0', & n = 0. \end{cases} \tag{4.7}$$

and

$$\hat{h}_n = \sum_m \hat{\boldsymbol{v}}_{n-m} \cdot \boldsymbol{D}_m\hat{\zeta}_m \tag{4.8}$$

are the y-components of the nth harmonic of the vorticity $\boldsymbol{\zeta} = \boldsymbol{\nabla} \times \boldsymbol{v}$ and that of the *curl* of the non-linear term $\boldsymbol{h} = \boldsymbol{\nabla} \times (\boldsymbol{v} \cdot \boldsymbol{\nabla})\boldsymbol{v}$. By separating the terms involving $\hat{u}_0$ in the sum (4.8), it can be rewritten as $\hat{h}_n = \mathrm{i}\alpha_n^{-1}(\hat{h}_n^w + \hat{h}_n^u)$, where

$$\hat{h}_n^w = n\sum_{m\neq 0} m^{-1}(\hat{w}_{n-m}\boldsymbol{D}_n^2\hat{w}_n' - \hat{w}_m'\boldsymbol{D}_{n-m}^2\hat{w}_{n-m}), \tag{4.9}$$

$$\hat{h}_n^u = \mathrm{i}\alpha_n[\hat{u}_0 - \hat{u}_0''\boldsymbol{D}_n^2]\hat{w}_n = \mathcal{N}_n(\hat{u}_0)\hat{w}_n. \tag{4.10}$$

Eventually, using the expressions above, Eq. (4.6) can be written concisely as

$$\mathcal{L}_n(\mathrm{i}\omega, \hat{u}_0)\hat{w}_n = \hat{h}_n^w, \tag{4.11}$$

where

$$\mathcal{L}_n(\mathrm{i}\omega, \hat{u}_0) = [\boldsymbol{D}_n^2 - \mathrm{i}\omega n]\boldsymbol{D}_n^2 - \mathcal{N}_n(\hat{u}_0). \tag{4.12}$$

This equation governs all of the harmonics except the zeroth one, for which it implies that $\hat{w}_0 \equiv 0$ in accordance with the incompressibility constraint (4.5). The equation governing the zeroth velocity harmonic, which only has the streamwise component $\hat{u}_0$, follows directly from the x-component of Navier-Stokes equation (4.1):

$$\hat{u}_0'' = -\hat{P}_0 + \hat{g}_0, \tag{4.13}$$

where $\hat{P}_0$ is a dimensionless applied pressure gradient and

$$\hat{g}_0 = \mathrm{i} \sum_{m \neq 0} \alpha_m^{-1} \hat{w}_m^* \hat{w}_m'' \tag{4.14}$$

is the x-component of the zeroth harmonic of the nonlinear term $\boldsymbol{g} = (\boldsymbol{v} \cdot \boldsymbol{\nabla})\boldsymbol{v}$. The velocity harmonics are subject to the no-slip and impermeability boundary conditions

$$\hat{w}_n = \hat{w}_n' = \hat{u}_0 = 0 \text{ at } z = \pm 1. \tag{4.15}$$

4.3 Amplitude expansion

The equations obtained in Sec. 4.2 govern the equilibrium states of two-dimensional travelling waves which have an arbitrary amplitude. In the vicinity of the linear stability threshold, which represents the main interest here, the problem can be simplified by expansion as a small perturbation amplitude. As discussed previously, the basic harmonic (4.3) with a small amplitude $O(\epsilon)$ interacting with itself through the quadratically non-linear term in Eq. (4.1) produces a zeroth harmonic, which modifies the mean flow, and the second harmonic, both with amplitude $O(\epsilon^2)$. Further, these two harmonics interacting with the basic one produces a $O(\epsilon^3)$ correction to the latter. The interaction of the second and basic harmonics also produces a third harmonic with amplitude $O(\epsilon^3)$. This perturbation series is represented by the following expansion:

$$\hat{w}_n = \sum_{m=0}^{\infty} \epsilon^{|n|+2m} \tilde{A}^{|n|} |\tilde{A}|^{2m} \hat{w}_{n,|n|+2m}, \tag{4.16}$$

where $\epsilon\tilde{A} = A$ is an equilibrium amplitude of the first harmonic to be found and $\tilde{A} = O(1)$ is its normalized counterpart. The mean flow, which as mentioned needs to be considered separately, is correspondingly expanded as

$$\hat{u}_0 = \hat{u}_{0,0} + \epsilon^2 |\tilde{A}|^2 \hat{u}_{0,2} + \dots. \tag{4.17}$$

In a similar way, we expand also Reynolds number and the frequency

$$Re = Re_0 + \epsilon^2 \tilde{Re}_2 + \ldots, \tag{4.18}$$

$$\omega = \omega_0 + \epsilon^2 \tilde{\omega}_2 + \ldots, \tag{4.19}$$

where Re_0 is the marginal Reynolds number satisfying $\Re[\lambda_0] = 0$ and $\omega_0 = \Im[\lambda_0]$ for the mode $\hat{w}_{1,1}$ with the wavenumber α; $\epsilon^2 \tilde{Re}_2 = Re_2$ is the deviation of the Reynolds number from its marginal value and $\epsilon^2 \tilde{\omega}_2 = \omega_2$ is the associated frequency deviation. Substituting these expansions into Eqs. (4.11) and (4.13), and collecting the terms at equal powers of ϵ, the following equations are obtained. At $O(\epsilon^0)$ the equation for the base flow is

$$\hat{u}''_{0,0} = -P_{0,0}, \tag{4.20}$$

where $P_{0,0} = 2Re_0$ and $\hat{u}_{0,0} = Re_0(1 - z^2) = Re_0 \bar{u}(z)$. At $O(\epsilon)$

$$\mathcal{L}_1(\mathrm{i}\omega_0, \hat{u}_{0,0})\hat{w}_{1,1} = 0, \tag{4.21}$$

which is the Orr-Sommerfeld equation defining the linear stability threshold. The solution of this eigenvalue problem for a given wavenumber α yields the marginal Reynolds number Re_0, the frequency ω_0, and the eigenfunction $\hat{w}_{1,1}(z)$. The latter is defined up to an arbitrary factor, which for $\hat{w}_{1,1}(z)$ being an even function is fixed by the standard normalization condition

$$\hat{w}_{1,1}(0) = 1. \tag{4.22}$$

At $O(\epsilon^2)$, two equations are obtained

$$\hat{u}''_{0,2} = -P_{0,2} - 2\alpha^{-1}\Im[\hat{w}^*_{1,1}\hat{w}''_{1,1}], \tag{4.23}$$

$$\mathcal{L}_2(\mathrm{i}\omega_0, \hat{u}_{0,0})\hat{w}_{2,2} = 2[(\hat{w}_{1,1}\hat{w}'_{1,1})' - 2\hat{w}'^2_{1,1}]', \tag{4.24}$$

which define the mean-flow perturbation $\hat{u}_{0,2}$ and the second harmonic $\hat{w}_{2,2}$ in terms of $\hat{w}_{1,1}(z)$ found previous. The mean-flow perturbation depends also on the perturbation of the mean pressure gradient $P_{0,2}$, which is zero when the flow is driven by a fixed pressure difference. Alternatively, if it is the flow rate rather than the pressure difference which is fixed, then $P_{0,2}$ is an additional unknown which has be determined so that to satisfy the flow-rate conservation constraint $\int_{-1}^{1} \hat{u}_{0,2}(z)\, dz = 0$. Start with the case of fixed mean pressure gradient, $P_{0,2} = 0$. The latter case can readily be reduced to the former by including $P_{0,2}$ into Re_2 as shown in the next section. To complete the solution, proceed to the order $O(\epsilon^3)$, which yields

$$\mathcal{L}_1(\mathrm{i}\omega_0, \hat{u}_{0,0})\hat{w}_{1,3} = \hat{h}^w_{1,3} + |A|^{-2}[\mathcal{N}_1(Re_2\bar{u} + |A|^2\hat{u}_{0,2}) + \mathrm{i}\omega_2 \boldsymbol{D}_1^2]\hat{w}_{1,1}, \tag{4.25}$$

where

$$\hat{h}^w_{1,3} = \frac{1}{2}\left(\hat{w}^*_{1,1}\boldsymbol{D}_2^2\hat{w}'_{2,2} - \hat{w}'_{2,2}\boldsymbol{D}_1^2\hat{w}^*_{1,1}\right) - \left(\hat{w}_{2,2}\boldsymbol{D}_1^2\hat{w}'^*_{1,1} - \hat{w}'^*_{1,1}\boldsymbol{D}_2^2\hat{w}_{2,2}\right). \tag{4.26}$$

This equation defines the correction of the basic harmonic $\hat{w}_{1,3}$ in terms of the previously found quantities. It is important to notice that the l.h.s. operator of this equation is the same as that of the Orr-Sommerfeld equation (4.21), which has $\hat{w}_{1,1}$ as an eigenfunction with zero eigenvalue. Thus, for Eq. (4.25) to be solvable its r.h.s. has to be orthogonal to the adjoint eigenfunction $\hat{w}^+_{1,1}$:

$$\left\langle \hat{w}^+_{1,1}, \hat{h}^w_{1,3} + |A|^{-2}[\mathcal{N}_1(Re_2\bar{u} + |A|^2\hat{u}_{0,2}) + \mathrm{i}\omega_2 \boldsymbol{D}_1^2]\hat{w}_{1,1} \right\rangle = 0, \tag{4.27}$$

where the angle brackets denote the inner product [4]. The above solvability condition yields

$$\mathrm{i}\omega_2 = \mu_1 Re_2 + \mu_2|A|^2, \tag{4.28}$$

where

$$\mu_1 = - \left\langle \hat{w}^+_{1,1}, \mathcal{N}_1(\bar{u}) \right\rangle, \tag{4.29}$$

$$\mu_2 = - \left\langle \hat{w}^+_{1,1}, \mathcal{N}_1(\hat{u}_{0,2}) + \hat{h}^w_{1,3} \right\rangle \tag{4.30}$$

for the adjoint eigenfunction normalized as $\left\langle \hat{w}^+_{1,1}, \boldsymbol{D}_1^2 \hat{w}_{1,1} \right\rangle = 1$. The expression above represents a reduced Landau equation for the case of equilibrium solution, which requires ω_2 to be real. This reality condition yields the sought after equilibrium amplitude

$$|A|^2 = -Re_2 \Re[\mu_1] / \Re[\mu_2], \tag{4.31}$$

which is the same as that resulting from the full Landau equation with the first Landau coefficient μ_2 and the linear growth rate correction $\mu_1 Re_2$ [4]. Note that the non-standard choice of the characteristic velocity results in expressions (4.29) and (4.30) sharing the operator $\mathcal{N}_1$, which simplifies their numerical treatment.

The type of instability is determined by the sign of $\Re[\mu_2]$. For the instability to be supercritical, which supposes an equilibrium solution with $|A|^2 > 0$ to exist at positive linear growth rates $Re_2 \Re[\mu_1] > 0$, $\Re[\mu_2] < 0$ is required. Otherwise, the instability is subcritical. In order to calculate Landau coefficients (4.29) and (4.30) following the standard approach outlined above one needs to solve not only the Orr-Sommerfeld equation (4.21) but also its adjoint problem which defines $\hat{w}^+_{1,1}$. Both problems, the direct and the adjoint, as well as those posed by Eqs. (4.23) and (4.24) need to be solved numerically. Then the integrals behind the inner products defining μ_1 and μ_2 need to be evaluated numerically. This standard approach can be significantly simplified by avoiding both the solution of the adjoint problem and the subsequent approximate evolution of the inner product integrals. This is achieved by applying the solvability condition to the discretized numerical problem as demonstrated in the following section.

4.4 Numerical method

In this section, the numerical evaluation of Landau coefficients is demonstrated using a Chebyshev collocation method with Chebyshev-Lobatto nodes

$$z_i = \cos\left(i\pi/N\right), \quad i = 0, \cdots, N, \tag{4.32}$$

at which the discretized solution $(\hat{w}_n, \hat{u}_0)(z_i) = (\mathbf{w}_n, \mathbf{u}_0)_i$ and its derivatives are sought. The latter are expressed in terms of the former by using the so-called differentiation matrices which for the first and second derivatives are denoted by $D^{(1)}_{i,j}$ and $D^{(2)}_{i,j}$. Explicit expressions for these matrices can be found in the Sec. (2.3) and Peyret [93]. Equations (4.21), (4.23) and (4.24) are approximated at the internal collocation points $0 < i < N$ and the boundary conditions (4.15) are imposed at the boundary points $i = 0, N$. The operator $\mathcal{L}_n(\mathrm{i}\omega_0, \hat{u}_{0,0})$ defined by Eq. (4.12), which appears in Eqs. (4.21) and (4.24) is represented by the matrix $\mathbf{L}_n(\mathrm{i}\omega_0, \mathbf{u}_{0,0}) = \mathbf{M}_n(\mathbf{u}_{0,0}) - \mathrm{i}\omega_0\mathbf{A}_n$ consisting of

$$\mathbf{M}_n(\mathbf{u}_{0,0}) = \mathbf{F}_n[\mathbf{A}_n^2 + Re_0\mathbf{N}_n(\bar{\mathbf{u}})], \tag{4.33}$$

$$(\mathbf{A}_n)_{i,j} = (\boldsymbol{D}_n^2)_{i,j}, \quad 0 < (i,j) < N, \tag{4.34}$$

where the latter represents the part of the collocation approximation of the operator

$$(\boldsymbol{D}_n^2)_{i,j} = D^{(2)}_{i,j} - \alpha_n^2\delta_{i,j} \tag{4.35}$$

related with the internal nodes. The other matrix in Eq. (4.33), defined as

$$(\mathbf{N}_n(\bar{\mathbf{u}}))_{i,j} = \mathrm{i}\alpha_n[\bar{u}_i\delta_{i,j} - \bar{u}_i''(\mathbf{A}_n)_{i,j}], \tag{4.36}$$

represents the collocation approximation of the operator defined by Eq. (4.10). Finally, the factor matrix

$$\mathbf{F}_n = \mathbf{I} - \mathbf{B}_n(\mathbf{C}\mathbf{A}_n^{-1}\mathbf{B}_n)^{-1}\mathbf{C}\mathbf{A}_n^{-1} \tag{4.37}$$

in Eq. (4.33) ensures the no-slip boundary condition $\hat{w}'(\pm 1) = 0$, which is represented by the matrix

$$C_{ij} = D^{(1)}_{i,j}, \quad i = 0, N; 0 < j < N \tag{4.38}$$

and also involves the part of the operator (4.35) related with the boundary nodes:

$$(\mathbf{B}_n)_{i,j} = (\boldsymbol{D}^2_n)_{i,j}, \quad 0 < i < N, j = 0, N. \tag{4.39}$$

Further details concerning Eq. (4.36) can be found in Sec. (3.2) and [90].

Starting with the Orr-Sommerfeld equation, whose collocation approximation is

$$\mathbf{L}_1(\lambda, Re\bar{\mathbf{u}})\mathbf{w}_{1,1} = [\mathbf{M}_1(Re\bar{\mathbf{u}}) - \lambda\mathbf{A}_1]\mathbf{w}_{1,1} = \mathbf{0} \tag{4.40}$$

can be reduced to the standard complex matrix eigenvalue problem

$$\mathbf{A}_1^{-1}\mathbf{L}_1(\lambda, Re\bar{\mathbf{u}})\mathbf{w}_{1,1} = [\mathbf{A}_1^{-1}\mathbf{M}_1(Re\bar{\mathbf{u}}) - \lambda\mathbf{I}]\mathbf{w}_{1,1} = \mathbf{0}, \tag{4.41}$$

which can be solved using, for example, LAPACK's ZGEEV routine [94].

4.5 Results

The marginal Reynolds number Re_0 for a given wavenumber α is determined by the condition $\Re[\lambda_0] = 0$ for the eigenvalue λ_0 with the largest real part. Simultaneously with the right eigenvector $\mathbf{w}_{1,1}$, we find also the associated left eigenvector $\mathbf{w}^\dagger_{1,1}$[103]. The right eigenvector is normalized using condition (4.22) and the left one is normalized against the former using the dot product of complex vectors $\mathbf{w}^\dagger_{1,1} \cdot \mathbf{w}_{1,1} = 1$. This normalization simplifies the expressions of Landau coefficients obtained in the following. Having found $\mathbf{w}_{1,1}$, it can be straightforwardly used to solve the discretized counterparts of Eqs. (4.23) and (4.24), which yield the mean-flow perturbation $\mathbf{u}_{0,2}$ and the complex amplitude distribution of the second harmonic $\mathbf{w}_{2,2}$. For the case of fixed flow rate considered later, the stream function of the mean-flow perturbation

$_{0,2}$ is needed. This is obtained by solving the collocation approximation of $\hat{\psi}'_{0,2} = \hat{u}_{0,2}$ with the symmetry condition $\hat{\psi}_{0,2}(0) = 0$.

Now, the final equation (4.25) can be solved, whose collocation approximation can be written similarly to Eq. (4.40) as

$$\mathbf{L}_1(\mathrm{i}\omega_0, Re_0\bar{\mathbf{u}})\mathbf{w}_{1,3} = \mathbf{F}_1\mathbf{h}^w_{1,3} + |A|^{-2}[\mathbf{F}_1\mathbf{N}_1(Re_2\bar{\mathbf{u}} + |A|^2\mathbf{u}_{0,2}) + \mathrm{i}\omega_2\mathbf{A}_1]\mathbf{w}_{1,1}, \tag{4.42}$$

which represents a matrix eigenvalue perturbation problem. For this equation to be solvable, its r.h.s multiplied by $\mathbf{A}_1^{-1}$ as in Eq. (4.41) has to be orthogonal to $\mathbf{w}^\dagger_{1,1}$[100]. This solvability condition leads to the reduced Landau equation (4.28), whose coefficients can now be defined as

$$\mu_1 = -\mathbf{w}^\dagger_{1,1} \cdot \mathbf{A}_1^{-1}\mathbf{F}_1\mathbf{N}_1(\bar{\mathbf{u}})\mathbf{w}_{1,1}, \tag{4.43}$$

$$\mu_2 = -\mathbf{w}^\dagger_{1,1} \cdot \mathbf{A}_1^{-1}\mathbf{F}_1(\mathbf{N}_1(\mathbf{u}_{0,2}) + \mathbf{h}^w_{1,3}). \tag{4.44}$$

Owing to the symmetry of the problem, both $\hat{w}_{1,1}$ and $\hat{u}_{0,2}$ are even, whereas $\hat{w}_{2,2}$ is an odd function of z. This allows the solution to be sought in one half of the layer so reducing the number of required collocation points by half. $M = N/2 = 32$ collocation points in a half layer is sufficient to obtain the critical Reynolds number $Re_l = 5772.22$, frequency $\omega_l = -1555.18$ and wavenumber $\alpha_l = 1.02055$ with six significant figures [17].

The real and imaginary parts of the critical perturbation $\hat{w}_{1,1}$, which are given by the right eigenvector $\mathbf{w}_{1,1}$ are shown in Fig. 4.1 together with the corresponding left eigenvector $\mathbf{w}^\dagger_{1,1}$. Note that the latter is orthogonal to all other right eigenvectors but $\mathbf{w}_{1,1}$. Since about a half of the right eigenvectors are numerically spurious [82], $\mathbf{w}^\dagger_{1,1}$ has only a numerical but no physical meaning. Because of different inner product definitions for the continuous and discrete problems, $\mathbf{w}^\dagger_{1,1}$ is also distinct from the adjoint eigenfunction $\hat{w}^+_{1,1}$ considered in the previous section. Distributions of the mean-flow perturbation and that of the complex amplitude of the second harmonic are plotted for the top half of the layer in Fig. 4.2. Note that due to the non-standard

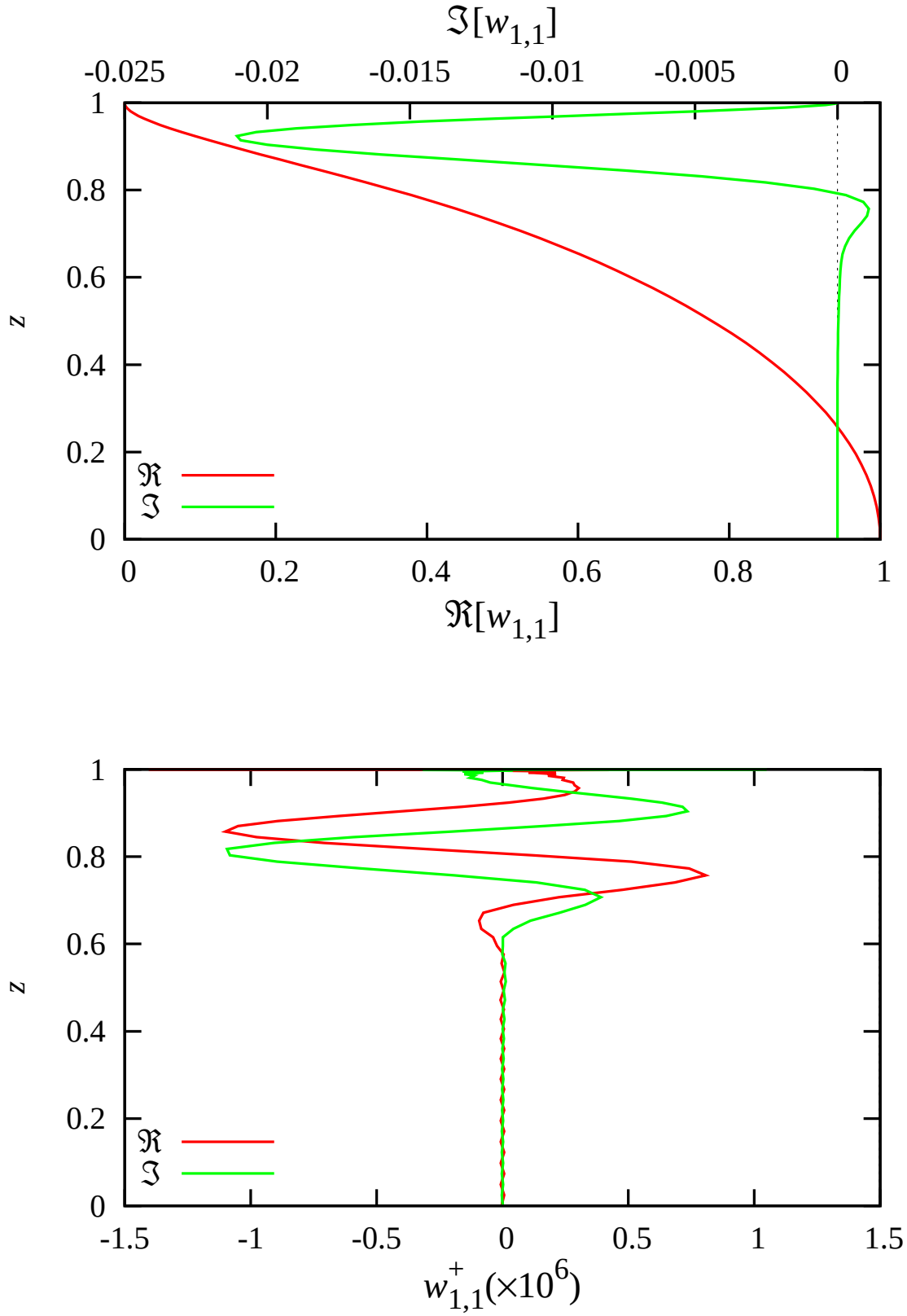

Figure 4.1: Real and imaginary parts of the critical perturbation $\hat{w}_{1,1}$ given by the right eigenvector $\mathbf{w}_{1,1}$ (a) and the corresponding left eigenvector $\mathbf{w}^{\dagger}_{1,1}$ plotted against the collocation point coordinates (b).

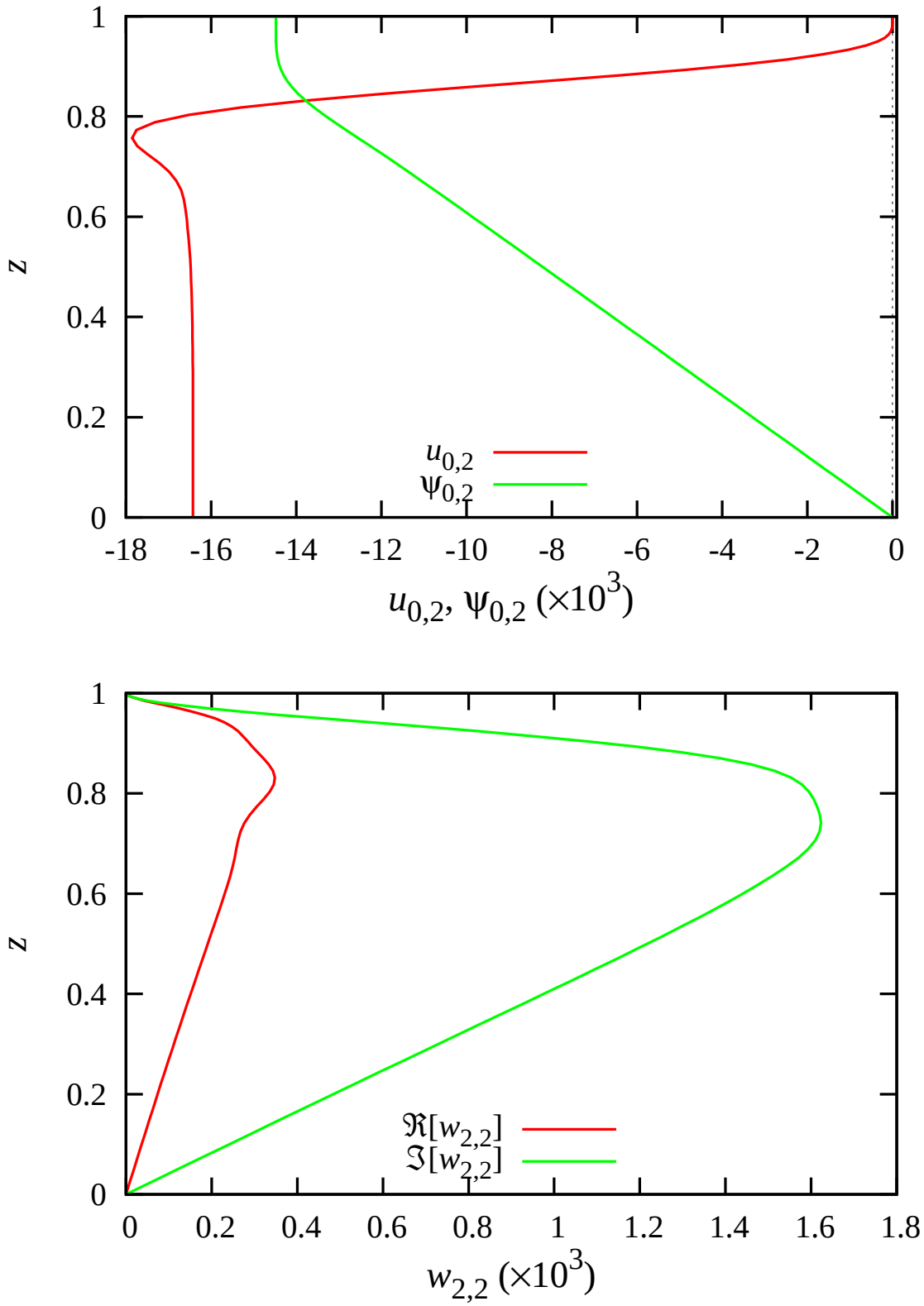

Figure 4.2: Velocity $\hat{u}_{0,2}$ and the associated stream function $\hat{\psi}_{0,2}$ of the mean-flow perturbation (a); the real and imaginary parts of the second harmonic amplitude $\hat{w}_{2,2}$ (b).

scaling, the dimensionless frequency and velocity differ by a factor of Re_l from the results obtained with the conventional scaling based on the center-line velocity.

Substituting the above results into Eqs. (4.29) and (4.30), then the following is values for μ_1 and μ_2 can be obtained:

$$\begin{aligned} \mu_1 &= 0.0097118 - \mathrm{i}0.222596, \\ \mu_2 &= 0.0049382 - \mathrm{i}0.0239131. \end{aligned}$$

As seen from Fig. 4.3, $M \gtrsim 40$ collocation points are required to obtain Landau coefficients with about six significant figures. The first and most important result is $\Re[\mu_2] > 0$, which confirms the subcritical nature of this instability in agreement with the previous findings. The coefficient μ_1 has been computed explicitly by Stewartson and Stuart [46] who found $d_1 = (0.17 + \mathrm{i}0.8) \times 10^{-5}$ for the standard normalization. Rescaling this result with the center-line velocity, $\tilde{\mu}_1 = \mu_1/Re_l = (0.168251 - \mathrm{i}3.85633) \times 10^{-5}$ is obtained, whose real part is close to that of d_1. This is not the case for the imaginary part. The μ_1 can also be plotted against the complex growth rate supplied by the linear stability analysis in the vicinity of the stability threshold, where $\delta\lambda = \lambda - \lambda_l \approx \mu_1(Re - Re_l)$. As seen in Fig. 4.4, the variation of the complex phase speed $c = -\mathrm{i}\lambda/Re\alpha$, which is commonly used instead of λ, is accurately reproduced by μ_1 in the vicinity of Re_l.

In order to compare the calculated Landau coefficient μ_2 with the values found in the previous studies it is necessary to take into account not only the non-standard choice of the characteristic velocity but also the fact that in here A stands for the amplitude of the transverse velocity component w, whereas in the previous studies it stands for the amplitude of the stream function ψ, which is related to the former as $w = \mathrm{i}\alpha\psi$. As a result, μ_2 is rescaled as

$$\tilde{\mu}_2 = \mu_2 \alpha_l^2 Re_l = 29.659 - \mathrm{i}143.622.$$

This result is close to $\tilde{\mu}_2 = \mathrm{i}\alpha_l K_1 = 29.46 - \mathrm{i}143.41$ found by Sen and Venkateswarlu

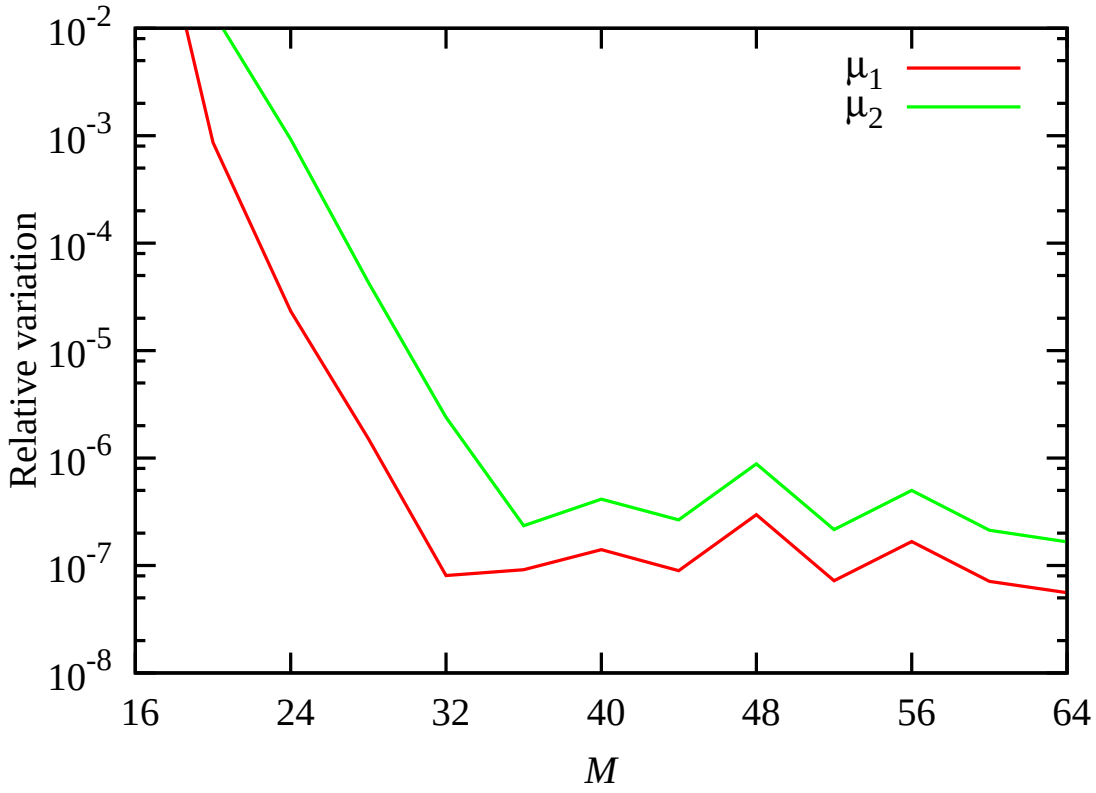

Figure 4.3: Relative variation of Landau coefficients with the number of collocation points M.

[44] using the method of Reynolds and Potter [43] for $Re_l = 5774$, $\alpha_l = 1.02$ and $c_r = 0.2639$. Note that K_1 has been mistaken for $\tilde{\mu}_2$ by Schmid and Henningson [4] who have denoted it by λ_2.

Alternatively, rescaling μ_2^q with Re_l based on the centerline velocity and the accurate value of α_l, we obtain

$$\tilde{\mu}_2^q = \mu_2^q \alpha_l^2 Re_l = 30.957 - \mathrm{i}172.83,$$

which agrees well with $\tilde{\mu}_2 = 30.96126 - \mathrm{i}172.8268$ and $\tilde{\mu}_2 = 30.95616 - \mathrm{i}172.8335$ obtained respectively by the amplitude expansion using a highly accurate Chebyshev collocation method [48] and by the centre manifold reduction using an expansion in linear eigenfunctions [49].

Reynolds and Potter [43] used their original method of "false solution" to obtain the first relatively accurate values of Landau coefficients for the case of fixed flow rate.

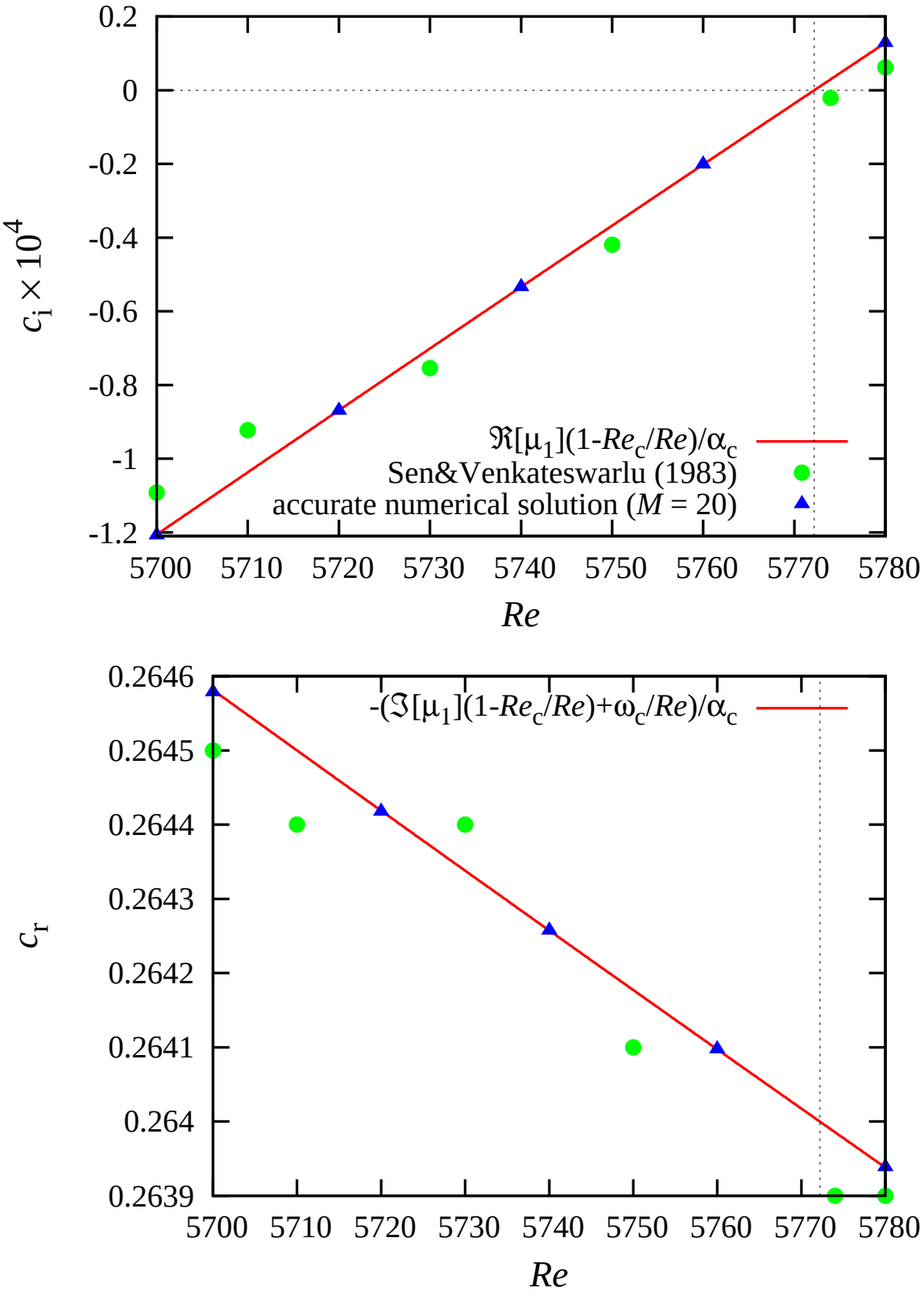

Figure 4.4: Imaginary (a) and real (b) parts of the complex phase velocity $c = -\mathrm{i}\lambda/Re\alpha$ of the most unstable mode in the vicinity of the critical Reynolds number Re_c calculated using μ_1 and supplied by the linear stability analysis (triangles) and taken from [44] (dots).

The solution found here for fixed pressure gradient can easily be converted to the fixed flow rate by using the non-zero pressure gradient correction $P_{0,2}$ in Eq. (4.23). As seen from Eq. (4.20), this correction, which affects only the magnitude of the base flow, is equivalent to the substitution of Re_2 by

$$Re_2^q = Re_2 + |A|^2 P_{0,2}/2.$$

The pressure correction $P_{0,2}$, which according to the expression above produces a flow rate perturbation $|A|^2 P_{0,2}\bar{\psi}(1)$, has to compensate for $2|A|^2\hat{\psi}_{0,2}(1)$ flow rate perturbation, which occurs at fixed pressure gradient. This results in

$$P_{0,2}/2 = -\hat{\psi}_{0,2}(1)/\bar{\psi}(1) = 0.00217238,$$

where $\bar{\psi}(1) = \int_0^1 \bar{u}(z)\,dz = \frac{2}{3}$. Substitution of Re_2 by Re_2^q in Eq. (5.26) results in μ_2 replaced by

$$\mu_2^q = \mu_2 + \mu_1 P_{0,2}/2 = 0.0051492 - \mathrm{i}0.0287487.$$

Rescaling μ_2^q with the critical Reynolds number based on the mean velocity $\bar{Re}_l = \frac{2}{3}Re_l = 3848.08$ and $\alpha_l = 1.02071$ used by Reynolds and Potter [43], then the expression

$$\tilde{\mu}_2^q = \mu_2^q \alpha_l^2 \bar{Re}_l = 20.64 - \mathrm{i}115.26,$$

is obtained, which is close to the value $\tilde{\mu}_2^q = a^{(2)} + \mathrm{i}b^{(2)} = 19.7 - \mathrm{i}111$ obtained by Reynolds and Potter [43].

Chapter 5

2-D travelling waves in Hartmann flow

Having established that there is a subcritical bifurcation in plane Poiseuille flow from linear and weakly nonlinear analysis, how far the subcritical equilibrium states exist below the linear stability threshold will be investigated. The perturbation is no longer considered to be small. A travelling wave solution will be sought, using the derivations in Sec. 4.2. The weakly nonlinear analysis is only valid when the expansion parameter is small, that is, when the Reynolds number is close to the linear stability threshold $Re_c = 5772.2$. The method will be validated by considering the hydrodynamic stability problem, i.e. $Ha = 0$, before calculating results for Hartmann flow. The neutral stability curve for linear stability will be extended to neutral finite-amplitude states [96, 97, 98]. Since the equilibrium states are sensitive to the number of Fourier components (harmonics) included, for accurate results $N \gg 2$ is required [4].

5.1 Problem Formulation

Consider the flow of an incompressible viscous electrically conducting liquid with density ρ, kinematic viscosity ν and electrical conductivity σ driven by a constant gradient of pressure p in the channel of the width $2h$ between two parallel walls in the presence of a transverse homogeneous magnetic field $\boldsymbol{B}$. The velocity distribution of the flow,

$\boldsymbol{v}(\boldsymbol{r}, t)$, is governed by the Navier-Stokes equation

$$\partial_t \boldsymbol{v} + (\boldsymbol{v} \cdot \boldsymbol{\nabla})\boldsymbol{v} = -\rho^{-1}\boldsymbol{\nabla} p + \nu \boldsymbol{\nabla}^2 \boldsymbol{v} + \rho^{-1}\boldsymbol{f}, \tag{5.1}$$

where $\boldsymbol{f} = \boldsymbol{j} \times \boldsymbol{B}$ is the electromagnetic body force containing the induced electric current $\boldsymbol{j}$, which is governed by Ohm's law for a moving medium

$$\boldsymbol{j} = \sigma(\boldsymbol{E} + \boldsymbol{v} \times \boldsymbol{B}). \tag{5.2}$$

The flow is assumed to be sufficiently slow that the induced magnetic field is negligible relative to the imposed one. This supposes a small magnetic Reynolds number $Rm = \mu_0 \sigma v_0 d \ll 1$, where μ_0 is the permeability of vacuum and v_0 is the characteristic velocity of the flow. In addition, we assume that the characteristic time of velocity variation is much longer than the magnetic diffusion time $\tau_m = \mu_0 \sigma h^2$. This allows use of the quasi-stationary approximation leading to $\boldsymbol{E} = -\boldsymbol{\nabla}\phi$, where ϕ is the electrostatic potential [61]. By assuming the magnetic Reynolds number is small, the Lorentz force and Ohm's law can be simplified to $\boldsymbol{f} = \boldsymbol{j} \times \boldsymbol{B}$ and Eq. (5.2) respectively [5, 61]. The velocity and current satisfy mass and charge conservation $\boldsymbol{\nabla} \cdot \boldsymbol{v} = \boldsymbol{\nabla} \cdot \boldsymbol{j} = 0$. Applying the latter to Ohm's law (5.2) yields

$$\boldsymbol{\nabla}^2 \phi = \boldsymbol{B} \cdot \boldsymbol{\omega}, \tag{5.3}$$

where $\boldsymbol{\omega} = \boldsymbol{\nabla} \times \boldsymbol{v}$ is the vorticity. At the channel walls S, the normal (n) and tangential (τ) velocity components satisfy the impermeability and no-slip boundary conditions $v_n|_s = 0$ and $v_\tau|_s = 0$. For a fixed pressure gradient, electrical conductivity of the walls affects only the magnitude of the base flow but not its profile. Moreover, the conductivity of the walls does not affect the electric current which is induced tangentially to the boundaries by the 2D disturbances considered in this study. Thus, the stability of the flow, which is determined by the centreline velocity, is not affected by the electrical conductivity of the walls.

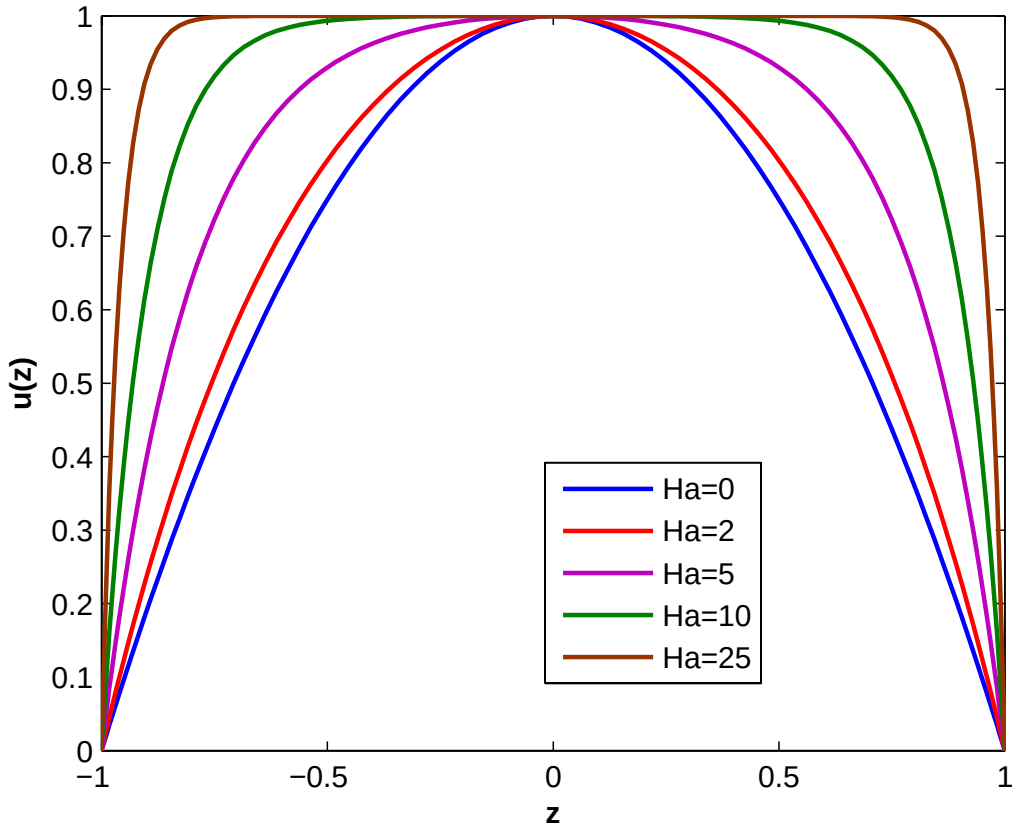

Figure 5.1: Streamwise base flow velocity $\bar{u}(z)$ for increasing Hartmann number.

Right-handed Cartesian coordinates are employed with the origin set at the mid-height of the channel, the x- and the z-axes directed, respectively, against the applied pressure gradient $\boldsymbol{\nabla} p_0 = P\boldsymbol{e}_x$ and along the magnetic field $\boldsymbol{B} = B\boldsymbol{e}_z$ so that the channel walls are located at $z = \pm h$, as shown in figure 1.1, and the velocity is defined as $\boldsymbol{v} = (u, v, w)$. Subsequently, all variables are non-dimensionalised by using h, h^2/ν and $B\nu$ as the length, time and electric potential scales, respectively. The velocity is scaled by the viscous diffusion speed ν/h, which is employed as the characteristic velocity instead of the commonly used centreline velocity. The problem admits a rectilinear base flow

$$\boldsymbol{v}_0(z) = \bar{u}_0(z)\boldsymbol{e}_x = Re\bar{u}(z)\boldsymbol{e}_x \tag{5.4}$$

for which Eq. (5.1) reduces to

$$\bar{u}'' - Ha^2\bar{u} = \bar{P}, \tag{5.5}$$

where $Re = Uh/\nu$ is the Reynolds number based on the centreline velocity U, $Ha = hB\sqrt{\sigma/\rho\nu}$ is the Hartmann number, and $\bar{P}$ is a dimensionless pressure gradient satisfying the normalization condition $\bar{u}(0) = 1$. This equation defines the well-known Hartmann flow profile

$$\bar{u}(z) = \frac{\cosh(Ha) - \cosh(zHa)}{\cosh(Ha) - 1} \tag{5.6}$$

with $\bar{P} = -\frac{Ha^2 \cosh(Ha)}{\cosh(Ha)-1}$, which relates the centreline velocity with the applied pressure gradient $P = \bar{P}U\nu\rho/h^2$. In the weak magnetic field ($Ha \ll 1$), the Hartman flow reduces to the classic plane Poiseuille flow $\bar{u}(z) = 1 - z^2$. Fig. 5.1 shows visually the effect of an increased Hartmann number on the velocity profile of the base flow.

5.2 Theoretical background

5.2.1 Linear stability analysis

The present study is concerned with two-dimensional travelling waves that are expected to bifurcate from the Hartmann flow as a result of linear instability. Therefore, start with determining the linear stability of the Hartmann flow with respect to infinitesimal perturbations $\boldsymbol{v}_1(\boldsymbol{x}, t)$ and search for the velocity as $\boldsymbol{v} = \boldsymbol{v}_0 + \boldsymbol{v}_1$. Since the base flow is invariant in both t and $\boldsymbol{x} = (x, y)$, perturbation can be sought as a Fourier mode

$$\boldsymbol{v}_1(\boldsymbol{r}, t) = \hat{\boldsymbol{v}}(z)\mathrm{e}^{\lambda t + \mathrm{i}\boldsymbol{k}\cdot\boldsymbol{x}} + \text{c.c.}, \tag{5.7}$$

which is defined by a complex amplitude distribution $\hat{\boldsymbol{v}}(z)$, temporal growth rate λ and the wave vector $\boldsymbol{k} = (\alpha, \beta)$. The incompressibility constraint, which takes the form $\boldsymbol{D}_k \cdot \hat{\boldsymbol{v}} = 0$, where $\boldsymbol{D}_k \equiv \boldsymbol{e}_z \frac{d}{dz} + \mathrm{i}\boldsymbol{k}$ is a spectral counterpart of the nabla operator, is satisfied by expressing the component of the velocity perturbation in the direction of the wave vector as $\hat{u}_{\shortparallel} = \boldsymbol{e}_{\shortparallel} \cdot \hat{\boldsymbol{v}} = \mathrm{i}k^{-1}\hat{w}'$, where $\boldsymbol{e}_{\shortparallel} = \boldsymbol{k}/k$ and $k = |\boldsymbol{k}|$. Taking the *curl* of the linearised counterpart of Eq. (5.1) to eliminate the pressure gradient and then projecting it onto $\boldsymbol{e}_z \times \boldsymbol{e}_{\shortparallel}$, after some transformations a modified Orr-Sommerfeld type

equation is obtained which includes a magnetic term

$$\lambda \boldsymbol{D}_k^2 \hat{w} = \left[\boldsymbol{D}_k^4 - Ha^2 (\boldsymbol{e}_z \cdot \boldsymbol{D}_k)^2 + \mathrm{i}kRe(\bar{u}'' - \bar{u}\boldsymbol{D}_k^2) \right] \hat{w}. \tag{5.8}$$

The no-slip and impermeability boundary conditions require

$$\hat{w} = \hat{w}' = 0 \quad \text{at} \quad z = \pm 1. \tag{5.9}$$

The equation (5.8) is written in a non-standard form corresponding to the choice of the characteristic velocity. Note that the Reynolds number appears in this equation as a factor at the convective term rather than its reciprocal at the viscous term as in the standard form. As a result, the growth rate λ differs by a factor Re from its standard definition.

Since the equation above, similarly to its non-magnetic counterpart, admits Squire's transformation [104], in the following we consider only two-dimensional perturbations ($k = \alpha$), which are the most unstable [59]. The linear stability problem is solved numerically using a Chebyshev collocation method which is described in detail in Sec. (3.2) and Hagan & Priede [90].

5.2.2 Nonlinear 2D travelling waves

Two-dimensional travelling waves emerge as follows. The neutrally stable mode (5.7) with a purely real frequency $\omega = -\mathrm{i}\lambda$ interacting with itself through the quadratically nonlinear term in Eq. (5.1) gives rise to a steady streamwise invariant perturbation of the mean flow as well as to a second harmonic $\sim \mathrm{e}^{2\mathrm{i}(\omega t + \alpha x)}$. Subsequent nonlinear interactions produce higher harmonics, which behave similarly to the fundamental and second harmonic travel with the same phase speed $c = -\omega/\alpha$. Thus, the solution can be sought in the form

$$\boldsymbol{v}(\boldsymbol{r}, t) = \sum_{n=-\infty}^{\infty} E^n \hat{\boldsymbol{v}}_n(z), \tag{5.10}$$

where $E = \mathrm{e}^{\mathrm{i}(\omega t+\alpha x)}$ contains ω, which, in general, needs to determined together $\hat{\boldsymbol{v}}_n$ by solving a non-linear eigenvalue problem. The reality of solution requires $\hat{\boldsymbol{v}}_{-n} = \hat{\boldsymbol{v}}_n^*$, where the asterisk stands for the complex conjugate. The incompressibility constraint applied to the nth velocity harmonic results in $\boldsymbol{D}_{\alpha_n}\cdot\hat{\boldsymbol{v}}_n = 0$, where $\boldsymbol{D}_{\alpha_n} \equiv \boldsymbol{e}_z\frac{d}{dz}+\mathrm{i}\boldsymbol{e}_x\alpha_n$ with $\alpha_n = \alpha n$ stands for the spectral counterpart of the nabla operator. This constraint can be satisfied by expressing the streamwise velocity component

$$\hat{u}_n = \boldsymbol{e}_x \cdot \hat{\boldsymbol{v}}_n = \mathrm{i}\alpha_n^{-1}\hat{w}_n' \tag{5.11}$$

in terms of the transverse component $\hat{w}_n = \boldsymbol{e}_z \cdot \hat{\boldsymbol{v}}_n$, which is employed instead of the commonly used stream function. Henceforth, the prime is used as a shorthand for d/dz. Note that Eq. (5.11) is not applicable to the zeroth harmonic, for which it yields $\hat{w}_0 \equiv 0$. Thus, $\hat{u}_0$ needs to be considered separately in this velocity-based formulation.

Taking the *curl* of Eq. (5.1) to eliminate the pressure gradient and then projecting it onto $\boldsymbol{e}_y$, the result is

$$[\boldsymbol{D}^2_{\alpha_n} - \mathrm{i}\omega n]\hat{\zeta}_n - Ha^2\hat{u}_n' = \hat{h}_n, \tag{5.12}$$

where

$$\hat{\zeta}_n = \boldsymbol{e}_y \cdot \boldsymbol{D}_{\alpha_n} \times \hat{\boldsymbol{v}}_n = \begin{cases} \mathrm{i}\alpha_n^{-1}\boldsymbol{D}^2_{\alpha_n}\hat{w}_n, & n \neq 0; \\ \hat{u}_0', & n = 0. \end{cases} \tag{5.13}$$

and

$$\hat{h}_n = \sum_m \hat{\boldsymbol{v}}_{n-m} \cdot \boldsymbol{D}_{\alpha_m}\hat{\zeta}_m \tag{5.14}$$

are the y-components of the nth harmonic of the vorticity $\boldsymbol{\zeta} = \boldsymbol{\nabla} \times \boldsymbol{v}$ and that of the *curl* of the nonlinear term $\boldsymbol{h} = \boldsymbol{\nabla} \times (\boldsymbol{v} \cdot \boldsymbol{\nabla})\boldsymbol{v}$. Henceforth, the omitted summation limits are assumed to be infinite. Separating the terms involving $\hat{u}_0$ in sum (5.14), it can be rewritten as $\hat{h}_n = \mathrm{i}\alpha_n^{-1}(\hat{h}_n^w + \hat{h}_n^u)$, where

$$\hat{h}_n^w = n\sum_{m\neq 0} m^{-1}(\hat{w}_{n-m}\boldsymbol{D}^2_{\alpha_m}\hat{w}_m' - \hat{w}_m'\boldsymbol{D}^2_{\alpha_{n-m}}\hat{w}_{n-m}), \tag{5.15}$$

$$\hat{h}_n^u = \mathrm{i}\alpha_n[\hat{u}_0 - \hat{u}_0''\boldsymbol{D}^2_{\alpha_n}]\hat{w}_n \equiv \mathcal{N}_n(\hat{u}_0)\hat{w}_n. \tag{5.16}$$

Eventually, using the expressions above, Eq. (5.12) can be expressed as

$$\mathcal{L}_n(\mathrm{i}\omega, \hat{u}_0)\hat{w}_n = \hat{h}^w_n, \tag{5.17}$$

with the operator

$$\mathcal{L}_n(\mathrm{i}\omega, \hat{u}_0) = [\boldsymbol{D}^2_{\alpha_n} - \mathrm{i}\omega n]\boldsymbol{D}^2_{\alpha_n} - Ha^2(\boldsymbol{e}_z \cdot \boldsymbol{D}_{\alpha_n})^2 - \mathcal{N}_n(\hat{u}_0). \tag{5.18}$$

The equation above governs all harmonics except the zeroth one, for which it implies $\hat{w}_0 \equiv 0$ in accordance with the incompressibility constraint (5.11). The zeroth velocity harmonic, which has only the streamwise component $\hat{u}_0$, is governed directly by the x-component of the Navier-Stokes equation (5.1):

$$\hat{u}_0'' - Ha^2\hat{u}_0 = \hat{P}_0 + \hat{g}_0, \tag{5.19}$$

where $\hat{P}_0 = \bar{P}Re$ is a dimensionless mean pressure gradient and

$$\hat{g}_0 = \mathrm{i}\sum_{m\neq 0} \alpha_m^{-1}\hat{w}^*_m\hat{w}''_m \tag{5.20}$$

is the x-component of the zeroth harmonic of the nonlinear term $\boldsymbol{g} = (\boldsymbol{v}\cdot\boldsymbol{\nabla})\boldsymbol{v}$. Velocity harmonics are subject to the usual no-slip and impermeability boundary conditions

$$\hat{w}_n = \hat{w}'_n = \hat{u}_0 = 0 \text{ at } z = \pm 1. \tag{5.21}$$

5.2.3 Weakly nonlinear analysis

The equations obtained in the previous section govern the equilibrium states of two-dimensional travelling waves of arbitrary amplitude. In the vicinity of the linear stability threshold, solution can be simplified by expanding it in a small perturbation amplitude. As discussed above, the basic harmonic (5.7) with amplitude $O(\epsilon)$ interacting with itself through the quadratically nonlinear term in Eq. (5.1) produces a

zeroth harmonic, which modifies the mean flow, and a second harmonic, both of which have amplitude $O(\epsilon^2)$. These two harmonics further interacting with the basic one produce an $O(\epsilon^3)$ correction to the latter. The second harmonic interacting with the basic one also gives rise to a third harmonic with amplitude $O(\epsilon^3)$. This perturbation series is represented by the following expansion:

$$\hat{w}_n = \sum_{m=0}^{\infty} \epsilon^{|n|+2m} \tilde{A}^{|n|} |\tilde{A}|^{2m} \hat{w}_{n,|n|+2m}, \tag{5.22}$$

where $\epsilon\tilde{A} = A$ is an unknown equilibrium amplitude of the basic harmonic and $\tilde{A} = O(1)$ is its normalized counterpart. The mean flow, which needs to be considered separately, is expanded as

$$\hat{u}_0 = \hat{u}_{0,0} + \epsilon^2 |\tilde{A}|^2 \hat{u}_{0,2} + \dots. \tag{5.23}$$

Similarly, the Reynolds number and the frequency are expanded as

$$Re = Re_0 + \epsilon^2 \tilde{R}e_2 + \dots, \tag{5.24}$$

$$\omega = \omega_0 + \epsilon^2 \tilde{\omega}_2 + \dots, \tag{5.25}$$

where Re_0 is the marginal Reynolds number satisfying $\Re[\lambda_0] = 0$ for the mode $\hat{w}_{1,1}$ with the frequency $\omega_0 = \Im[\lambda_0]$ and the wavenumber α; $\epsilon^2\tilde{R}e_2 = Re_2$ and $\epsilon^2\tilde{\omega}_2 = \omega_2$ are deviations of the respective quantities from their linear stability threshold values. Substituting these expansions into Eqs. (5.17) and (5.19), collecting terms at equal powers of ϵ and applying the solvability condition to the equation for $\hat{w}_{n,|n|+2m}$ we eventually obtain

$$\mathrm{i}\omega_2 = \mu_1 Re_2 + \mu_2 |A|^2. \tag{5.26}$$

The coefficients of this equation are defined as

$$\mu_1 = - \hat{w}^+_{1,1}, \mathcal{N}_1(\bar{u})\hat{w}_{1,1}\rangle\,, \tag{5.27}$$

$$\mu_2 = -\left\langle \hat{w}^+_{1,1}, \mathcal{N}_1(\hat{u}_{0,2})\hat{w}_{1,1} + \hat{h}^w_{1,3}\right\rangle, \tag{5.28}$$

where the angle brackets denote the inner product and the expressions are written for the adjoint eigenfunction normalized as $\hat{w}^+_{1,1}, \boldsymbol{D}_1^2\hat{w}_{1,1}\rangle = 1$. The eigenfunction $\hat{w}_{1,1}$ can be normalized in several different ways which will be specified later on. Equation (5.26) represents a reduced Landau equation for the case of equilibrium solution, which requires ω_2 to be real and, thus, yields the sought equilibrium amplitude

$$|A|^2 = -Re_2\Re[\mu_1]/\Re[\mu_2]. \tag{5.29}$$

The type of instability is determined by the sign of $\Re[\mu_2]$. Namely, $\Re[\mu_2] > 0$ corresponds to a subcritical instability, which means that an equilibrium solution with $|A|^2 > 0$ is possible at negative linear growth rates $Re_2\Re[\mu_1] < 0$. Otherwise, instability is supercritical. The coefficients (5.27 and 5.28) are calculated using an efficient numerical approach based on the application of the solvability condition directly to the discretized problem [90]. This allows both the solution of the adjoint problem to be bypassed, as well as the subsequent evaluation of the integrals defining the inner products.

5.2.4 Linear stability of 2-D travelling waves

Weakly nonlinear subcritical equilibrium states considered in the previous section can easily be shown to be linearly unstable [4]. Instability straightforwardly follows from the fact the growth rate of these perturbations increases with their amplitude. Thus, perturbations with an amplitude slightly lower or higher than the equilibrium one will respectively decay or grow so moving away from the equilibrium state. Stability of strongly subcritical equilibrium states is not that obvious. Orszag & Patera [31] originally suggested that the subcritical equilibrium state emanating at the linear

stability threshold remain linearly unstable down the lowest possible Reynolds number admitting such states. At this critical Reynolds number, which will be the main concern of the present study, the unstable subcritical state disappears by merging with another equilibrium state of a higher amplitude which was thought to be linearly stable. This simple picture was amended by Pugh & Saffman [99] who showed it to hold for the Reynolds number based on the flow rate but not on the pressure gradient. It is important to notice that these two Reynolds numbers are just alternative parametrisations of the same physical problem, i.e. plane Poiseuille flow [71].

Linear stability of travelling-wave states, which in contrast to the rectilinear base state are periodic rather than invariant in both in time and the streamwise direction, can be analysed using Floquet theory according to which small-amplitude velocity disturbance can be sought similarly to (5.10) as

$$\boldsymbol{v}_1(\boldsymbol{r},t) = e^{\tilde{\lambda}t+\mathrm{i}\tilde{\alpha}x} \sum_{n=-\infty}^{\infty} E^n \tilde{\boldsymbol{v}}_n(z) + \text{c.c.}, \tag{5.30}$$

where $\tilde{\lambda}$ is generally a complex growth rate and $|\tilde{\alpha}| \leq \alpha/2$ is the subharmonic wavenumber [41]. Adding this disturbance to the travelling wave base state (5.10), a linearised counterpart of Eq. (5.12) for transverse velocity harmonics $\tilde{w}_n$ is obtained:

$$\left[\boldsymbol{D}^2_{\tilde{\alpha}_n} - \tilde{\lambda} - \mathrm{i}\omega n\right] \boldsymbol{D}^2_{\tilde{\alpha}_n}\tilde{w}_n - Ha^2\tilde{w}_n'' = -\mathrm{i}\tilde{\alpha}_n \sum_m \boldsymbol{D}_{\tilde{\alpha}_n} \cdot (\hat{\boldsymbol{v}}_{n-m}\tilde{\zeta}_m + \tilde{\boldsymbol{v}}_m\hat{\zeta}_{n-m}), \tag{5.31}$$

where $\tilde{\alpha}_n = \alpha_n + \tilde{\alpha}$ is a modified wavenumber for the nth harmonic, $\tilde{u}_n = \boldsymbol{e}_x \cdot \tilde{\boldsymbol{v}}_n = \mathrm{i}\tilde{\alpha}_n^{-1}\tilde{w}_n'$ is the streamwise velocity and $\tilde{\zeta}_n = \mathrm{i}\tilde{\alpha}_n^{-1}\boldsymbol{D}^2_{\tilde{\alpha}_n}\tilde{w}_n$ is the spanwise vorticity of the disturbance. The boundary conditions, as usual, are $\tilde{w}_n(1) = \tilde{w}_n'(1) = 0$.

Cutting the series (5.30) off at $n = \pm N$, a linear eigenvalue problem represented by $2N+1$ complex equations is obtained (5.31) for the eigenvector consisting of the same number of harmonics $\tilde{w}_n$ with the eigenvalue $\tilde{\lambda}$, which depends on the subharmonic wavenumber $\tilde{\alpha}$. This eigenvalue problem is solved in the same as that for the linear stability of the rectilinear base flow. To avoid the division by zero in the expressions for $\tilde{u}_0$ and $\tilde{\zeta}_0$ above, which occurs for superharmonic disturbances corresponding to

$\tilde{\alpha} = 0$, we use the substitution as $\tilde{w}_n = -\mathrm{i}\tilde{\alpha}_n\tilde{\psi}_n$, where $\tilde{\psi}_n$ is the stream function. This makes superharmonic disturbances treatable in the same way as subharmonic ones. In the following, we consider only the superharmonic disturbances corresponding to $\tilde{\alpha} \to 0$.

Note that subharmonic disturbances with $\tilde{\alpha} \neq 0$ affect neither the mean pressure gradient nor the flow rate. Both of these quantities are associated with the zero wavenumber mode, which occurs only for superharmonic disturbances. $\tilde{\alpha}_0 = 0$. In the limit $\tilde{\alpha} \to 0$, the growth rate of subharmonic disturbances is expected to tend to that of superharmonic ones. This is obviously the case for the formulation above based on the fixed flow rate but not so when the condition of constant mean pressure gradient is applied to superharmonic disturbances in the form which was originally suggested by Pugh & Saffman [99] and later amended by Soibelman and Merion [71]. This condition results in the stability characteristics of superharmonic disturbances which substantially differ from those in the cases of fixed flow rate. Thus, the growth rate, in this case, varies discontinuously as $\tilde{\alpha} \to 0$ which is obviously unphysical. This inconsistency seems to be due to the incorrect assumption of constant flux Reynolds number when fixed mean pressure gradient is considered. Taking into account the variation of the flux Reynolds number caused by the flow disturbance when the mean pressure gradient is fixed eliminates the unphysical difference between the stability characteristics of superharmonic disturbances for the fixed flow rate and the fixed mean pressure cases.

5.3 Numerical approach

The problem is solved numerically using a Chebyshev collocation method with the Chebyshev-Lobatto nodes

$$z_i = \cos\left(i\pi/2M\right), \quad i = 0, \cdots, M, \tag{5.32}$$

at which the discretized solution $(\hat{w}_n, \hat{u}_0)(z_i) = (\mathbf{w}_n, \mathbf{u}_0)_i$ is sought in the upper half of the layer. The reduction to the half layer is due to the following symmetries implied by Eq. (5.15). Harmonics of the transverse velocity $\hat{w}_n$ with even indices are odd functions of z, whereas those with odd indices have the same parity as the fundamental mode ($n = 1$). The latter may be either odd or even, which gives rise to two types of possible 2D solutions. The same two symmetries apply also to the perturbations of the even travelling wave mode. The deformed base flow $\hat{u}_0(z)$ according to Eq. (5.20) is an even function.

The equations above are approximated at the internal collocation points $1 \leq i \leq M$ by using the differentiation matrices which express the derivatives in terms of the collocation variables $(\mathbf{w}_n, \mathbf{u}_0)_i$. The boundary conditions (5.9) are imposed at the boundary point $i = 0$ [93]. Cutting series (5.10) off at $n = \pm N$, Eqs. (5.17) give rise to $N \times M$ complex algebraic equations with respect to the same number of complex unknowns $\mathbf{w}_n$ for $n = 1, 2, \ldots, N$. Note that $\mathbf{w}_0 \equiv 0$ and $\mathbf{w}_{-n} = \mathbf{w}_n^*$. These equations contain also M real unknowns $\tilde{u}_0$, which are governed by the same number of real equations resulting from the collocation approximation of Eq. (5.19). These linear equations can be solved for $\tilde{u}_0$ in terms of $\mathbf{w}_n$. This results in a system of $N \times M$ nonlinear complex equations for the same number of complex unknowns $\mathbf{w}_n$. Since the equations contain also $\mathbf{w}_n^*$, the actual unknowns are the real and imaginary parts of $\mathbf{w}_n$, which need to be determined by solving the same number, i.e. $2N \times M$, real equations given by the real and imaginary parts of the original complex equations.

There is one more unknown: the frequency ω, which represents an eigenvalue of this non-linear problem, and needs to be determined along with $\mathbf{w}_n$. There are two ways to balance the number of unknowns and equations. First, as the problem is homogeneous, a non-trivial solution requires a certain nonlinear solvability condition to be satisfied, which provides an additional equation analogous to the characteristic determinant in the case of linear eigenvalue problem. The second possibility, which is used in this study, follows from the fact that $\mathbf{w}_n$ is defined up to an arbitrary phase due to the translational invariance of the problem. The phase, which defines the x-offset

of solution, can be fixed by imposing the condition $\Im[\mathbf{w}_{1,i}] = 0$ at some collocation point i where the solution is not already fixed. This is equivalent to setting $\mathbf{w}_{1,i} = A$, where A is a real parameter defining the amplitude of velocity. Thus, the number of unknowns is reduced by one and the system of $2N \times M$ nonlinear algebraic equations can be written in general form as

$$\mathbf{F}(\mathbf{w}, A, \omega; \alpha, Re)\mathbf{w} = \mathbf{0}, \tag{5.33}$$

where $\mathbf{w}$ are the real and imaginary parts of $\mathbf{w}_n$ normalized with the real amplitude A and $\mathbf{F}$ is a real square matrix of size $2N \times M$ depending on the listed parameters. For given α and Re, this problem can be solved by the Newton-Raphson method with respect to A, ω and $2N \times M - 2$ unknown $\mathbf{w}$. In some cases, instead of Re, it is more convenient to fix A and then to solve for Re depending on A and α.

The solution is traced using a quadratic extrapolation along arc length in logarithmic coordinates. For a general function f of an argument p the scale-independent arc length element is defined as $\delta s^2 = \ln^2(1 + \frac{\delta f}{f}) + \ln^2(1 + \frac{\delta p}{p})$. Using a reference arc length based on the solution at the chosen first three parameter values, a subsequent parameter value and an initial guess for the Newton-Raphson method are extrapolated from the previous three parameter values and respective solutions. When the Newton-Raphson iterations fail, the step along the arc length is reduced until the solution is recovered.

5.4 Results

5.4.1 Linear stability of Hartmann flow

The linear stability analysis of the Hartmann flow is considered first. The marginal Reynolds number defines the threshold at which perturbations with positive temporal growth rate $\Re[\lambda]$ appear. Numerically calculated marginal Reynolds numbers and the associated phase velocities of neutrally stable modes are plotted in Fig. 5.2 (a) and

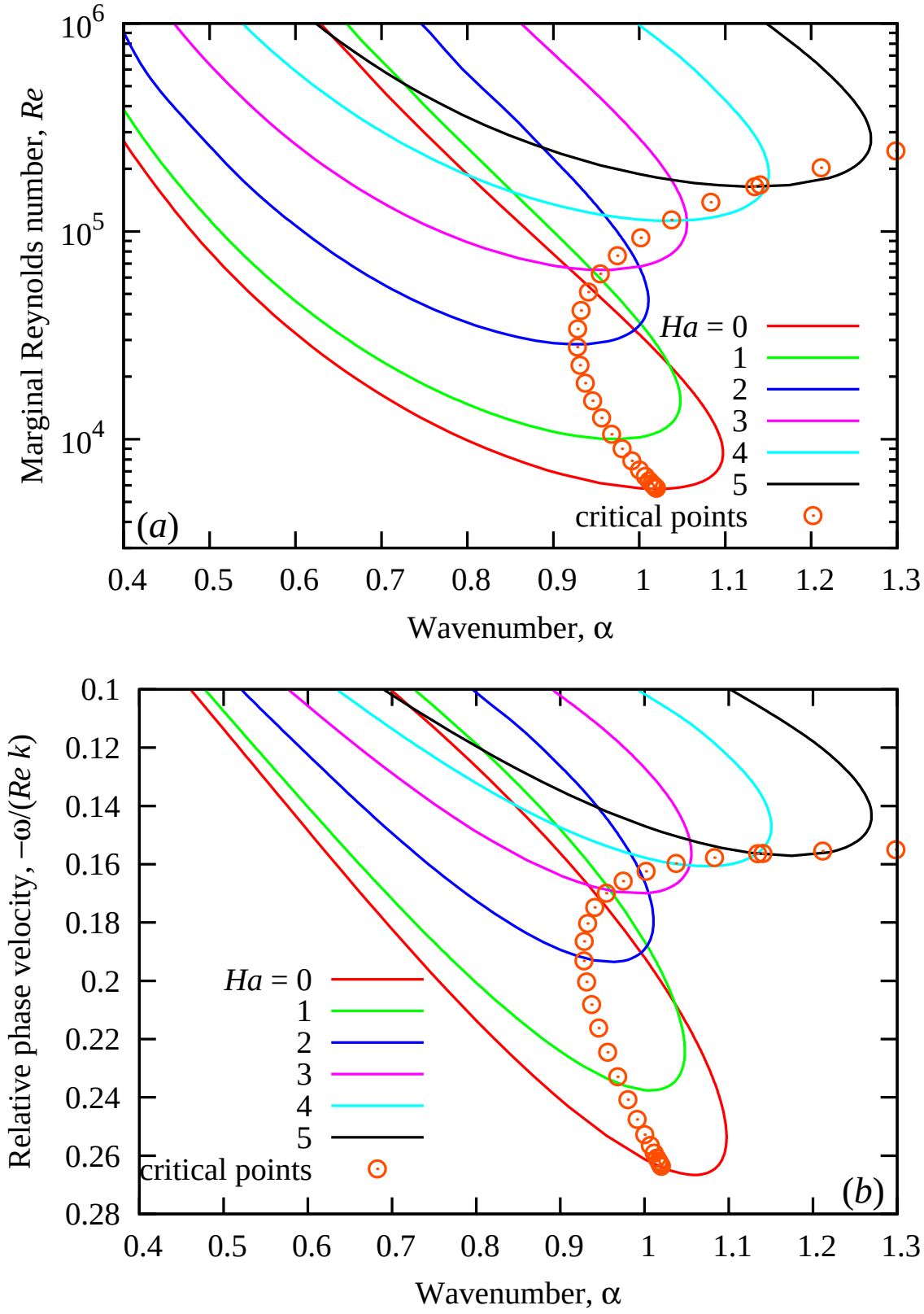

Figure 5.2: Marginal Reynolds number (a) and the relative phase velocity (b) of neutrally stable modes against the wavenumber for various Hartmann numbers.

(b) respectively versus the wavenumber α for several Hartmann numbers. The non-magnetic case ($Ha = 0$) corresponds to the classic plane Poiseuille flow. First, it is seen that only the modes with sufficiently small wavenumbers, i.e. sufficiently long waves, can become linearly unstable. Second, each such mode can be linearly unstable only in a limited range of Reynolds numbers. Namely, besides the lower marginal Reynolds number by exceeding which mode of a given wavenumber turns linearly unstable, there is also an upper marginal Reynolds number by exceeding which it becomes linearly stable. Linear stability threshold corresponds to the lowest marginal Reynolds number which is referred to as the critical Reynolds number. For the non-magnetic case, ($Ha = 0$), the critical Reynolds number is $Re_l = 5772.22$, and it occurs at the critical wavenumber $\alpha_l = 1.02055$ [17]. The former is seen in Fig. 5.2 to rise with the Hartmann number, which means that the flow is stabilized with the increase in the magnetic field. The critical wavenumber first decreases and then starts to rise at $Ha \gtrsim 2$.

As seen in Figures 5.3 (a) - (c), the critical Reynolds number Re_l and the associated wavenumber α_l both increase in a sufficiently strong magnetic field ($Ha \gtrsim 10$) directly with the Hartmann number while the relative phase speed $c = -\omega/Re\alpha$ tends to a constant. The best fit of the numerical results yields

$$Re_l \sim 4.83 \times 10^4 Ha, \tag{5.34}$$

$$\alpha_l \sim 0.162 Ha, \tag{5.35}$$

$$c_l \sim 0.155, \tag{5.36}$$

These asymptotics agree well with the highly accurate results of Takashima [60]. Note that besides the original instability mode, which develops from the non-magnetic one, another linearly unstable mode appears at $Ha \gtrsim 6.5$. At higher Hartmann numbers, the second mode closely approaches the original one. Both modes differ by their z-parity; the transverse velocity distribution is an even function of z for the former and an odd function for the latter. This difference becomes unimportant in a sufficiently

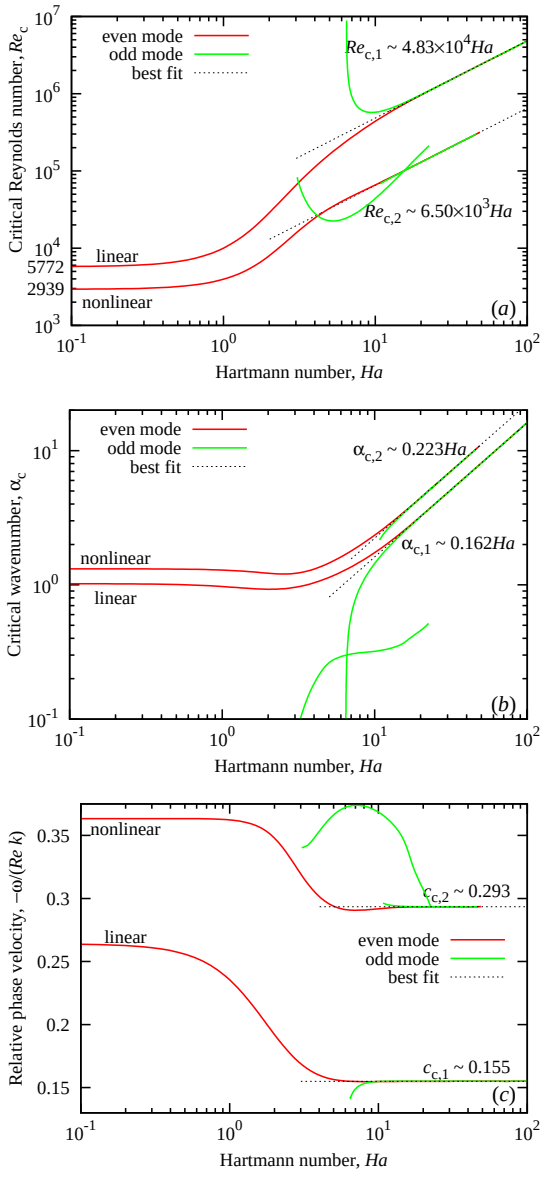

Figure 5.3: Critical Reynolds number (a), wavenumber (b) and phase speed (c) for even and odd modes of linear and nonlinear instabilities against the Hartmann number.

strong magnetic field when $Ha \gtrsim 20$. In such a magnetic field the instability becomes localized in the so-called Hartmann boundary layers of characteristic thickness

$$\delta \sim h/Ha. \tag{5.37}$$

First, this is implied by the above variations of Re_l and α_l, which both become independent of Ha when δ is used instead of h as the characteristic length scale. Second, it is also confirmed by the streamline patterns of the critical perturbations for both modes which are seen in Fig. 5.4 to be very similar to each other. The perturbations differ by the direction of circulation in the vortices at the opposite walls, which is the same for the even mode and opposite for the odd mode. The co-rotating vortices in the even mode are connected through the mid-plane and, thus, enhance each other, whereas the counter-rotating vortices in the odd mode tend to suppress each other. The interaction of the vortices at the opposite walls becomes insignificant in strong magnetic field where the vortices are effectively separated by a stagnant liquid core. This effect has implications for the subsequent weakly nonlinear analysis.

5.4.2 Weakly nonlinear subcritical equilibrium states

As noted previously, the coefficients (5.27, 5.28) and, thus, the equilibrium amplitude (5.29) determined by them depend on the normalization of the linear eigenfunction. This is because the equilibrium perturbation (5.22), which is supposed to be independent of normalization, is given by the product of both quantities. For the classic plane Poiseuille flow, Landau coefficients are usually calculated by normalizing the linear eigenfunction at the middle of the layer as $\hat{w}_{1,1}(0) = 1$. This standard normalization, however, is not suitable for the Hartmann flow. First, it is not compatible with the odd mode, which satisfies the symmetry condition $\hat{w}_{1,1}(0) = 0$. Second, as discussed above, the same condition is effectively satisfied also by the even mode when it becomes suppressed in the core of the layer by a sufficiently strong magnetic field. Thus, instead of the standard normalization condition, it is necessary to use $\hat{w}''_{1,1}(0) = 1$,

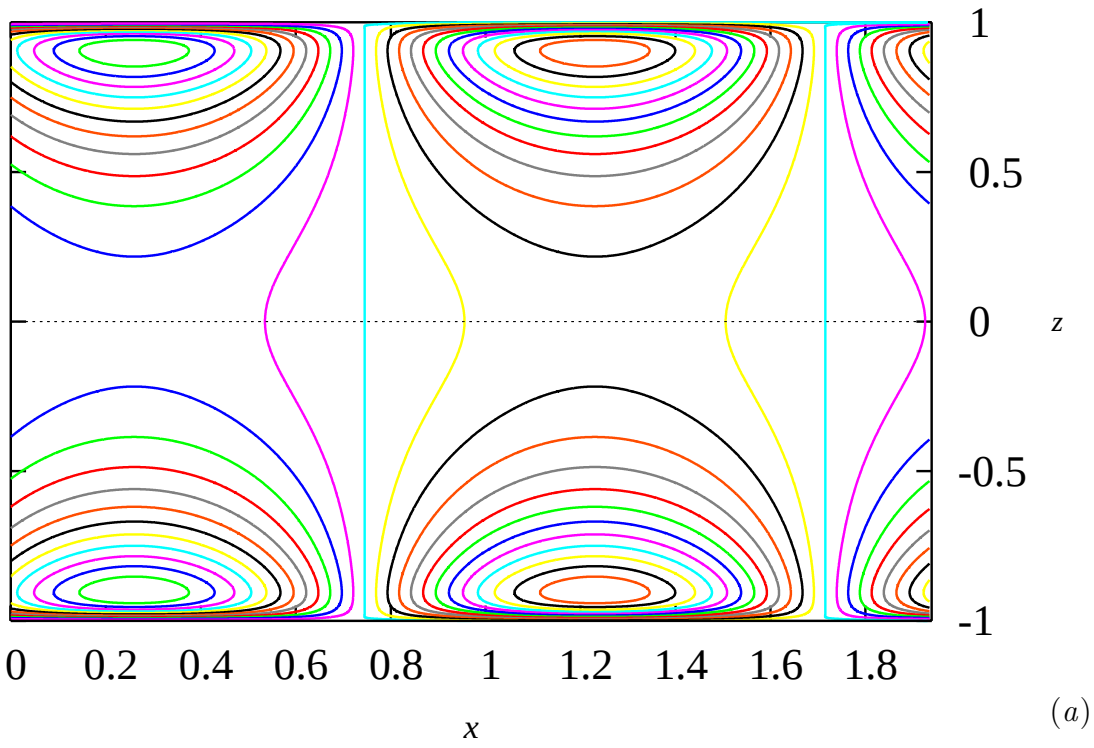

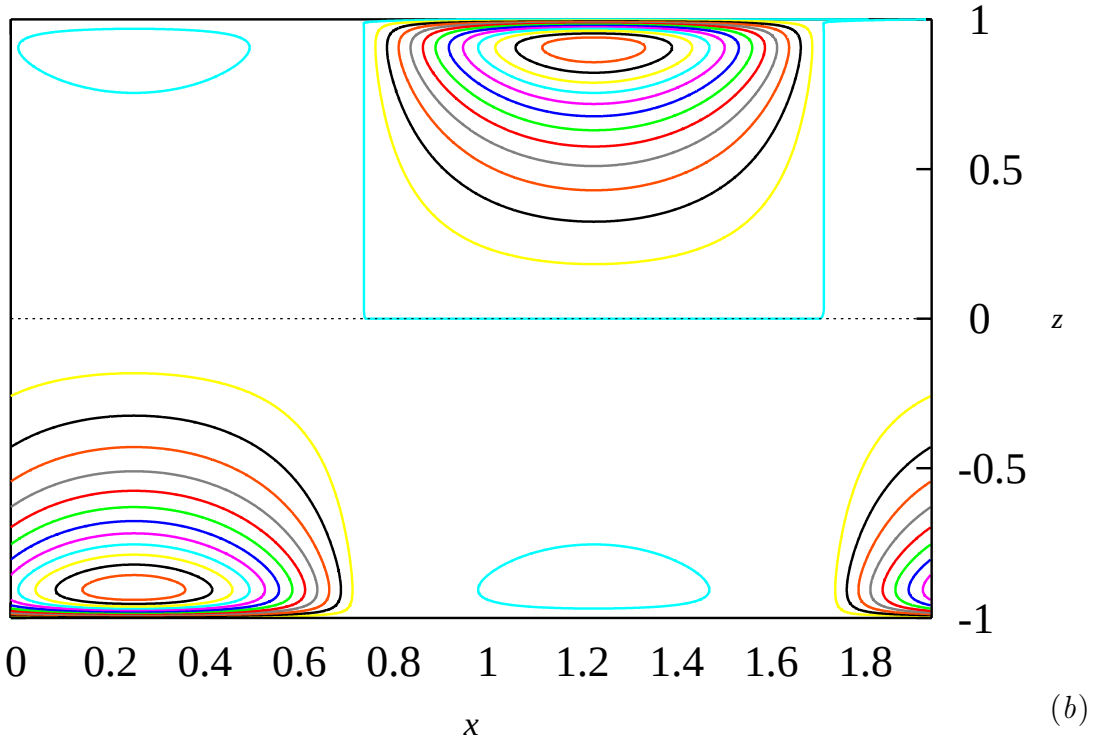

Figure 5.4: Instantaneous streamlines of critical perturbations for even (a) and odd (b) modes at $Ha = 20$. The x-offset is defined by the normalization condition $\hat{w}''_{1,1}(1) = 1$.

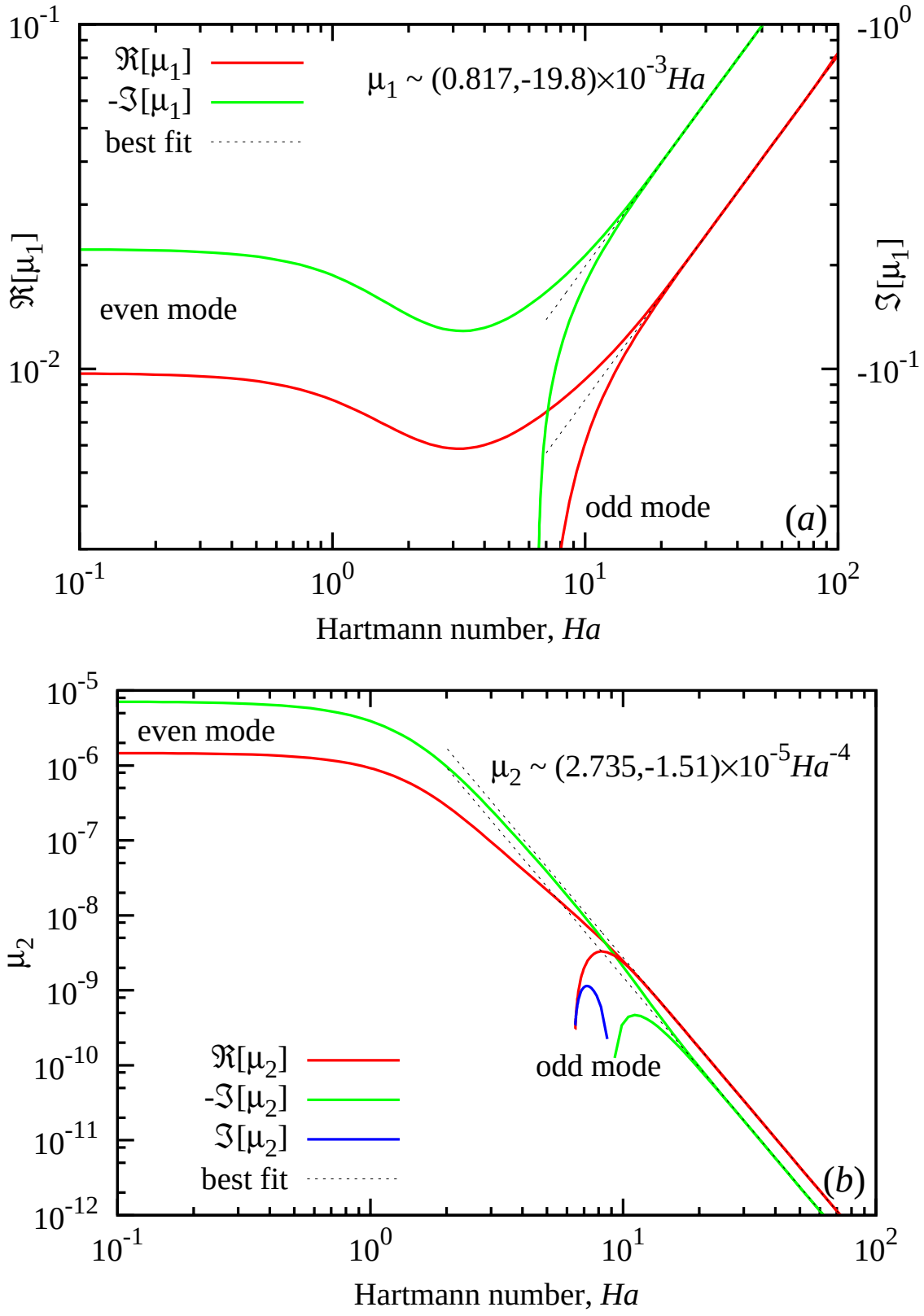

Figure 5.5: Linear growth rate coefficient μ_1 (a) and and the first Landau coefficient μ_2 (b) for odd and even instability modes normalized with $\hat{w}''_{1,1}(1) = 1$.

which can related by Eq. (5.13) to the vorticity at the wall. This normalization condition is straightforwardly applicable to both even and odd modes regardless of the field strength.

The linear growth rate coefficient μ_1 and the first Landau coefficient μ_2 computed with this normalization condition for both critical modes are plotted in Fig. 5.5, against the Hartmann number. As seen from Eq. (5.26) these coefficients define the variation of the complex growth rate $\lambda_2 = \mathrm{i}\omega_2$. The coefficient μ_1 is associated with the deviation of the Reynolds number from its linear stability threshold Re_2, while μ_2 accounts for the effect of amplitude A. The real part of μ_1 is positive because the critical mode becomes linearly unstable as Re exceeds Re_l. The positive $\Re[\mu_2]$, which is seen in Fig. 5.5(b) to be the case for all Hartmann numbers, means that the perturbation amplitude has a positive feedback on its growth rate. Consequently, the Hartmann flow is sub-critically unstable regardless of the magnetic field strength. In sufficiently strong magnetic fields, the best fit of numerical results yields

$$\mu_1 \sim (0.814 - \mathrm{i}19.8) \times 10^{-3} Ha, \tag{5.38}$$

$$\mu_2 \sim (2.73 - \mathrm{i}1.50) \times 10^{-5} Ha^{-4}, \tag{5.39}$$

which substituted into Eq. (5.29) results in

$$|A|^2 \sim 29.8 Ha^6 (R_l - R), \tag{5.40}$$

where $R = Re/Ha$ is a Reynolds number based on the the Hartmann layer thickness (5.37). The scaling above is consistent with the relevant length scale of instability determined by Eq. (5.37) which for the choice of the characteristic velocity $v_\delta = \nu/\delta$ leads to $A \sim w'' \sim Ha^3$. This last result implies that the velocity of equilibrium perturbation increases asymptotically as $w \sim Ha$, which is similar to the variation of Re_l.

The perturbation of the mean flow $\hat{u}_{0,2}(z)$ and the complex amplitude distribution of the second harmonic $\hat{w}_{2,2}$, which both are produced by the nonlinear self-interaction

$M \times N$	Re_n	α_n	$c_n = -\omega/Re_n\alpha$	$A_E^2(\times 10^3)$	$A = \hat{w}_1(0)$
32×1	2825.56	1.22223	0.345828	6.14777	131.655
32×2	2701.72	1.31294	0.366290	4.92982	118.206
32×3	2911.36	1.31824	0.364025	4.33693	119.120
32×4	2933.53	1.32425	0.364470	4.50019	121.571
32×6	2940.08	1.31701	0.363147	4.26584	119.171
32×8	2939.05	1.31752	0.363251	4.28277	119.330
32×10	2939.04	1.31751	0.363250	4.28224	119.324
40×10	2939.04	1.31750	0.363249	4.28224	119.320

Table 5.1: Critical parameters for the appearance of 2D travelling waves in plane Poiseuille flow computed with various number of collocation points M and harmonics N.

of the basic harmonic, are plotted in Fig. 5.6. The perturbation of the flow rate is defined by the stream function $\hat{\psi}_{0,2}(z) = \int_0 \hat{u}_{0,2}(z)\, dz$. For a strong magnetic field, the best fit yields

$$\hat{\psi}_{0,2}(1) \sim -4.45 \times 10^{-5} Ha^{-6}, \tag{5.41}$$

which according to Eq. (5.23) needs to be multiplied with the $|A|^2$ given by Eq. (5.40) to obtain the dimensionless perturbation of the flow rate over the half channel. Note that Ha cancels out in this product which is consistent with the dimensional arguments considered in the paragraph above. Similarly, we can introduce stream functions for higher harmonics which satisfy $w_n = -\partial_x \psi_n$ and, thus, lead to the following simple expressions for the complex amplitudes $\hat{\psi}_n = \mathrm{i}\alpha_n^{-1}\hat{w}_n$. The streamlines of the combined second-order perturbation given by $\hat{\psi}_{0,2}(z) + 2\Re[\hat{w}_{2,2}(z)\mathrm{e}^{\mathrm{i}2\alpha_c x}]$ are shown in Fig. 5.7 for the even mode near the upper wall at $Ha = 20$.

5.4.3 Nonlinear 2D travelling waves

The goal of this section is to find out how far the subcritical for equilibrium states extend below the linear stability threshold of the Hartmann flow. It means that it is no longer assumed that the perturbation amplitude is small and a travelling wave solution is searched for as described in Sec. 5.2.2. This method is first validated by computing the critical Reynolds number for 2D travelling waves in the plane Poiseuille flow which corresponds to $Ha = 0$. It means that Eq. (5.33) is solved for Re as a function of A

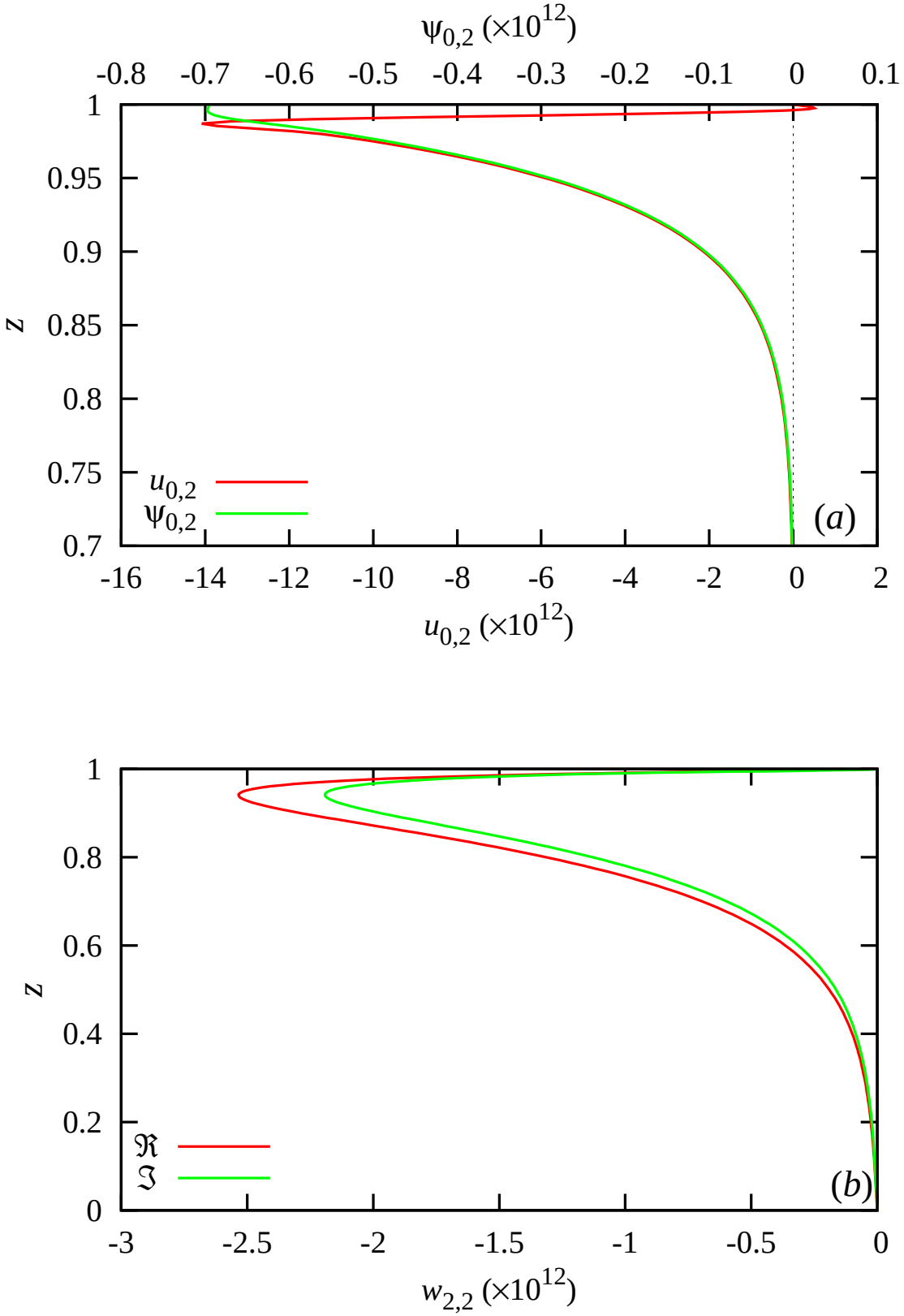

Figure 5.6: Velocity $\hat{u}_{0,2} = \hat{\psi}'_{0,2}$ and the associated stream function $\hat{\psi}_{0,2}$ of the mean flow perturbation (a); the real and imaginary parts of the second harmonic amplitude $\hat{w}_{2,2}$ (b) for the even mode at $Ha = 20$.

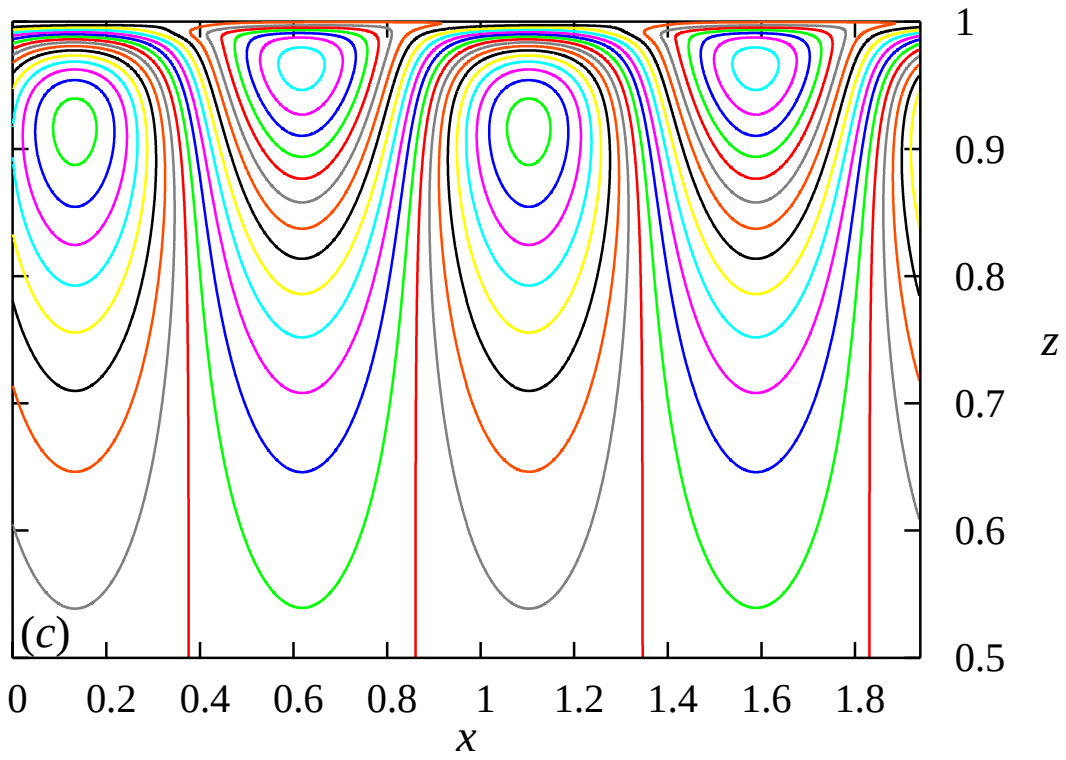

Figure 5.7: Streamlines of the combined second-order perturbation given by $\hat{\psi}_{0,2}(z) + 2\Re[\hat{w}_{2,2}(z)\mathrm{e}^{\mathrm{i}2\alpha_c x}]$ for the even mode near the upper wall.

and α and then the solution is minimised over both variables. This yields the critical values which are shown in Table 5.1 for various number of collocation points M and harmonics N. The critical parameters for the first three resolutions perfectly agree with those found by [71], whereas for the last three resolutions both Re and α agree up to 5 dp with the accurate results obtained by [72] using $2M = 70$ Chebyshev polynomials and $N = 22$ Fourier modes. To characterise the deviation of velocity distribution (5.10) from the base state (5.4), besides the transverse velocity normalization amplitude A introduced in Eq. (5.33) the amplitude associated with the energy of perturbation scaled by energy of the basic flow is used

$$A_E^2 = \int_0^1 \overline{|\boldsymbol{v}(x,z) - \boldsymbol{v}_0(z)|^2} dz \Big/ \int_0^1 |\boldsymbol{v}_0(z)|^2 dz, \tag{5.42}$$

where the overbar stands for streamwise average. This quantity slightly differs from that used by [71] which neglects the contribution of the mean flow perturbation.

By starting with a relatively low Hartmann number $Ha = 1$ for which the flow becomes linearly unstable at $Re_n = 10016.3$ with $\alpha_n = 0.971827$ (see Fig. 5.2). Energy amplitude of equilibrium states versus the wavenumber is plotted in Fig. 5.8 for various subcritical values of Re. As for plane Poiseuille flow, equilibrium states form closed contours, which shrink as Re is reduced and collapse to a point at the critical $Re_n = 3961.36$ where 2D travelling waves vanish. It means that for subcritical Reynolds numbers there is not only an equilibrium perturbation with a minimum amplitude but also one with maximum amplitude. Both these amplitude extremes are plotted in Fig. 5.8 together with the respective value of $\hat{w}_1''(1)$. The latter can be compared with the weakly nonlinear equilibrium amplitude (5.29). As seen, the lower branch of $\hat{w}_1''(1)$ is predicted well by weakly nonlinear solution for subcritical Reynolds numbers down to $Re \approx 7000$.

A similar structure of subcritical equilibrium states is seen also in Fig. 5.9 for $Ha = 5$ and $Re_n = 43\,8302$. At this large Re, it becomes difficult to compute accurately the upper equilibrium states which require a numerical resolution of at least 48×16. The strongly subcritical states, which in this case extend down to $Re_n \approx 32860$, can

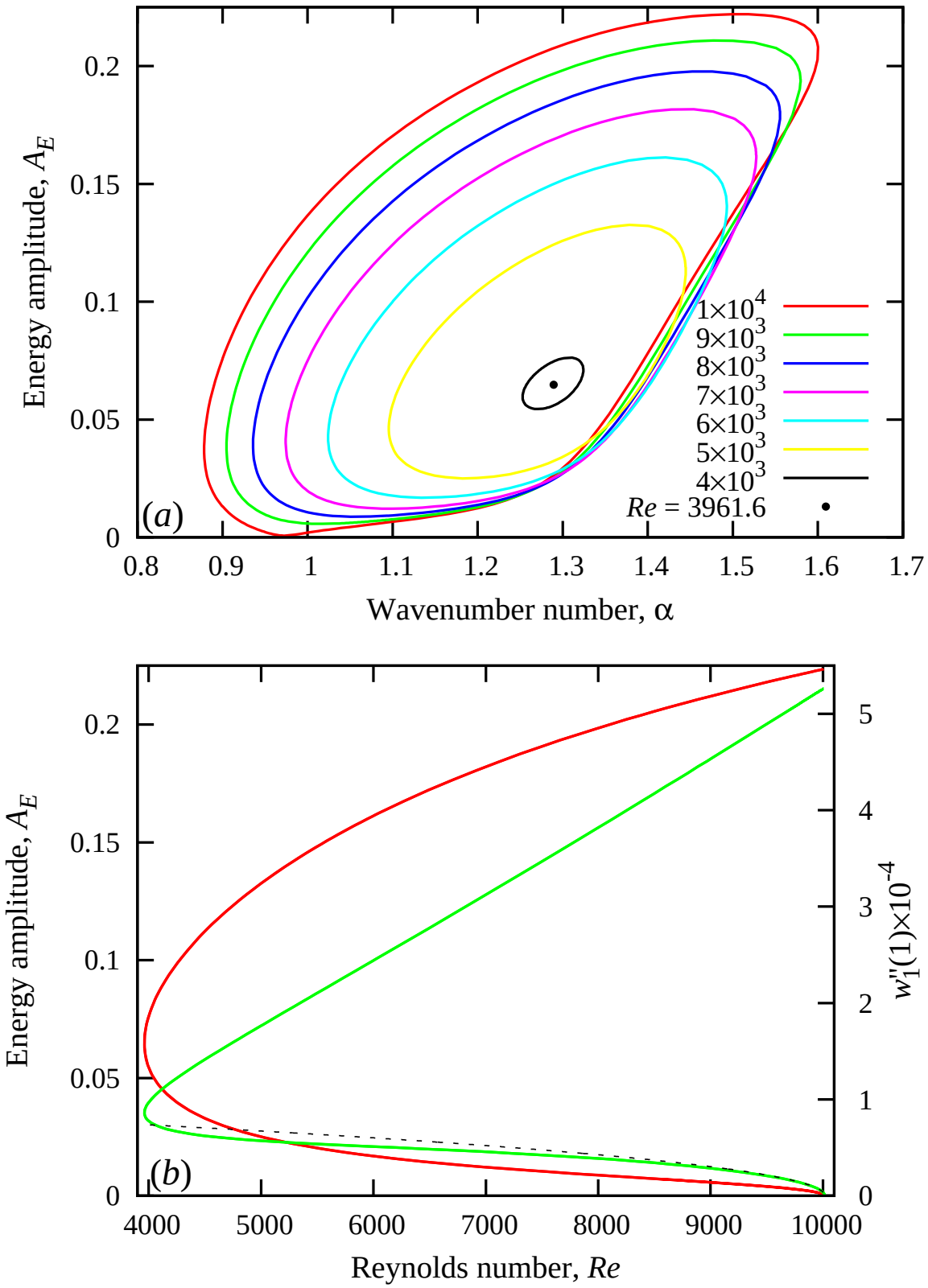

Figure 5.8: The energy amplitude of equilibrium states versus the wavenumber α for $Ha = 1$ and various Re computed with $M \times N = 32 \times 8$.

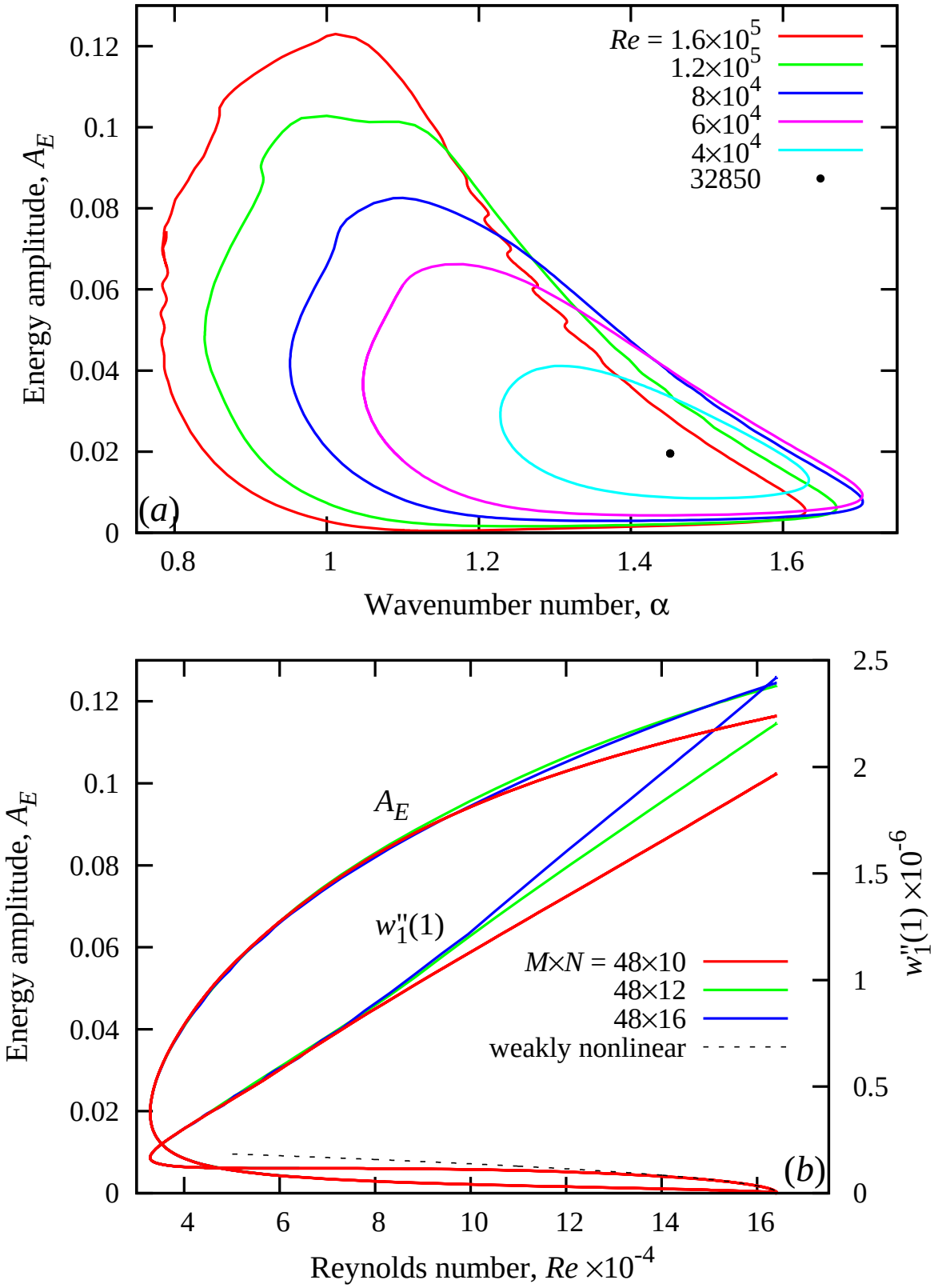

Figure 5.9: The energy amplitude of equilibrium states versus the wavenumber α for $Ha = 5$ and various Re computed with $M \times N = 48 \times 10 \cdots 16$.

reliably be computed with a substantially lower resolution of 48×10. In the following, the focus is on such strongly subcritical Reynolds numbers at which two-dimensional travelling waves emerge. The respective Reynolds number defines what is subsequently referred to as the two dimensional nonlinear stability threshold.

The critical Reynolds number and the wavenumber for the 2D nonlinear stability threshold are shown in Fig. 5.3 together with the critical parameters for the linear stability versus the Hartmann number. At small Hartmann numbers, instability is associated with the even mode for which 2D travelling waves appear at $Re_n = 2939$, which is the 2D nonlinear stability threshold of plane Poiseuille flow shown in Table 5.1. As the Hartmann number exceeds $Ha \approx 2.8$, which is about half of the respective value for the linear instability, an odd equilibrium mode appears with a large Reynolds number and a small wavenumber. This long-wave odd mode exists only within a limited range of Hartmann numbers up to $Ha \approx 20$. At $Ha \approx 10$ another odd mode appears with a slightly higher Reynolds number and much shorter wavelength. At $Ha \approx 15$ the Reynolds number of the latter mode becomes smaller than that for the long-wave mode while the characteristics of this short-wave odd mode closely approach those of the original even mode. In sufficiently strong magnetic field, the critical Reynolds number and wavenumber for both nonlinear modes increase with the Hartmann number similarly to the respective threshold parameters for the linear instability. Namely, for $Ha \gtrsim 20$ the best fit yields

$$Re_n \sim 6.50 \times 10^3 Ha, \tag{5.43}$$

$$\alpha_n \sim 0.223 Ha, \tag{5.44}$$

$$c_n \sim 0.293. \tag{5.45}$$

It is important to notice that the critical Reynolds number above is almost by an order of magnitude lower than that for the linear instability given by Eq. (5.34). In the mean-field approximation using only one harmonic, it is found that $Re_n \sim 12.3 \times 10^3 Ha$, which is almost by a factor of two higher than the accurate result above and coincides

with the result of Lifshits and Shtern [63].

Besides the threshold parameters above the critical two-dimensional travelling wave is characterised also by its energy amplitude A_E and the flow rate perturbation

$$\hat{\psi}_0(1) = \int_0^1 (\hat{u}_0(z) - \bar{u}_0(z))\, dz \tag{5.46}$$

which are plotted in Fig. 5.10 versus the Hartmann number. At large Ha the latter is seen to approach a constant value $\hat{\psi}_0(1) \sim -242$, which means that in strong magnetic field critical flow rate perturbation becomes independent of the magnetic field strength. This is because the flow rate is determined by the product of the characteristic length and velocity scales where the latter varies inversely with the former. Thus, as the Hartmann layer thickness represents the characteristic length scale in a strong magnetic field, this cancels out the flow rate perturbation. The same arguments also explain the scaling of the energy perturbation (5.42) inversely with Ha which leads to $A_E \sim 0.0317 Ha^{-1/2}$ for the even mode as well as for the odd short-wave mode (see Fig. 5.10). The same relation for both instability modes again implies that the perturbations originating in the Hartmann layers at the opposite walls do not affect each other in strong enough magnetic field.

Streamlines of the critical finite-amplitude perturbations of both symmetries are plotted in Fig. 5.11 for $Ha = 10$ and Fig. 5.12 for $Ha = 20$. Note that the streamlines of the odd mode are mirror-symmetric with respect to the mid-plane $z = 0$ whereas those of the even mode possess a central rather than a $z-$reflection symmetry. As discussed in the description of the numerical method, this is because all stream function harmonics of the odd mode are odd functions of z while those of the even mode have alternating z parities. It is interesting to note that the long-wave odd mode at $Ha = 10$ represents a localized disturbance consisting of a pair of mirror-symmetric vortices. As discussed above, this long-wave equilibrium state disappears at $Ha \gtrsim 20$. The short-wave state, which replaces the former at higher Hartmann numbers, is seen in Fig. 5.11 and Fig. 5.12 to differ from that of the even mode only by a half wave length shift between the top and bottom parts of the layer.

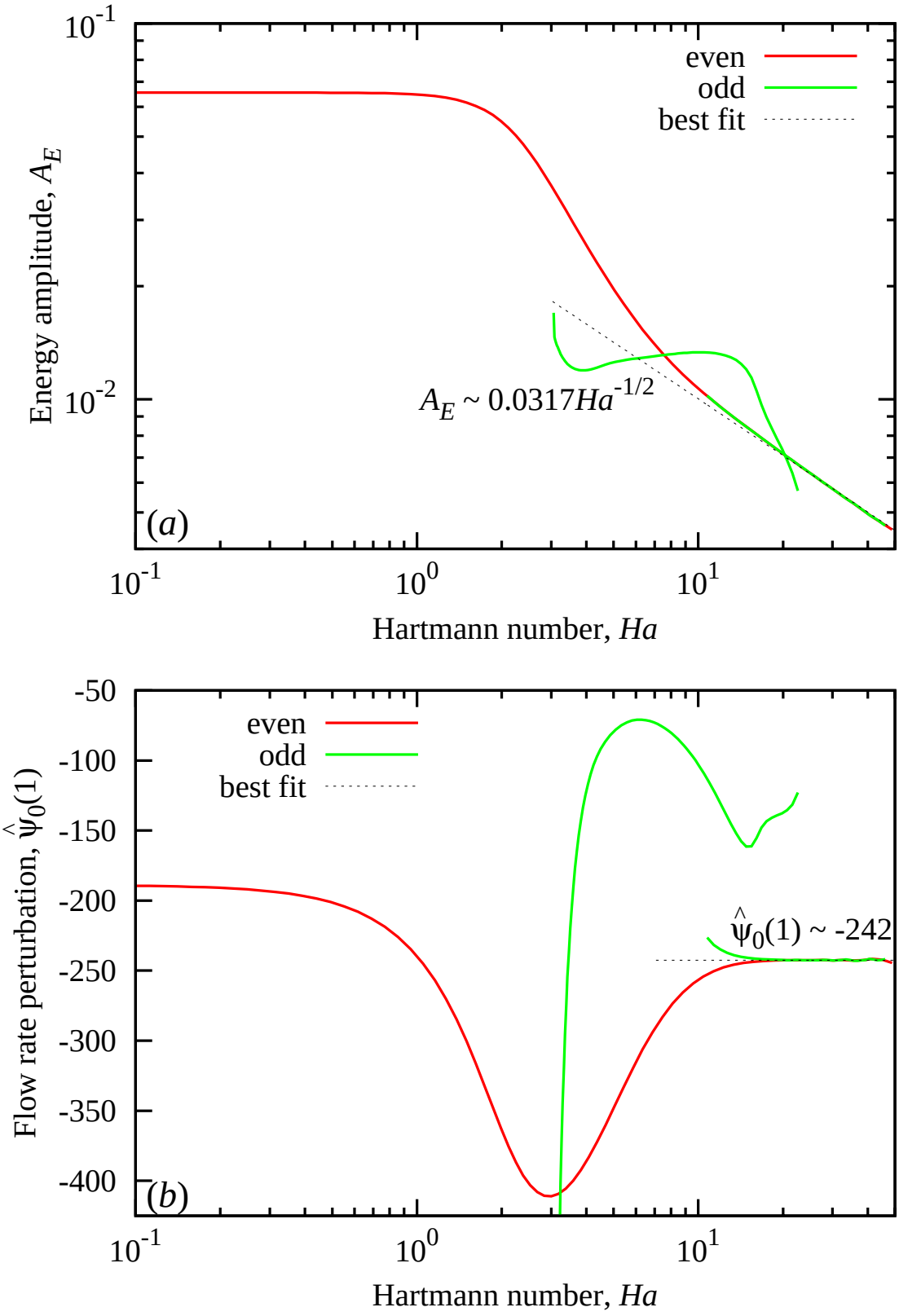

Figure 5.10: Energy amplitude (top) and the flow rate perturbation (bottom) at the 2D nonlinear instability threshold for even and odd modes versus the Hartmann number.

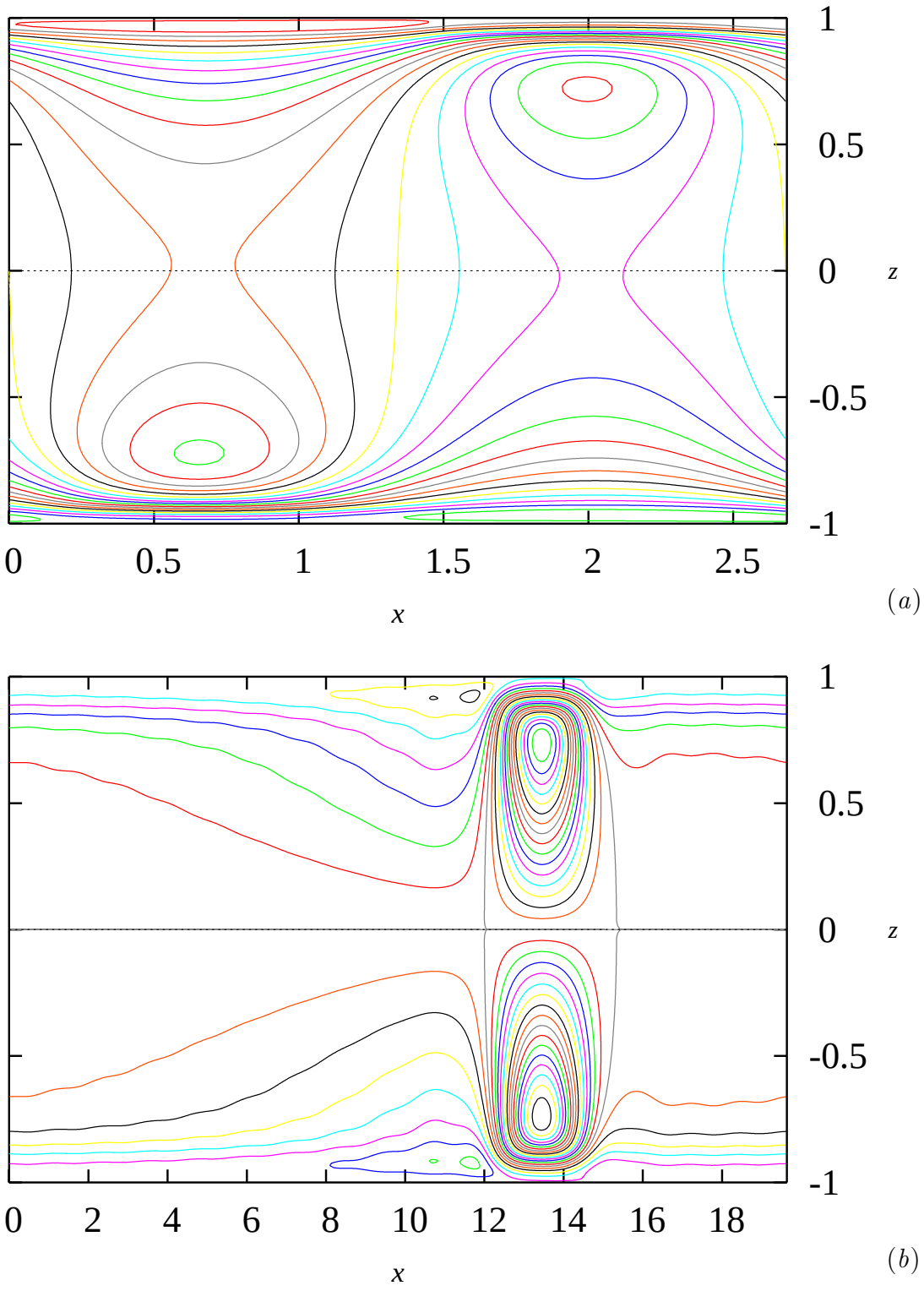

Figure 5.11: Streamlines of even (top) and odd (bottom) critical finite-amplitude perturbations for $Ha = 10$.

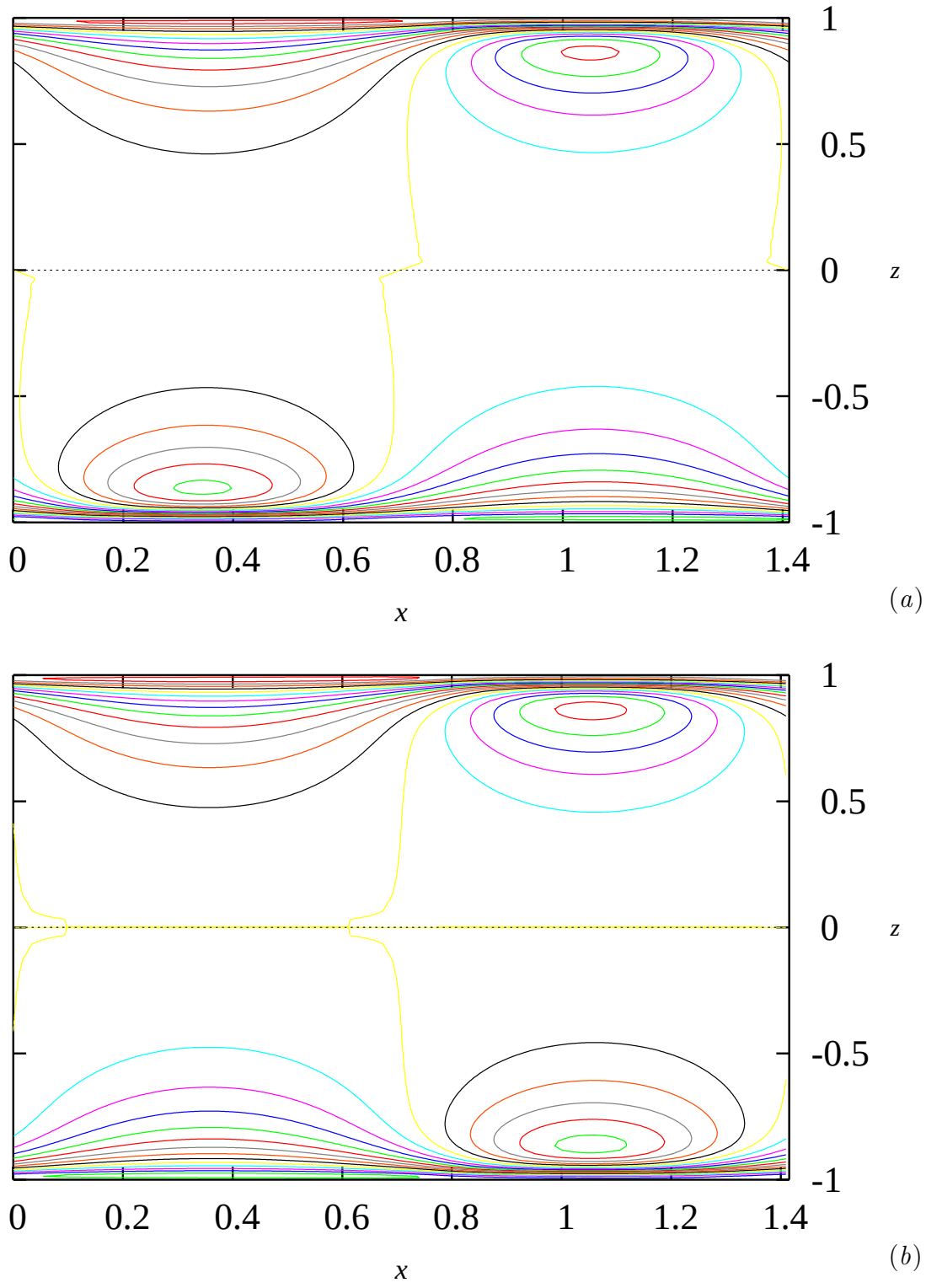

Figure 5.12: Streamlines of even (top) and odd (bottom) critical finite-amplitude perturbations for $Ha = 20$.

5.4.4 2D superharmonic stability of travelling waves

Growth rates of even and odd superharmonic disturbances of the even travelling wave mode are plotted in Fig. 5.13 for $Ha = 1$ and $Ha = 5$. As discussed in Sec. 5.2.2, the subcritical equilibrium states bifurcating from the base flow are unconditionally unstable. This is confirmed by the positive growth rate of the even disturbance, which is seen in Fig. 5.13 (top) to persist down the lowest possible Reynolds number Re_q based on the flow rate. The latter is linked to the original Reynolds number Re based on the mean pressure gradient as

$$Re_q = Re + \hat{\psi}_0(1)/\bar{\psi}(1),$$

where $\bar{\psi}(1) = \int_0^1 \bar{u}(z)\,dz = (\cosh(Ha) - Ha^{-1}\sinh(Ha))/(\cosh(Ha) - 1)$ is the flow rate of the unperturbed Hartmann flow (5.6) and $\hat{\psi}_0(1)$ is the flow rate perturbation defined by Eq. (5.46) and plotted in Fig. 5.10 (bottom). The change of stability of the even mode coincides with the lowest value of Re_q because the superharmonic disturbance, like the subharmonic ones, limiting case of which the former represents, preserves the flow rate and, thus, also Re_q. Consequently, the solution at the lowest value of Re_q, where two different equilibrium solutions merge, is invariant and, thus, neutrally stable with respect to the small-amplitude superharmonic perturbation given by the difference between these two solution branches. Note that owing to the phase invariance of the travelling wave solution there is another neutrally stable disturbance corresponding to a small phase shift of the original solution which is present at all possible Re.

The growth rate of the even disturbance, which was positive and purely real for the unstable lower solution branch turns negative as the solution passes through the turning point at the critical Re_q and proceeds to the upper branch. For $Ha = 1$ the original purely negative eigenvalue subsequently merges with another similar eigenvalue which results in two complex conjugate eigenvalues with negative real part. Note that a purely real growth rate describes disturbances that travel synchronously with the

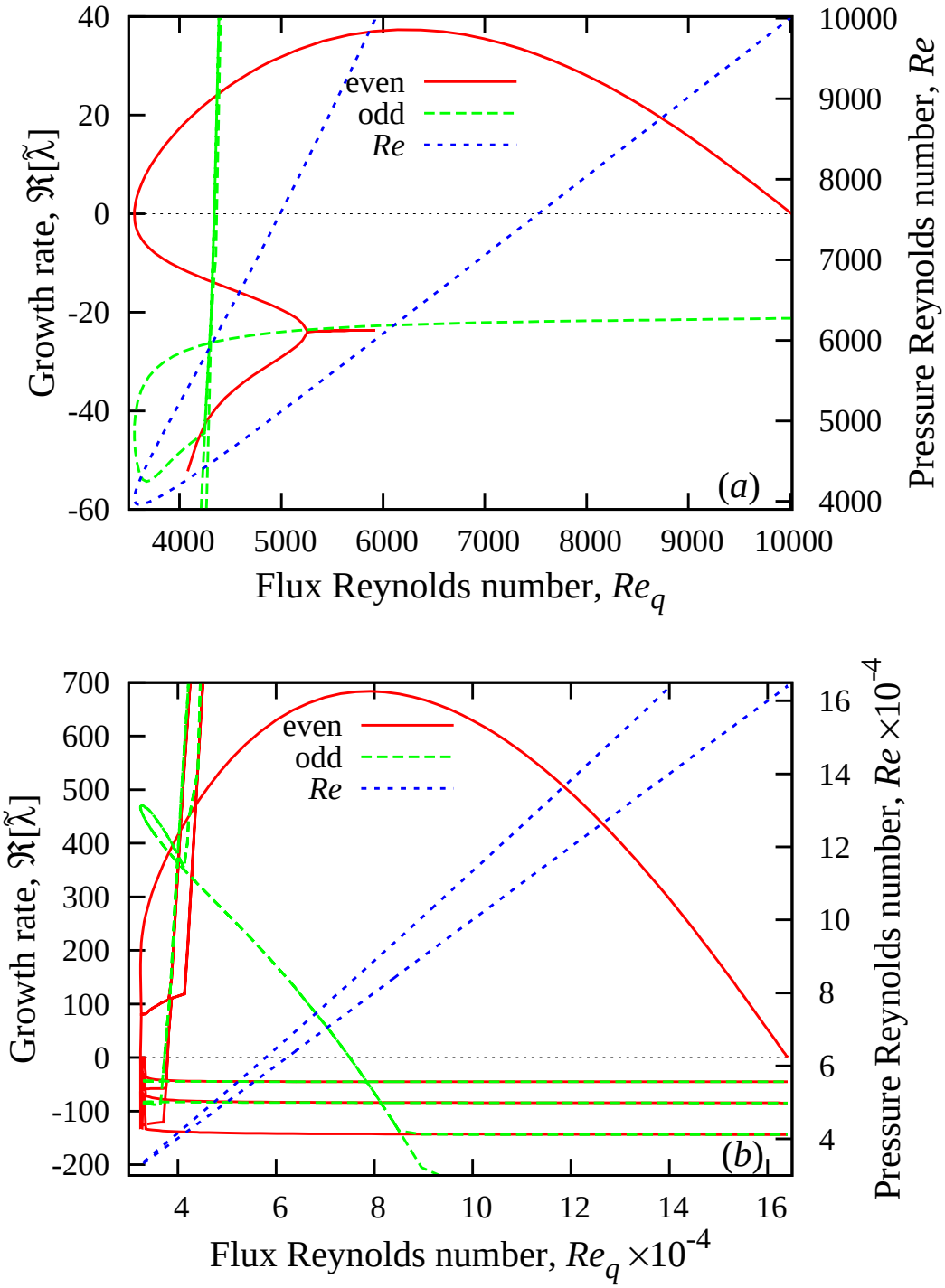

Figure 5.13: Growth rates of even and odd superharmonic 2D disturbances versus the flux Reynolds number for the even travelling wave mode at $Ha = 1$ (top) and $Ha = 5$ (bottom). The original Reynolds number based on the mean pressure gradient is shown on the right hand side axis.

same phase speed as the background wave whereas the complex growth rate describes asynchronous disturbances which lead to the solutions which are quasiperiodic in the laboratory frame of reference and periodic in the frame of reference moving with the phase speed of travelling wave. Several strongly unstable asynchronous disturbances of the odd symmetry are seen in Fig. 5.13 (top) to emerge shortly after the turning point. More such type of disturbances of both symmetries are present at $Ha = 5$. Some of these quasiperiodic solutions may extend to the subcritical Reynolds numbers below the limit point for travelling waves, which, however, is outside the scope of the present study. For the non-magnetic case, this problem has been considered by Barkley [106] using a generalization of the fixed pressure gradient condition whose physical consistency was discussed in Sec. 5.2.4.

Chapter 6

Conclusions and Summary

The present study was concerned with the stability of MHD channel flow in a transverse magnetic field. First, linear stability of this flow was revisited and its critical Reynolds number Re_l reproduced. As the magnetic field increases, Re_l was found to rise in agreement with the previous results from its hydrodynamic limit $Re_l = 5772$ to $Re_l \sim 4.83 \times 10^4 Ha$ in strong magnetic field. Two different instability modes were found to become linearly unstable when Reynolds number exceeds the latter limit. The first mode, which is related to the original hydrodynamic instability, has a symmetric (even) transverse velocity distribution over the channel depth. The second mode, which emerges at $Ha \approx 6$, has an anti-symmetric (odd) transverse velocity distribution. Physically, the two instability modes differ by the direction in which vortices at the opposite walls rotate. For the even mode, the vortices at the opposite walls rotate in the same sense, whereas for the odd mode they do it in the opposite senses. The vortices at opposite walls enhance each other in the first case, and hinder in the second case. This results in the stability threshold for the even mode being slightly lower than that for the odd mode. Note that the interaction of the vortices occurs mostly through their circulation which adds up for the co-rotating vortices and cancels out for counter-rotating ones. Namely, co-rotating vortices are weakly connected by common streamlines along which they share some flow rate, which is not the case for the counter-rotating vortices. As the magnetic field increases, the interaction of

vortices at opposite walls weakens and becomes virtually negligible in strong magnetic fields, where the critical Reynolds numbers for the two instability modes converge. This is because the size of unstable vortices shrinks directly with the thickness of the Hartmann boundary layer, which represents the essential length scale of this instability and is roughly Ha times smaller than the channel width. Therefore, both the critical Reynolds number and the wavenumber in a strong magnetic field scale directly with the Hartmann number.

Next, using an efficient numerical approach, which was developed for the purpose of this study, the first Landau coefficient and the linear growth rate correction were computed. These coefficients determine weakly nonlinear evolution of finite small-amplitude disturbances in the vicinity of linear stability threshold. Hartmann flow was found to be subcritically unstable regardless of the magnetic field strength. Namely, finite amplitude disturbances can be become unstable at Reynolds numbers below the linear stability threshold of Hartmann flow. Equilibrium amplitude of subcritical transverse velocity disturbances, which are inherently unstable, were found to vary as $A \sim Ha(R_l - R)^{1/2}$, where $R = Re/Ha$ is a Reynolds based on the Hartmann layer thickness.

Finally, using the Newton-Raphson method the fully nonlinear 2D travelling wave solutions were traced. These solutions emanate at the linear stability threshold as a result of subcritical bifurcation. Such equilibrium states, which without the magnetic field extended down to $Re_n = 2939$, were found in strong magnetic field down to $Re_n \sim 6.50 \times 10^3 Ha$. Although this critical Reynolds number is almost an order of magnitude lower than the linear stability threshold of Hartmann flow, it is still more than an order of magnitude greater than that at which turbulence is observed in this type of flow. Subcritical equilibrium states in the Hartmann flow, as those in plane Poiseuille flow, are likely to be unstable not only with respect to 2D superharmonic disturbances considered in this study but also to more general 3D disturbances like those considered originally by Orszag and Patera [31]. Three-dimensional equilibrium states bifurcating either from the 2D travelling waves [98] or infinity [87], as in plane

Poiseuille flow, may extend to lower subcritical Reynolds numbers and thus provide a more adequate threshold for the onset of turbulence in Hartmann flow. Such a possibility is supported by a very simple model involving interaction of just two mirror-symmetric oblique waves with the 2D second harmonic they produce, which yields for the Hartmann layer $R_n \approx 4670$ [107]. As for the 2D waves considered in this study, it is likely that a more accurate model including a sufficient number of higher harmonics would result in a substantially lower R_n.

The by-product of this study are two developments of numerical techniques for linear and weakly nonlinear stability analysis. Firstly, a simple technique for avoiding physically spurious eigenmodes in the solution of hydrodynamic stability problems was developed. The method was demonstrated on the Orr-Sommerfeld equation for plane Poiseuille flow, but then also used for Hartmann flow. The original fourth order differential equation was factorised into two second order differential equations using a vorticity-type auxiliary variable which has no explicit boundary conditions. The elimination of the vorticity boundary values using a capacitance matrix approach results in a standard eigenvalue problem. It was demonstrated that this can be achieved in two different ways. Apart from its simplicity, the main advantage of this method of eliminating spurious eigenmodes is that it can be applied to more general stability problems with more complex boundary conditions.

Secondly, an efficient method for evaluating Landau coefficients was developed. By applying the solvability condition to the discretised problem as opposed to the continuous problem, by using the left eigenvectors, was the main novelty. By not having to solve the adjoint problem the method was greatly simplified.

Bibliography

[1] Batchelor, G. K. (1967) *An Introduction to Fluid Dynamics*, Cambridge University Press.

[2] Reynolds, O. (1883) 'An experimental investigation of the circumstances which determine whether the motion of water shall be direct or sinuous, and of the law of resistance in parallel channels.' *Phil. Trans. Roy. Soc.* **174**, 935-82.

[3] Drazin, P. G. and Reid, W. H. (1981) *Hydrodynamic Stability*, Cambridge University Press.

[4] Schmid, P. J. and Henningson D. S. (2001) *Stability and Transition in Shear Flows*, Springer, New York.

[5] Davidson, P. A. (2001) *An Introduction to Magnetohydrodynamics*, Cambridge University Press, Cambridge, UK.

[6] Proctor, M. R. E. and Gilbert, A. D. (1964) *Lectures on solar and planetary dynamos*, Cambridge University Press

[7] Helmholtz, H. von (1968) 'Über discontinuirliche Flüssigkeitsbewegungen.' *Monats. Königl. Preuss. Akad. Wiss. Berlin.* **23**, 215-28.

[8] Kelvin, L. (1887) 'On the stability of steady and of periodic fluid motion.' *Philos. Mag.* **23**, 459-464.

[9] Rayleigh, L. (1880) 'On the stability, or instability, of certain fluid motions.' *Proc. London Math. Soc.* **11**, 57-70.

[10] Orr, W. M. F. (1907) 'The stability of instability of the steady motions of a perfect liquid and of a viscous liquid. Part I: A perfect liquid. Part II: A viscous liquid.'

[11] Sommerfeld, A. (1908) 'Ein Betrag zur hydrodynamischen Erklärung der turbulenten Flüssigkeitbewegungen.' In *Atti. del 4. Congr. Internat. dei Mat. III*, 116-124, Roma.

[12] Grosch, C. E. and Salwen, H. (1978) 'The continuous spectrum of the Orr-Sommerfeld equation. Part I: The spectrum and the eigenfunctions.' *J. Fluid Mech.* **87** 33-54

[13] Heisenberg, W. (1924) 'Über Stabilität und Turbulenz von Flüssigkeitsströmen.' *Ann. Phys. Lpz. (4)*, **74**, 577-627.

[14] Tollmien, W. (1929) 'Über die Entstehung der Turbulenz.' *Nachr. Ges. Wiss. Göttingen, Math-phys. Kl*, 21-44.

[15] Lin, C. C. (1945) 'On the stability of two-dimensional parallel flows.' *Quart. Appl. Math.* **3**, 117-142, 218-234 and 277-301.

[16] Lin, C. C. (1955) *The theory of hydrodynamic stability*, Cambridge University Press.

[17] Orszag, S. A. (1971) 'Accurate solution of the Orr-Sommerfeld stability equation.' *J. Fluid Mech.* **50**, 689-703.

[18] Thomas, L. H. (1953) 'The stability of plane Poiseuille flow.' *Phys. Rev. (2)*, **91**, 780-783.

[19] Davey, A. and Drazin, P. G. (1969) 'The stability of Poiseuille flow in a pipe.' *J. Fluid. Mech.* **36**, 209-218.

[20] Davey, A. (1973) 'A simple numerical method for solving Orr-Sommerfeld problems.' *Quart. J. Mech. Appl. Math.* **26**, 401-411

[21] Lee, L. H. and Reynolds, W. C. (1967) 'On the approximate and numerical solution of Orr-Sommerfeld problems.' *Quart. J. Mech. Appl. Math.* **20**, 1-22.

[22] Lanczos, C. (1938) 'Trigonometric interpolation of empirical and analytical functions.' *J. Math. Phys.* **17**, 123-199.

[23] Gottlieb, D. and Orszag, S. A. (1977) *Numerical Analysis of Spectral Methods: Theory and Applications*, SIAM, Philadelphia.

[24] Davies, S. J. and White, C. M. (1928) 'An experimental study of the flow of waiter in pipe of rectangular section.' *Proc. R. Soc. Lond.* **119**, 90-107.

[25] Patel, V. C. and Head, M. R. (1969) 'Some observations in skin friction and velocity profiles in fully developed pipe and channel flows.' *J. Fluid Mech.* **38**, 181-201.

[26] Nishioka, M., Iida, S. and Ichikawa, H. (1975) 'An experimental investigation on the stability of plane Poiseuille flow.' *J. Fluid Mech.* **172**, 731-751.

[27] Kozlov, V. V. and Ramazanov, M. P. (1980) 'Experimental investigation of the growth process of disturbances in Poiseuille flow.', *Preprint 21*, Inst. Theor. Appl. Mech., AN SSSR SO, Novosibirskj.

[28] Carlson, D. R., Widnall, S. E. and Peeters, M. F. (1982) 'A flow-visualisation study of turbulence in plane channel flow.' *J. Fluid Mec.* **121**, 487-505.

[29] Nishioka, M. and Asai, M. (1985) 'Some observations of the subcritical transition in plane Poiseuille flow.' *J. Fluid Mech.* **150**, 441-450.

[30] Alavyoon, F., Henningson, D. S. and Alfresson, P. H. (1986) 'Turbulent spots in plane Poiseuille flow - flow visualisation', *Phys. Fluids*, **29**, 1328-1331.

[31] Orszag, S. A. and Patera A. T. (1983) 'Secondary instability of wall-bounded shear flows.' *J. Fluid Mech.* **128**, 347-385.

[32] Landau, L. D. (1944) 'On the problem of turbulence.' *C.R. Acad. Sci. URSS*, **44**, 311-314.

[33] Landau L. and Lifshitz, E. M. (1987) *Fluid Mechanics*, Pergamon, London.

[34] Hopf, E. (1948) 'A mathematical example displaying features of turbulence.' *Comm. Appl. Math.* **1**, 303-322.

[35] Stuart, J. T. (1958) 'On the nonlinear mechanics of hydrodynamic stability.' *J. Fluid Mech.* **4**, 1-21.

[36] Gor'kov, L. P. (1957) 'Stationary convection in a plane liquid layer near the critical heat transfer point.' *Zh. Eksp. Teor. Fiz.* **33**, 402-407.

[37] Malkus, W. V. R. and Veronis, G. (1958) 'Finite amplitude cellular convection.' *J. Fluid Mech.* **4**, 225-260.

[38] Palm, E. (1960) 'On the tendency towards hexagonal cells in steady convection.' *J. Fluid Mech.* **8**, 183-192.

[39] Stuart, J. T. (1960) 'On the non-linear mechanics of wave disturbances in stable and unstable parallel flows.' *J. Fluid Mech.* **9**, 353-370.

[40] Watson, J. (1960) 'On the non-linear mechanics of wave disturbances in stable and unstable parallel flows.' *J. Fluid Mech.* **9**, 371-389.

[41] Huerre, P. and Rossi, M. (1988) 'Hydrodynamic instabilities in open flows.' In *Hydrodynamics and Nonlinear Instabilities*, 81-294, Ed. Godreche, C. and Manneville, P. Cambridge University Press

[42] Yaglom, A. M. (2012) *Hydrodynamic Instability and Transition to Turbulence*, ed. Frisch, U. Springer Verlag, New York.

[43] Reynolds, W. C. and Potter, M. C. (1967) 'Finite-amplitude instability of parallel shear flows.' *J. Fluid Mech.* **27**, 465-492.

[44] Sen, P. K. and Venkateswarlu, D. (1983) 'On the stability of plane Poiseuille flow to finite-amplitude disturbances, considering the higher-order Landau coefficients.' *J. Fluid Mech.* **133**, 179-206.

[45] Herbert, Th. (1983) 'On perturbation methods in nonlinear stability theory.' *J. Fluid Mech.* **126**, 167-186.

[46] Stewartson, K. and Stuart, J.T. (1971) 'A non-linear instability theory for a wave system in plane Poiseuille flow.' *J. Fluid Mech.* **48**, 529-545.

[47] Aranson, I. S. and Kramer, L. (2002) 'The world of the complex Ginzburg-Landau equation.' *Rev. Mod. Phys.* **74**, 99-143.

[48] Fujimura, K. (1989) 'The equivalence between two perturbation methods in weakly nonlinear stability theory for parallel shear flows.' *Proc. R. Soc. Lond. A*, **424**, 373-392.

[49] Fujimura, K. (1997) 'Centre manifold reduction and the Stuart-landau equation for fluid motions.' *Proc. R. Soc. Lond. A*, **453**, 181-203.

[50] Crouch, J. D. and Herbert, Th. (1993) 'A note on the calculation of Landau constants.' *Phys. Fluids A*, **5**, 283-285.

[51] Jeffrey, A. and Kawahara, T. (1982) *Asymptotic methods in nonlinear wave theory*, Pitman books, London.

[52] Moreau, R. (1990) *Magnetohydrodynamics*, Kluwer Academic Publishers, Netherlands.

[53] Hartmann, J. (1937) 'Hg–dynamics I. Theory of the laminar flow of an electrically conductive liquid in a homogeneous magnetic field.' *K. Dan. Vidensk. Selsk. Mat. Fys. Medd.* **15**(6), 1-28.

[54] Hartmann, J. and Lazarus, F. (1937) 'Experimental investigations on the flow of mercury in a homogeneous magnetic field.' *K. Dan. Vidensk. Selsk Mat. Fys. Medd.* **15(7)**, 1.

[55] Lock, R. C. (1955) 'The stability of the flow of an electrically conducting fluid between parallel planes under a transverse magnetic field.' *Proc. Roy. Soc. Lond.* ***A*****233**, 105-125.

[56] Murgatroyd, W. (1953)'Experiments on magnetohydrodynamic channel flow.' *Philos. Mag.* **44**, 1348-1354.

[57] Stuart, J. T. (1954) 'On the stability of viscous flow between parallel planes in the presence of a co-planar magnetic field.' *Proc. Roy. Soc. Lond. A* **221**, 189.

[58] Hunt, J. C. R. (1966) 'On the stability of parallel shear flows with parallel magnetic fields.' *Proc. R. Soc. Lond. A* **293**, 342-358.

[59] Potter, M. C. and Kutchey, J. A. (1973) 'Stability of plane Hartmann flow subject to a transverse magnetic field.' *Phys. Fluids.* **16**, 1848-1851.

[60] Takashima, M. (1996) 'The stability of the modified plane Poiseuille flow in the presence of a transverse magnetic field.' *Fluid Dyn. Res.* **17**, 293-310.

[61] Roberts, P. H. (1967) *An Introduction to Magnetohydrodynamics*, Longmans, §6.2

[62] Likhachev, O. A. (1976) 'Self-oscillatory flow in asymptotic boundary layers.' *J. Appl. Mech. Tech. Phys.* **17**, 194-197.

[63] Lifshits, A. M. and Shtern, V. N. (1979) 'Monoharmonic analysis of the nonlinear stability of Hartmann flow.' *Magnitnaya Gidrodinamika.* **3**, 17-22.

[64] Lingwood, R. J. and Alboussière, T. (1999) 'On the Stability of the Hartmann layer.' *Phys. Fluids.* **8**, 2058-2068.

[65] Lykoudis, P. S. (1960) 'Transition from laminar to turbulent flow in magneto-fluid mechanic channels.' *Rev. Mod. Phys.* **32**, 796-798.

[66] Branover, G. G. (1967) 'Resistance of magnetohydrodynamic channels.' *Magnetohydrodynamics*, **3**, 1-11.

[67] Moresco, P. and Alboussière, T. (2003) 'Experimental study of the instability of the Hartmann layer.' *J. Fluid Mech.* **504**, 167-181.

[68] Krasnov, D. S., Zienicke, E., Zikanov, O., Boeck, T. & Thess, A. (2004) 'Numerical study of the instability of the Hartmann layer.' *J. Fluid Mech.* **504**, 181-211.

[69] Hocking, L. M. (1975) 'Non-linear stability of the asymptotic suction velocity profile.' *Quart. J. Mech. Appl. Math.* **28**, 341-353.

[70] Moresco, P. and Alboussière, T. (2003) 'Weakly nonlinear stability of Hartmann boundary layers.' *Eur. Jour. Mec B.* **22**, 345-353.

[71] Soibelman, I. & Meiron, D. I. (1991) 'Finite-amplitude bifurcations in plane Poiseuille flow: two-dimensional Hopf bifurcation.' *J. Fluid Mech.* **229**, 389-416.

[72] Casas, P. S. & Jorba, À. (2012) 'Hopf bifurcations to quasi-periodic solutions for the two-dimensional plane Poiseuille flow.' *Comm. Nonlinear. Sci. Numer. Simulat.* **17**, 2864-2882.

[73] Gerard-Varet, D. (2002) 'Amplification of small perturbations in a Hartmann layer.' *Phys. Fluids* **14**, 1458-1467.

[74] Airiau, C. & Castets, M. (2004) 'On the amplification of small disturbances in a channel flow with a normal magnetic field.' *Phys. Fluids* **16**, 2991-3015.

[75] Waleffe, F. (1995) 'Transition in shear flows: non-linear normality versus non-normal linearity.' *Phys. Fluids* **7**, 3060-3066.

[76] Chapman, S. J. (2002) 'Subcritical transition in channel flows.' *J. Fluid Mech.* **451**, 35-97.

[77] Canuto, C., Hussaini, M.Y., Quarteroni, A. and Zang, T.A. (1988) *Spectral Methods in Fluid Dynamics*, Springer, Berlin.

[78] McFadden, G.B., Murray, B.T. and Boisvert, R.F. (1990) 'Elimination of spurious eigenvalues in the Chebyshev tau spectral method.' *J. Comput. Phys.* **91**, 228-239.

[79] Slater, J. C. (1934) 'Electronic bands in metal.' *Phys. Rev.* **45**, 794-801.

[80] Kantorovic, L. V. (1934) 'On a new method of approximate solution of partial differential equations.' *Dokl. Aka. Nauk NSSSR*, **4**, 532-536.

[81] Frazer, R. A., Jones, W. P. and Skan, S. W. (1937) *Approximation to Functions and to the Solution of Differential Equations*. Rep. and Mem. 1799 (Aeronautical Research Council, London)

[82] Boyd, J.P. (2001) *Chebyshev and Fourier Spectral Methods*, Dover, New York.

[83] Zebib, A. (1987) 'Removal of spurious modes encountered in solving stability problems by spectral methods.' *J. Comput. Phys.* **70**, 521-525.

[84] Dawkins, P.T., Dunbar, S.R. and Douglass, R.W. (1998) 'The origin and nature of spurious eigenvalues in the spectral tau method.' *J. Comput. Phys.* **147**, 441-462.

[85] Gardner, D.R., Trogdon, S.A., and Douglass, R.W. (1989) 'A modified tau spectral method that eliminates spurious eigenvalues.' *J. Comput. Phys* **80**, 137-167.

[86] Zebib, A. (1984) 'A Chebyshev method for the solution of boundary value problems.' *J. Comput. Phys.* **53**, 443-455.

[87] Waleffe, F. (2001) 'Exact coherent structures in channel flow.' *J. Fluid Mech.* **435**, 93-102.

[88] Huang, W. and Sloan, D.M. (1994) 'The pseudospectral method for solving differential eigenvalue problems.' *J. Comp. Phys.* **111**, 399-409.

[89] Weideman, J.A.C. and Reddy, S.C. (2000) 'A MATLAB differentiation matrix suite.' *ACM Transactions on Mathematical Software*, **26**, 465-519.

[90] Hagan, J. & Priede, J. (2013) 'Capacitance matrix technique for avoiding spurious eigenmodes in the solution of hydrodynamic stability problems by Chebyshev collocation method.' *J. Comp Phys.* **238**, 210-216.

[91] Fox, L. and Parker, I. B. (1968) *Chebyshev Polynomials in Numerical Analysis*, Oxford University Press, London.

[92] Mason, J. C. and Handscomb, J. C.(2003) *Chebyshev Polynomials*, CRC Press LLC, Florida, USA.

[93] Peyret, R. (2002) *Spectral Methods for Incompressible Viscous Flow*, 1st ed. Springer-Valeg New York, Inc.

[94] Anderson, E., Bai, Z., Bischof, C., Blackford, S., Demmel, J., Dongarra, J., Du Croz, J., Greenbaum, A., Hammarling, S., McKenney, A., Sorensen, D. (1999) *LAPACK Users' Guide*, 3rd ed., SIAM, Philadelphia

[95] Joseph, D. D. & Sattinger, D. H. (1972) 'Bifurcating time periodic solutions and their stability,' Arch. Rat. Mech. Anal. **45**, 79.

[96] Herbert, T. (1977) 'Finite amplitude stability of plane parallel flows.' *AGARD Conf. Proc.* ***CP*–224**, 3/1.

[97] Zahn, J. P., Toomre, J., Spiegel, E. A. & Gough, D. O. (1974) 'Nonlinear cellular motions in plane Poiseuille channel flow.' *J. Fluid Mech.* **64**, 319-345.

[98] Ehrenstein, U. and Koch, W. (1991) 'Three-dimensional wavelike equilibrium states in plane Poiseuille flow.' *J. Fluid Mech.* **228**, 111-148.

[99] Pugh, J. D. & Saffman, P. G. (1988) 'Two-dimensional superharmonic stability of finite amplitude waves in plane Poiseuille flow.' *J. Fluid Mech.* **194**, 295-307.

[100] Hinch, E. J. (1991) *Perturbation methods* Cambridge University Press, p. 15.

[101] Bodoia, J. R. and Osterle, J. F. (1961) 'Finite difference analysis of Poiseuille and Couette flow developments.' *App. Sci. Res.* **10**, 265-276.

[102] Fujimura, K. (1987) 'Landau constant of plane Poiseuille flow near the neutral state,' *Phys. Fluids* **30**, 1216.

[103] Golub, G. H. & van Loan, C. F. (1996) *Matrix computations*, 3rd ed., Johns Hopkins University Press, Baltimore, p. 311.

[104] Squire, H. B. (1933) 'On the stability of three-dimensional disturbances of viscous flow between parallel walls.' *Proc. Roy. Soc.* ***A*142**, 621-628.

[105] Lin, C. C. (1961) 'Some mathematical problems in the theory of the stability of parallel flows.' *J. Fluid Mech.* **10**, 430-438.

[106] Barkley, D. (1990) 'Theory and predictions for finite-amplitude waves in two-dimensional plane Poiseuille flow.' *Phys. Fluids*, **29**, 1328-1331.

[107] Zinov'ev, A. T. & Shtern, V. N. (1987) 'Self-excited oscillations in Hartmann channel and boundary-layer flows.' *Magnetohydrodynamics* **23**, 24-30.

[108] J. Priede, S. Aleksandrova, S. Molokov, (2010) 'Linear stability of Hunt's flow. J. Fluid Mech.' **649**, 115-134.